Alkali-silica reaction in geopolymer concrete

Lei, Jiawei

2020

Lei, J. (2020). Alkali-silica reaction in geopolymer concrete. Doctoral thesis, Nanyang Technological University, Singapore.

https://hdl.handle.net/10356/146237

https://doi.org/10.32657/10356/146237

NANYANG TECHNOLOGICAL UNIVERSITY
SINGAPORE

ALKALI-SILICA REACTION IN GEOPOLYMER CONCRETE

LEI JIAWEI

SCHOOL OF CIVIL AND ENVIRONMENTAL ENGINEERING

2020

ALKALI-SILICA REACTION IN GEOPOLYMER CONCRETE

LEI JIAWEI

School of Civil and Environmental Engineering

A thesis submitted to the Nanyang Technological University
in partial fulfilment of the requirement for the degree of
Doctor of Philosophy

Statement of Originality

I hereby certify that the work embodied in this thesis is the result of original research, is free of plagiarised materials, and has not been submitted for a higher degree to any other University or Institution.

20/01/2020
Date

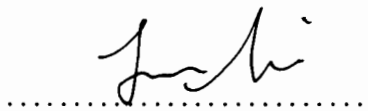
Lei Jiawei

Supervisor Declaration Statement

I have reviewed the content and presentation style of this thesis and declare it is free of plagiarism and of sufficient grammatical clarity to be examined. To the best of my knowledge, the research and writing are those of the candidate except as acknowledged in the Author Attribution Statement. I confirm that the investigations were conducted in accord with the ethics policies and integrity standards of Nanyang Technological University and that the research data are presented honestly and without prejudice.

20 Jan 2020
.....
Date

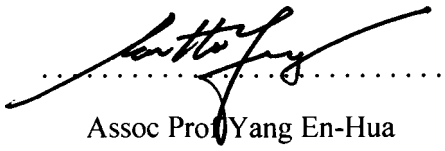
.....
Assoc Prof Yang En-Hua

Authorship Attribution Statement

This thesis contains material from paper accepted at conference in which I am listed as an author.

Chapter 3 contains material from the conference paper: Lei, JW, Fu, JJ, Yang, EH (2019), Pore Solution Chemistry of Fly Ash Geopolymer: Relation to Alkali-Silica Reaction Resistance of Geopolymer Concrete, 15th International Congress on the Chemistry of Cement, Prague, Czech Republic, September 16-20, 2019.

The contributions of the co-authors are as follows:

- Assoc Prof Yang En-Hua provided the initial research direction and revised the manuscript drafts.
- All the laboratory works were performed by Mr Fu Jia Jun and me.
- I analysed the data and prepared the manuscript drafts.

20/01/2020
.....
Date

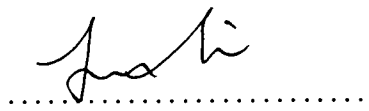
.....
Lei Jiawei

Acknowledgements

First and foremost, I would like to express my sincere gratitude and appreciation to my supervisor, Assoc Prof Yang En-Hua for his guidance, advice and encouragement throughout my four-year Ph.D. study. Being a man of trustworthiness and integrity was the first lesson I have learned since I joined the group. Through Prof. Yang's guidance and the discussions with him, I can see my improvement on the critical thinking and problem-solving skills, which I value more than the knowledge I learned in the studied area. He encouraged every group member to learn from each other so that I was not limited in my Ph.D. research topics but had a chance to see more interesting ideas, which broadened my horizon and were also inspiring to my research. All of the above mentioned learning formed the foundation for my Ph.D. works.

I would like to give my thanks to all the LiSt group members for their valuable suggestions and insightful discussions, especially to Dr. Chen Zhitao, Dr. Qiu Jishen and Dr. Li Junxia for their patient guidance on experiments and the selfless sharing of their experience. I would also like to thank Mr. Fu Jia Jun, Ms. Wang Wei Lin, Mr. See Zheng Hao, Mr. Law Wei Wee and Mr. Goh Han Sheng for helping me on the hand-on experiments.

Special thanks to Mr. Ong Chee Yung, Mr. Tan Han Khiang, Mr. Jee Kim Tian, Mr. Chan Chiew Choon, Mr. Choi Siew Pheng, Mr. Li Fali, Ms. Maria Chong and Ms. Pearlyn See for their technical support and assistance in the lab.

Last but not the least, I would like to thank my wife Wang Xin and my parents for always supporting me and always being there for me. I won't be where I am today without their love and support.

Table of Contents

Summary

The excavation of the Jurong Rock Cavern in Singapore produced rocks in a volume of about three million cubic meters. The excavated rocks potentially provide a valuable source for the local concrete aggregates, especially for Singapore, where the aggregates rely entirely on import. However, these rocks, mainly sedimentary siltstone and sandstone, were identified as alkali-silica reactive rocks, which would cause severer durability issues when they are used as aggregates in ordinary Portland cement (OPC) concrete.

Geopolymer cement, a promising low-CO_2 alternative binder to OPC, has been generally reported to be more resistant to ASR than the conventional OPC. The use of geopolymer concrete potentially provides a new solution to utilize the reactive aggregates. In addition, the local reactive rocks are rich in silica and alumina, two components which make them appealing for the geopolymer precursors.

The objective of this study is therefore to produce a reliable ASR-free geopolymer concrete by using the local ASR-suspicious rocks as both aggregates and precursors. On one hand, the influence of the geopolymer pore solution on the ASR resistance of the geopolymer concrete was investigated to understand the reason for the ASR resistance of the geopolymer concrete. On the other hand, the method of geopolymer precursor synthesis by using the local ASR-suspicious rocks was explored.

The results suggests the insufficient alkalinity and the deficiency of calcium in the geopolymer pore solution were the two controlling factors for the ASR resistance of the geopolymer concrete. The geopolymer precursor could be produced from the reactive rocks by the thermal treatment on a mix of rocks, alumina and sodium hydroxide in the powder form. The optimization of the binder was conducted by tailoring the composition of the precursor to improve the mechanical strength of the binder. Finally, an ASR-free geopolymer concrete was produced by using the local ASR-suspicious rocks as both aggregates and precursors.

List of Tables

List of Figures

Chapter 1 Introduction

1.1 Research background

The Jurong Rock Cavern (JRC) is the first commercial underground rock cavern for oil storage in Southeast Asia, which is located at a depth of 130 m beneath Banyan Basin on Jurong Island in Singapore. The excavation of the cavern resulted in the rocks in a volume of about three million cubic meters being dug out (Winn et al., 2017), which potentially provide a valuable source for the local concrete aggregates, especially for Singapore, where the aggregates rely entirely on import. However, the excavated rocks, mainly sedimentary siltstone and sandstone, were identified as alkali-silica reactive through petrography observations and accelerated mortar bar tests. The use of these JRC rocks as aggregates in ordinary Portland cement (OPC) concrete would cause severer durability issues.

In contrast to OPC concrete, recent studies on the ASR expansion behavior of geopolymer mortar or concrete generally showed that geopolymer concrete or mortar exhibited higher resistance to ASR compared with the conventional OPC counterpart. The adoption of geopolymer concrete potentially provides a new solution to ASR mitigation when reactive aggregates are used in concrete.

1.1.1 Alkali-silica reaction in geopolymer concrete

Alkali-silica reaction (ASR) is one of the major durability problems in OPC concrete. It was firstly identified as a reason for concrete deterioration 80 years ago (Stanton, 1940). In the reaction, the reactive forms of silica in aggregates are attacked and dissolved by the hydroxyl ions in the pore solution in the OPC matrix, resulting in the formation of a hydrophilic alkali-silicate gel, which is responsible for the expansion, cracking and even the disruption of the OPC concrete structures (Swamy, 1992). The problems associated with ASR have been recognized in the structures, including dams, pavements, bridges, barriers and nuclear/power plant structures, all around the world (Fournier and Bérubé, 2000) and ASR is a continuing concern as the progressive depletion of non-reactive aggregates (Swamy, 1992). Use of non-reactive aggregate in many locations is not often practical due to the local availability and the cost of shipping non-reactive aggregates from other locations are prohibitive

(Rajabipour et al., 2015). In addition, avoiding ASR in structures cannot be guaranteed even when aggregates believed to non-reactive are used in the construction exposed to aggressive environment, such as to seawater or de-icing salts (Thomas et al., 2013).

Using a sufficient quantity of supplementary cementitious materials (SCM) is one of the most common means of controlling ASR in OPC concrete containing reactive aggregates (Rajabipour et al., 2015). It was showed that the amount of SCM required to control ASR varies widely depending on the nature of the SCM, the reactivity of the aggregates, the availability of the alkalis within the concrete and the exposure conditions of the concrete (Michael Thomas, 2011). However, the appropriate SCM dosage in a concrete has to be determined by the ASR testing case by case (Wright et al., 2014). In addition, high replacement levels of Portland cement with SCM can negatively impact other concrete properties such as setting, strength development and freeze–thaw durability (Rajabipour et al., 2015).

Geopolymer cement is one of the promising low-CO_2 alternatives to OPC (Provis, 2018). It is produced by the reaction of an alkali source and an aluminosilicate precursor, which dissolves under alkaline conditions to release silicate and aluminate species, and the components then rearrange through solution and condense to form a dense binding gel with a three-dimensional aluminosilicate network (Duxson, et al., 2007). Geopolymer binders have been seen to provide comparable mechanical and rheological property to OPC binder in the hardened and the fresh states, respectively, but with reduced environmental footprint in contrast to OPC (Bernal and Provis, 2014; Li et al., 2010). Additionally, they exhibited a variety of attractive attributes such as high resistance to acid attack and fire (Lahoti et al., 2018; Provis, 2016) if proper formulation and curing condition are adopted. Moreover, recent studies on the resistance of geopolymer concrete to alkali-silica reaction (ASR) showed that geopolymer concrete were almost innocuous to ASR when reactive aggregates were used (García-Lodeiro et al., 2007; Kupwade-Patil and Allouche, 2012; Pouhet and Cyr, 2015; Williamson and Juenger, 2016).

García-Lodeiro et al (2007) found that the ASR-induced expansion in fly ash geopolymer mortar was much smaller than that of OPC mortar and was below the

expansion limit (0.1%) prescribed in the standard (Fig. 1.1). As can be seen, typical ASR map cracking could be observed on the OPC specimens, while the geopolymer mortar exhibited no surface cracking. Pouhet and Cyr (2015) also found that the incorporation of reactive silica did not lead to the ASR expansion- in metakaolin-based geopolymer concrete even though a small amount of ASR gel was found on the surface of the reactive aggregates. The work by William and Juenger (2016) studied the influence of activating solution concentration on the ASR behavior of fly ash geopolymer. The results showed that the geopolymer concrete has little expansion although the pore solution alkalinity within the binder was believed to be sufficient to trigger the ASR expansion. The reason for the ASR resistance of the geopolymer mortar or concrete is still unclear, although several hypotheses have been proposed.

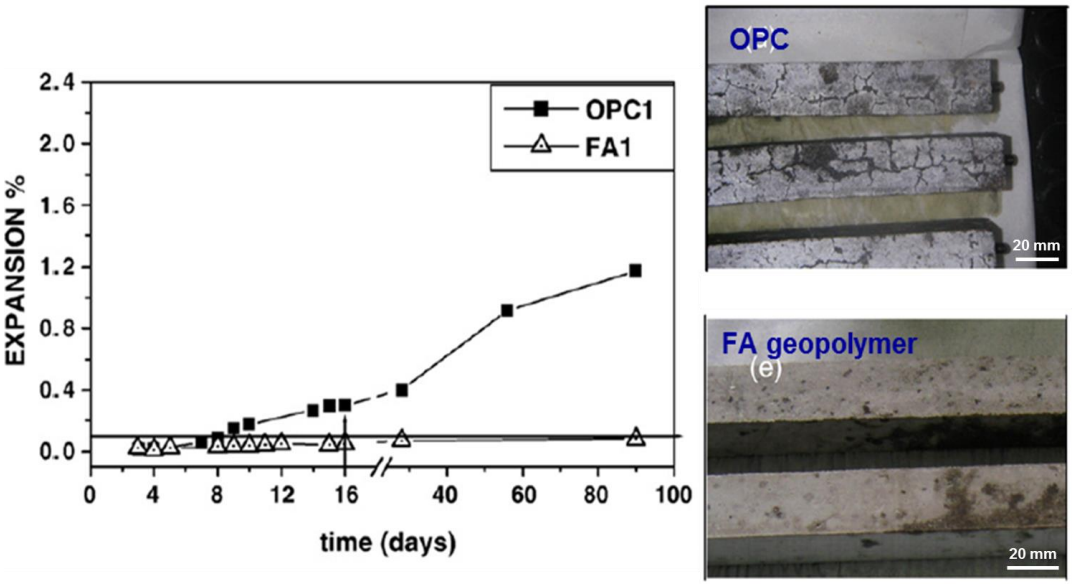

Fig. 1.1 ASR induced expansion in OPC and fly ash geopolymer mortars (García-Lodeiro et al., 2007)

Some researchers proposed that the lack of calcium hydroxide in geopolymer may account for this phenomenon (Fernández-Jiménez and Puertas, 2002; García-Lodeiro et al., 2007; Pacheco-Torgal et al., 2012; Pouhet and Cyr, 2015; Shi et al., 2015; Williamson and Juenger, 2016). It is known that large amount of calcium hydroxide are produced from the hydration of tri- and di-calcium silicates in OPC, whereas no calcium hydroxide appears in geopolymer binders (Shi et al., 2011; Shi et al., 2015). It is generally believed that calcium hydroxide plays an important role in ASR

expansion in OPC concrete but the effect of calcium is still controversial. Firstly, the calcium hydroxide provide a large reservoir of hydroxide ions to maintain the pH level of the pore solution, thus sustaining the attack on the reactive aggregates (Rajabipour et al., 2015). Secondly, a number of studies concluded that the presence of calcium influences the gelation process (Glasser and Kataoka, 1982; Gaboriaud et al., 1999). In the absence of calcium, it was reported that the reactive silica simply dissolved in the alkali hydroxide solution without forming any gel (Diamond, 1989; Leemann et al., 2011; Struble, 1987), probably because calcium promoted the gelation of silicate species in the solution (Gaboriaud et al., 1999). Thirdly, it was also proposed that calcium affects the physical and chemical properties of the ASR gel (Bleszynski and Thomas, 1998; Gholizadeh et al., 2016) in OPC concrete. Urhan (1987) speculated that the ASR gel with low calcium content has low viscosity, which is easily dispersed into the surrounding pastes without causing internal stress and expansion. However, a study on the composition-rheology relationship of ASR gel (Vayghan et al., 2016) indicated that calcium exhibited no significant effect on the osmotic pressure of the gel with low Na/Si ratio and the osmotic pressure was reduced for the gel with high Na/Si ratio, and an earlier work of Struble and Diamond (1981) concluded that the presence of calcium does not noticeably influence the swelling pressure when compared with calcium-free gel.

Moreover, the different alkalinity of the pore solution in geopolymer concrete and OPC concrete has also been proposed to explain the different expansion behaviors in these two systems. It has been reported that sufficient alkalinity of concrete pore solution is required to sustain the ASR at a certain rate that will lead to deleterious ASR expansions (Rajabipour et al., 2015; Shehata and Thomas, 2006), and the pH levels of the pore solution of OPC paste typically fall between 13.2 and 13.8 (Struble, 1988; Swamy, 1992), which is sufficient for the deleterious ASR to occur. The studies on the alkalinity of pore solution in geopolymer are limited and the results are not consistent with one another. Pouhet and Cyr (2015) found that the pH of the pore solution in a metakaolin-based geopolymer was initially as high as 14, but reduced rapidly to be lower than 12 after only 14 days. They suggested that this is likely due to the carbonation of the pore solution and proposed that the low ASR expansion may be attributed to the extremely high initial pH leading to rapid alkali-silica reaction in

the early period of hardening, or due to the rapid reduction of alkalinity which would not be sufficient for the pore solution to attack the reactive aggregates. However, Lloyd et al. (2010) showed that the pH level of the pore solution in the geopolymer pastes synthesized by different kinds of fly ash was generally above 13 at 90 days, and Williamson and Juenger (2016) suggested that the alkali contents in the pore solution of fly ash geopolymer at 7 days were 3-4 times higher than the thresholds previously proposed for ASR expansion in OPC concrete. Nonetheless, little ASR expansion was observed in these fly ash geopolymer concretes through laboratory investigations (Williamson and Juenger, 2016).

The presence of aluminum in geopolymer concrete is also one of the possible reasons for its ASR resistance. The role of aluminum in ASR in OPC concrete has been studied (Chappex and Scrivener, 2012a, 2012b, 2013; Leemann et al., 2015; Warner et al., 2012) and the results consistently showed that the presence of aluminum contributed to ASR expansion mitigation. Hong and Glasser (2002) concluded that incorporation of Al into C-S-H remarkably enhanced the alkali binding capability of the binder based on the test on the synthetic gel. The alkalinity of the pore solution was therefore reduced with the presence of aluminum, accounting for the lower ASR expansion. Chappex and Scrivener (2012a), however, found that the aluminum incorporation increased alkali fixation capacity very slightly in real cementitious system and suggested that the beneficial effect of aluminum on ASR was attributed to the incorporation of aluminum into the reactive silica structure, resulting in reduction of the silica dissolution rate. Also, Krivenko et al. (2014) reported that a dense zeolitic shell ($Na_2O \cdot Al_2O_3 \cdot mSiO_2 \cdot nH_2O$) was formed around the aggregate grains in the presence of active alumina, thus preventing the further reaction between the alkalis and aggregates. Geopolymer binder, synthesized from aluminosilicate precursors, is expected to contain higher aluminum content in the pore solution compared to OPC paste, which may account for its lower expansion due to ASR.

1.1.2 Synthesis geopolymer binder by utilizing local natural mineral resources

Industrial by-products such as coal fly ash are widely used nowadays as aluminosilicate precursors for geopolymer binder production, which is environmental friendly and cost-efficient. However, the utilization of these by-products are subjected to the variability in their characteristics and the local availability. The local availability of the precursors does not only determine the likelihood of adoption of the alkali-activated binder for a specific location, but also influences the environmental benefits when utilization the binder as the transport of bulk materials can dominate the emissions footprint of the binder as a whole if long distance transportation is required (McLellan et al., 2011; Provis, 2016). In addition, the competition in demand from the use of fly ash in blends with OPC may also restrain the available raw materials for alkali-activated binders. Thus increasing research efforts have been made recently to broaden the selection of precursors, especially to seek a local solution to utilize the local available sources for geopolymer binder productions (C. Shi et al., 2019).

Natural mineral resources such as common clay and feldspars are of interest to researchers in producing geopolymer binder due to the ecological benefits, low costs and local availability. Buchwald et al. (Buchwald et al., 2009) showed that illite/smectite clays can be used for alkali activation after thermal treatment and the calcination temperature should be carefully selected to ensure the full dehydroxylation of the clay minerals and prevent the formation of new stable phases. Valentini et al. (Valentini et al., 2018) produced alkali-activated binder by using the local thermal-treated smectite clay with moderate addition of waste calcium carbonates and the binder exhibited appealing mechanical property without high temperature curing. Dietel et al. (Dietel et al., 2017) concluded that specific surface area and the amount of soluble Si and Al are the key factors determining the strength of the alkali-activated binder by using local illitic clays.

Feldspars are the most widespread mineral group accounting for around 40% of the Earth's crust and contain silica and alumina, which are an appealing natural sources for the alkali-activated precursors. Feng et al. (Dingwu Feng et al., 2012) synthesized geopolymer precursors by thermal activation of albite feldspars with sodium

hydroxide and sodium carbonate. The crystalline albite structure broke down and an amorphous geopolymer precursor was formed with the addition of alkali source and thermal treatment at 1000℃. The geopolymer binder with acceptable compressive strength was formed just by mixing water with the synthesized precursors.

The chemical compositions analysis showed that the local JRC rocks are rich in silica and alumina, both constituting 77% by mass of the rocks. The two components make the JRC rocks a promising source material to produce the local available geopolymer precursors.

1.1.3 Summary

The previous studies generally suggested that the geopolymer binder system has higher resistance to ASR than the conventional OPC system. It potentially makes geopolymer concrete more appealing for commercial adoption in construction industry. The problem associated with ASR largely limits the option for available aggregates types that are suitable for use in OPC concrete. Reactive aggregates (including natural aggregates and waste material such as waste glass) that are prohibited to use in conventional OPC concrete are more readily and abundantly available compared to non-reactive aggregates in many locations (Thomas et al., 2013). The geopolymer concrete system with higher ASR resistance could potentially make the use of these reactive aggregates, such as the JRC rocks, in concrete possible without causing deleterious ASR expansions, which could produce much more options for aggregate resources with lower cost and reduced environmental impacts.

The local JRC rocks not only have the potential to be used as aggregates in geopolymer concrete, they are also the promising raw materials for the production of the locally available geopolymer precursors since they are rich in silica and alumina. It could broaden the selection of material as precursors and provide a local solution to the needs of the construction industry for geopolymer concrete production.

1.2 Research scope and objective

Based on the above introduction, hypotheses were proposed to explain the low ASR expansion of the geopolymer concrete with the focus on the differences in the pore

solution composition between the geopolymer and OPC systems, as the pore solution may directly influences the ASR process and the gel expansions. However, the underlying mechanism still remains unclear and inconclusive due to the controversies between the existed studies and the lack of understanding on the pore solution chemistry of geopolymer binders. It raises doubts on its reliability and durability when ASR-vulnerable aggregates are used in geopolymer concrete.

Moreover, it is expected that the locally available geopolymer precursors could be synthesized by using the local JRC rocks. While the studies on the geopolymer precursor synthesis by using mineral rocks are limited and there is no one-size-fits-all solution due to the variability of the composition and reactivity of the raw materials, the solution to effectively transform the local rocks into geopolymer precursor is required to be investigated.

The objective of this study is therefore to produce a reliable ASR-free geopolymer concrete by using the local ASR-suspicious rocks as both aggregates and precursors. To achieve this objective, the influence of the geopolymer pore solution on the ASR resistance of the geopolymer concrete need to be understood and the solution to the precursor synthesis by using the local rocks need to be investigated. Specifically, the main scope of the work is shown as follows.

- To understand the pore solution chemistry of the geopolymer binders;
- To study the effect of pore solution alkalinity on ASR expansion of geopolymer concrete;
- To investigate the influence of aluminum in pore solution on ASR expansion of geopolymer concrete;
- To investigate the influence of calcium in pore solution on ASR expansion of geopolymer concrete;
- To synthesis the geopolymer binder by using local rock minerals and optimize the mechanical property of the binder;
- To produce ASR-free geopolymer concrete by using the local alkali-silica reactive rocks as both aggregates and precursors.

1.3 Methodology

Fig. 1.2 shows the methodology of the present study. Macroscopic expansion tests including the accelerated approach (ASTM C1260) and the long-term method (ASTM C1293) were used to evaluate the ASR expansion of geopolymer concrete, which provided information directly associated to the ASR deterioration.

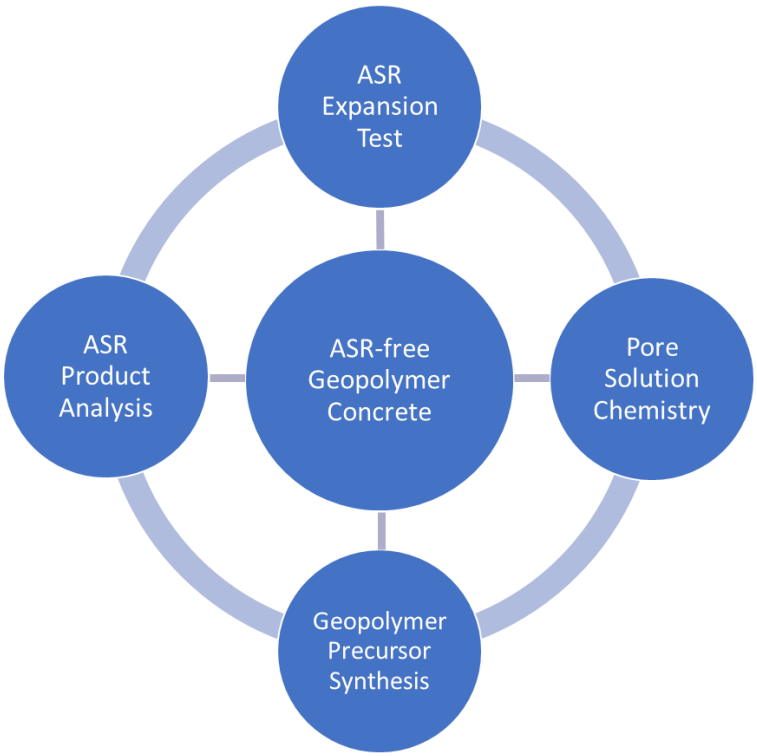

Fig. 1.2 Methodology of the present study

The accelerated mortar bar test (AMBT) according to ASTM C1260, which involves the immersion of mortar bars in 1 mol/L NaOH solution at 80 °C. Despite the method was proposed based on the conventional cementitious material, it is the most commonly used test applied in evaluating ASR in alkali-activated concrete (Provis and van Deventer, 2014). For the geopolymer concrete, however, the aggressive condition in AMBT was reported to influence the chemical stability of the geopolymer matrix. The external alkali source and the elevated temperature that the mortar bars experience in AMBT may lead to the transition of amorphous geopolymers to crystalline zeolitic phases (Fernandez-Jimenez et al., 2007; García-Lodeiro et al., 2007; Nguyen and Škvára, 2016), which makes the applicability of this

method to geopolymer mortar questionable. The concrete prism test (CPT), ASTM C1293, which is currently considered as the most representative ASR test method in laboratory investigations when compared to structures in actual field conditions (Michael Thomas et al., 2006), is more suitable to evaluate the ASR-behavior of the geopolymer concrete as the specimens are not immersed into NaOH solution and the temperature is closer to ambient temperature. In this study, the CPT was applied to evaluate the ASR expansion of the low-calcium geopolymer system. The AMBT was applied to the alkali-activated slag system, allowing a rapid test to evaluate ASR behavior of the mortar bars in 16 days.

The pore solution of the geopolymer binder was extracted from hardened samples at varied ages, which is the key to understand the mechanisms of the enhanced ASR resistance of the geopolymer concrete. The pore solution was analyzed to investigate the relationship between the alkalinity and composition of the pore solution with the ASR expansions.

The alkali-silica reaction products within the concrete were analyzed to show the composition and morphology. Due to the difficulty of extracting ASR products from concrete, further analysis on the structure of reaction product was conducted on the gel obtained directly from the reaction of pore solution and aggregates.

In addition, for the synthesis of geopolymer precursors, heat-treatment on the rock powder together with additives (such as heat flux and alumina) was employed to improve the reactivity of the materials, based on which the composition of the precursor was adjusted to achieve a binder with optimized mechanical strength.

1.4 Roadmap

The roadmap of the present study is showed in Fig. 1.3. To understand the influence of the geopolymer pore solution on the ASR resistance of the geopolymer concrete, the pore solution chemistry of the geopolymer concrete was firstly studied, followed by the individual investigation into the effect of pore solution alkalinity, aluminum and calcium in the pore solution on the ASR expansion behavior of the geopolymer concrete.

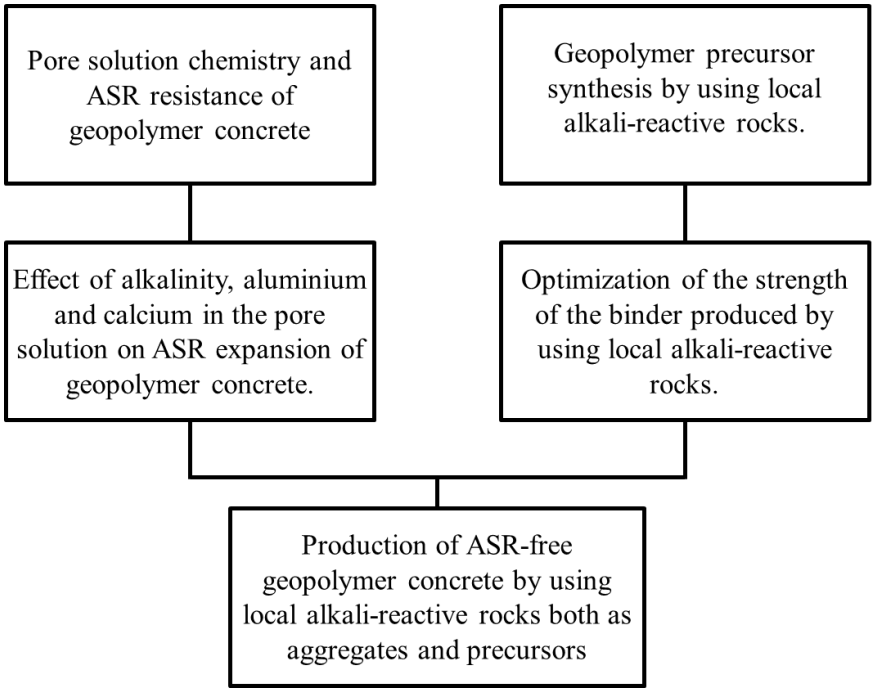

Fig. 1.3 Roadmap of the present study

Firstly, the pore solution of a fly ash-based geopolymer binder was systematically investigated in terms of ion concentrations, pH, chemical bonds, and short-range order of the silicon and aluminum within the pore solution. Fly ash is the most commonly used precursor for producing geopolymer concrete. The ASR expansion behaviors of the OPC and geopolymer concrete was compared by using concrete prism test (ASTM C1293). The reaction products within the specimens after the tests were analyzed and compared in terms of the morphology and chemical composition. Moreover, the relation of the pore solution and ASR expansion of the geopolymer concrete was illustrated.

To study the effect of pore solution alkalinity on the geopolymer concrete, geopolymer concrete with pore solution with varied alkalinity was produced. The geopolymer concrete was produced by the activating solution with varied alkalinity with all the other factors remain constant. Metakaolin was adopted as the precursor in this study due to its high reactivity and simple composition that allows a control of the pore solution composition through mix design compared to fly ash. The ASR expansions of the concrete with varied pore solution alkalinity were compared. In addition, the reaction product was investigated by directly mixing the extracted pore

solution from the geopolymer binder with different types of aggregates. Based on the results of the reaction between the pore solution and the aggregates, the effect of aluminum in the pore solution on the ASR in geopolymer concrete was discussed.

The effect of calcium hydroxide on the ASR expansion was investigated in an alkali-activated slag (AAS) system, due to the difficulty of adding calcium sources directly into geopolymer system, as the additional calcium would be incorporated into the geopolymer structure forming C-A-S-H gel, which is similar to the structure of AAS system. It is believed that the information provided by the study on the effect of calcium hydroxide on the ASR expansion in AAS mortar would contribute to understanding whether the absence of calcium in the geopolymer system accounts for the ASR resistance of the geopolymer concrete. In the study, the ASR products and the pore solution of the AAS mortars with varied amount of additional calcium hydroxide were analyzed and the relationship between the ASR expansion and the content of the calcium hydroxide within the binder was investigated. The role of calcium hydroxide in the ASR in AAS concrete was discussed.

For the utilization of the local rocks to produce geopolymer precursors, heat-treatment with additional heat flux and aluminum source were employed to transform the crystalline rocks into vitreous phases. The optimization of the binder was conducted in terms of the amount of heat flux and Si/Al ratio of the produced precursor to improve the mechanical strength of the binder.

Finally, based on the knowledge obtained from the aforementioned studies, the production of ASR-free geopolymer concrete by using the local alkali-silica reactive rocks both as aggregates and precursors were explored. The ASR expansion behavior of the produced geopolymer mortars was investigated by using the accelerated mortar bar test.

1.5 Layout of the thesis

The thesis consists of seven chapters. Chapter one is an introduction to the background, objective, scope, methodology and roadmap of the research. Chapter two covers a detailed review on the alkali-silica reaction, alkali-activated binder including geopolymer and AAS binder, and the recent research on the alkali-silica

reaction in geopolymer concrete. In the third chapter, the pore solution chemistry of a fly ash based geopolymer binder was investigated and the relation of the pore solution and the ASR expansion behavior of the geopolymer concrete was illustrated. Chapter four includes the effect of the pore solution alkalinity on the ASR expansion of the metakaolin geopolymer concrete and the influence of the aluminum on the ASR behavior of the geopolymer concrete is also discussed. Chapter five reports the study on the effect of calcium hydroxide on the ASR expansion of alkali-activated slag concrete. Chapter six reports the synthesis and optimization of the precursor produced by the local alkali-reactive rocks and the demonstration of the ASR resistance of the synthesized binder with local reactive aggregates is presented. Chapter seven gives the conclusion of the present study and the plan of future works.

Chapter 2 Literature Review

2.1 Overview

Literature relevant to the current study was introduced in the first chapter for the purpose of clarifying the research motivation and identifying the research objective. In this chapter, a more comprehensive literature review is provided to give readers an explicit overview of the alkali-silica reaction, alkali-activated binder and the recent research on the alkali-silica reaction in geopolymer concrete.

2.2 An overview of alkali-silica reaction

Alkali-silica reaction (ASR) is a widespread durability issue in OPC concrete and the problem associated with ASR have been recognized in important structures including dams, pavements, bridges, barriers and nuclear/power plant structures throughout the world (Fournier and Bérubé, 2000). Since it was first identified as a reason for concrete deterioration 80 years ago (Stanton, 1940), numerous investigations on ASR have been conducted on the level of materials and structures. In this section, a review of the chemistry of ASR, the controlling factors and the laboratory test methods for evaluating ASR in concrete are presented.

2.2.1 Mechanism of alkali-silica reaction

Alkali-silica reaction is a chemical reaction in the fabric of concrete between the alkaline pore solution of concrete and the reactive silica contained within natural or synthetic aggregates (Diamond, 1975). In this reaction a hydrophilic gel forms and internal pressure is developed as the gel absorbs water and increases its volume, eventually inducing expansion, cracking and disruption of the concrete structure.

The ASR is a multistage process which starts with the dissolution of reactive silica in the aggregates into concrete pore solution. At the interface between aggregates and the pore solution, the silanol groups (Si-OH) and the siloxane bonds (Si-O-Si) of poorly crystallized silica network were attacked by the hydroxyl ions in the pore solution, leading to the disintegration of the silica network. These processes can be represented as follows (Glasser and Kataoka, 1981):

? Si O- Si寒 + OH^- ? Si O^- + HO− Si ? (1)

? Si OH + OH^- Si - O^- + H_2O (2)

Siloxane bonds are ruptured and replaced by silanol bonds, i.e., reaction (1). These silanol bonds, together with the pre-existing one contained in hydrous silica aggregates, react with further hydroxyls. The resulting negative charges from (1) and (2) are balanced by the alkaline ions (K^+, Na^+ or Ca^{2+}) in the pore solution.

As a result, an alkali-silicate gel forms with porous structure, high surface areas and many hydrophilic groups (e.g., -OH, -O…Na, and $-O^-$) (Hench and Clark, 1978), resulting in osmosis, adsorption of water and swelling of the gel (Powers and Steinour, 1955). The gel formation generates increasing internal pressures within the concrete fabric that triggers macroscopic expansions, cracking, strength loss and potentially to failure of structures.

It can be concluded from the above discussion that the deleterious process caused by ASR requires at least three prerequisites: sufficient alkalis or hydroxyl ions in pore solution, a source of reactive silica from aggregates and access to moisture to allow gel expansion (Swamy, 1992).

The major source of alkalis in OPC concrete is from the cement used, while aggregates and SCMs can also provide additional alkali sources to further exacerbate the reaction (Rajabipour et al., 2015). It has been reported that sufficient alkali or hydroxyl concentration in concrete pore solution is required to sustain the alkali-silica reaction at a certain rate that will lead to significant ASR expansion (Rajabipour et al., 2015; Shehata and Thomas, 2006), and a number of minimum hydroxyl ion concentrations of pore solution have been proposed for deleterious expansion to occur in OPC concrete. Several researchers (Diamond, 1983; Kollek and Varma, 1986; Thomas et al., 2006) reported a minimum value of pore solution hydroxyl ion concentration between 0.2 to 0.3 mol/L under which deleterious ASR expansion is unlikely to occur, while Duchesne and Bérubé (Duchesne and Bérubé, 1994) proposed a relatively higher threshold in hydroxyl concentration around 0.65 mol/L and Struble (Struble, 1988) suggested a pH threshold between 13.65 and 13.83 which corresponds to 0.45 and 0.67 mol/L hydroxyl ion concentration, respectively. It

should be noted that the expansion thresholds determined are dependent on the reactivity of the reactive aggregates used in concrete and different binder system (e.g., different types of SCMs blended with cement) selected in the study also affect the expansion behavior as alkali concentration is not the only factor influencing the ASR expansion (Shehata and Thomas, 2006), which may explain the different expansion thresholds suggested in the above studies.

The significant role of alkali in the concrete pore solution for ASR expansion led to the investigation of pore solution chemistry in hardened concrete. The analysis on pore solution of normal OPC concrete (Diamond, 1989) showed that the solution is complex initially on setting, containing alkalis, sulphate, calcium and hydroxyl ions. The equilibrium of pore solution is reached after nearly a month consisting primarily of a relatively high concentration of sodium and potassium hydroxide with minor amount of calcium hydroxide and sulphates. Struble (1987) analyzed the pore solution at stable state from cement mortar made with different cements with a wide range of alkali contents, showing that hydroxyl ion concentration of pore solution lied in the range of 0.2-1.0 mol/L. The pH values of pore solution from many real cement systems were measured showing comparable results ranging from 13 to 14 (Swamy, 1992). Thus, the high concentration of hydroxyl ions in the normal concrete pore solution provides the driving force for ASR to proceed when reactive aggregates are used.

The role of water in ASR is twofold: firstly, it acts as a media for the transport of alkali and hydroxyl ions within concrete and, secondly, it is absorbed by the hydrophilic gel to allow expansion of the gel. With the exception of the dried outer layer, the relative humidity (RH) within concrete usually remains at a high level of 80-90%. It was reported that ASR expansion varies directly with the RH within concrete and the relationship is shown in Fig. 2.1 (Swamy, 1992). As can be seen, no expansion was observed once RH is below 50% and the expansion increases significantly as RH exceeds 80%, implying that limiting concrete's access to external moisture is a method to mitigate the expansion caused by ASR, while it is not feasible for most concrete structures exposed to outdoor environments.

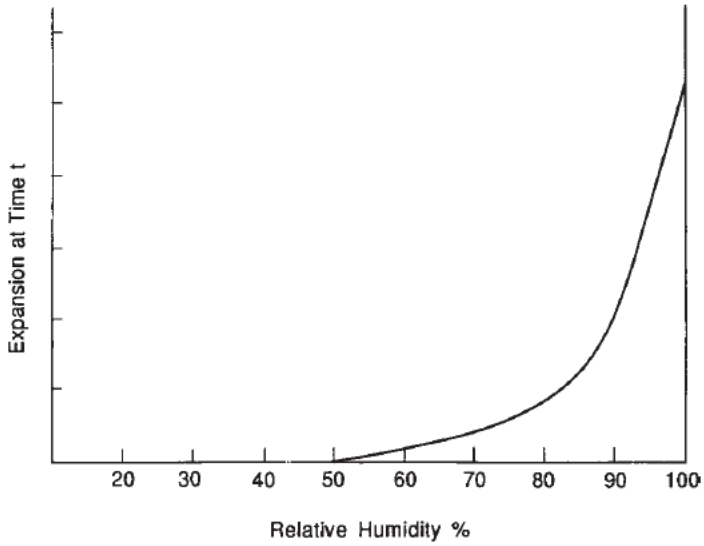

Fig. 2.1 The effect of relative humidity on the expansion of concrete due to ASR (Swamy, 1992)

2.2.2 Reactive aggregates

The presence of reactive silica within aggregates is an essential requirement for ASR to occur in concrete. The reactivity of silica mineral generally increases as the degree of nanostructure disorder increases. Amorphous silica such as opal, natural or synthetic glass is known to be most reactive, followed by meta-stable crystals (e.g., cristobalite and tridymite), micro-crystalline silica and other crystalline forms containing lattice defects, residual strains or internal cracks (Rajabipour et al., 2015). A list of reactive aggregates and minerals is provided in Table 2.1.

Rocks used as aggregates in concrete usually contain more than one type of mineral and might contain a proportion of reactive silica as either major or minor constituents. The volume of reactive components required to cause deleterious ASR could be as small as 2%. It is therefore suggested that the rock mineral constituents should be considered during the evaluation of aggregates' ASR potential rather than the rock type (Swamy, 1992).

Table 2.1 Some ASR-suspicious aggregates and minerals (Thomas et al., 2013)

Reactive substance (mineral)	**Chemical composition**	**Physical character**
Opal	$SiO_2 \cdot nH_2O$	Amorphous
Chalcedony	SiO_2	Microcrystalline to cryptocrystalline; commonly fibrous
Certain forms of quartz	SiO_2	Microcrystalline to cryptocrystalline; crystalline, but intensely fractured, strained, and/or inclusion-filled
Cristobalite	SiO_2	Crystalline
Tridymite	SiO_2	Crystalline
Rhyolitic, dacitic, latitic, or andesite glass or cryptocrystalline devitrification products	Siliceous with small proportions of Al_2O_3, Fe_2O_3,alkaline earths and alkalis	Glass or cryptocrystalline material as the matrix of volcanic rocks or fragments in tuffs
Synthetic siliceous glass	Siliceous, with small proportions of alkalis, Al_2O_3, and/or other substances	Glass

Aggregates can be identified as non-reactive in concrete only based on service records or thorough and careful test results data, such as standardized tests ASTM C1260 (2014) and C1293 (2015). Use non-reactive aggregates is certainly a viable method to prevent ASR-associated damage, while it is not often practical due to the limited availability of truly non-reactive aggregates in many locations (Rajabipour et al., 2015). For instance, Singapore is a country lack of natural resources. The aggregates in Singapore rely entirely on import. Recently, the excavation of a underground Jurong Rock Cavern (JRC) in Singapore resulted in the rocks in a volume of about three million cubic meters being dug out (Winn et al., 2017), which provide a valuable source for the local concrete aggregates. However, the excavated rocks, mainly sedimentary siltstone and sandstone, were identified as alkali-silica reactive through a combination of petrographic examination and concrete mortar bar tests. In addition, for the construction exposed to aggressive environment, such as

exposed to seawater or de-icing salts, avoiding ASR in structures cannot be guaranteed even when aggregates believed to non-reactive are used (Thomas et al., 2013).

2.2.3 Effect of calcium on alkali-silica reaction

The important role of calcium in ASR was not recognized initially in early studies but received great interest in the last few decades. Calcium's effect on ASR expansion can be summarized as two parts: (1) it could free up alkalis back into pore solution by exchanging the alkalis from ASR gel, which is called "alkali recycling"; (2) it could influence the ASR expansion by modifying the ASR gel properties or the gelation process of the gel (Rajabipour et al., 2015).

The calcium could exchange with alkali from the ASR gel was firstly proposed by Hansen (1944) based on the observation that portlandite is depleted in the paste neighboring the gel-filled cracks. The reaction is shown as follows:

$$2(\equiv \mathrm{Si} - \mathrm{O} \ldots \mathrm{Na}) + Ca^{2+} \rightarrow 2Na^{+} + \equiv Si - O \ldots Ca \ldots O - Si \equiv$$

Once the calcium in pore solution is consumed and incorporated into the gel, further dissolution of solid portlandite will compensate the calcium deficiency in pore solution, resulting in the increase of the pore solution alkalinity. This hypothesis was supported by other reported observations. Knudsen and Thaulow (1975) showed that the ASR gel that formed originally within or close to the aggregates has chemical composition of high alkali and low calcium content. The further the distance of the gel from the aggregate, the higher calcium content of the gel was detected. It is believed that the calcium was incorporated into the gel once the gel contacted with the cement pastes. Thomas (2001) reported similar observation by comparing the gel composition in aggregates and paste and suggested that alkali recycling could continue to fuel ASR and sustain ASR expansion for decades which was observed in many large concrete dams.

Besides the alkali recycling effect, a number of studies proposed that the presence of calcium influences the gelation process (Glasser and Kataoka, 1982; Gaboriaud et al., 1999) as well as the physical and chemical properties of the ASR gel (Bleszynski and

Thomas, 1998; Vayghan et al., 2016). However, the role of calcium in ASR expansion is not consistent according to the reported results.

Chatterji (1979) and Thomas (1998) showed that expansion and signs of ASR was absent in the mortar bars with $Ca(OH)_2$ removed either by leaching or carbonation. A series of studies (Alasali and Malhotra, 1991; Aquino et al., 2001; Chatterji et al., 1987; Kawamura et al., 1988) suggested that the efficacy of pozzolans in controlling the expansion of concrete caused by ASR is attributed to the consumption of $Ca(OH)_2$ by pozzolanic reaction, which reduces the source of calcium for ASR. It was therefore believed by many researchers that calcium is essential for ASR expansion and several mechanisms have been proposed as follows.

- It was proposed that the calcium could promote the gelation of silicate species in the solution (Gaboriaud et al., 1999). It was supported by the observations that the presence of calcium facilitated the dissolution of reactive silica forming C-S-H with a low Ca/Si ratio containing alkalis (Leemann et al., 2011), while in the absence of calcium, the reactive silica simply dissolved in the alkali hydroxide solution without forming any gel (Diamond, 1989; Leemann et al., 2011; Struble, 1987).
- It was proposed that the incorporation of calcium in the gel influences the viscosity and yield strength of the gel (Bleszynski and Thomas, 1998; Urhan, 1987). It was observed that high sodium gel could easily disperse into the surrounding pastes alleviating internal stress (Bleszynski and Thomas, 1998). Based on previous studies on the alkali silicate solutions, Urhan (1987) speculated that the presence of calcium may increase the viscosity of the alkali silicate gel and made a hypothesis that low viscosity alkali silicate gel could transfer to CSH progressively as the increase of the calcium and decrease of alkali in the composition of the reaction products, as shown in Fig. 2.2. As can be seen, gel with low calcium content may have a high swelling capacity but low viscosity. On the other hand, gel with calcium content as high as C-S-H is rigid and does not swell. The speculation indicates that the gel with moderate calcium content may have sufficient viscosity and swelling capacity to cause ASR expansion.

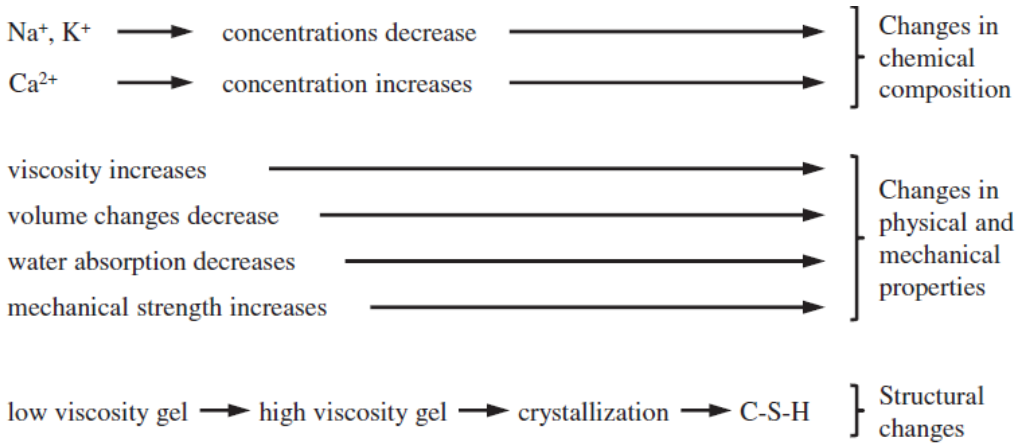

Fig. 2.2 Property changes of reaction products with variation of chemical composition (Urhan, 1987)

- Chatterji et al. (1986) proposed the higher calcium content reduced the dissolved silica diffusing out of the reaction sites and increased the penetration of alkali and hydroxyl ions into the reactive grains, thus promoting the expansion. But no direct evidence was provided.
- Wang and Gillott (1991) believed that the calcium-alkali-silicate gel was non-expansive. The effect of calcium hydroxide was probably due to it can maintain high pH in pore solution as well as exchange for alkali ions, which will be released for further production of ASR gel.

However, some researchers concluded the opposite, that calcium may decrease the expansion caused by ASR. Powers and Steinour (1955) speculated that calcium-alkali-silicate gel was non-expansive and the build-up of this non-expansive layer on the reactive silica controls the formation of swelling type alkali-silicate gel. If calcium is sufficient high, the reaction products are mainly non-swelling calcium-alkali-silicate, resulting in little ASR expansion. In a recent study (Vayghan et al., 2016) on composition-rheology relationship of ASR gel, the osmotic pressure of the synthetic ASR gel with varied compositions (Ca/Si and Na/Si ratio) was measured. The results showed that calcium exhibited no significant effect on the osmotic pressure of the gel with low Na/Si ratio and the osmotic pressure was reduced for the gel with high Na/Si ratio. Moreover, Struble and Diamond (1981) measured the free swelling capacity of the synthetic ASR gel. The results showed that the presence of

calcium does not significantly reduce the swelling pressure when compared with calcium-free gel.

2.2.4 Effect of aluminum on alkali-silica reaction

The role of aluminum in ASR in OPC concrete has been studied recently (Chappex and Scrivener, 2012a, 2012b, 2013; Leemann et al., 2015; Warner et al., 2012) and the results consistently showed that the presence of aluminum contributed to reducing the ASR expansions. It is known that the replacement of cement by SCMs (e.g., fly ash, metakaolin or silica fume) is effective to mitigate the ASR expansion. Additionally, researchers (Chappex and Scrivener, 2012a; Ramlochan et al., 2004; Warner et al., 2012) observed that the alumina-rich SCMs, such as fly ash, metakaolin, were more efficient than silica fume, which was rich only in silica. Warner (2012) showed that ASR expansion is further reduced by adding fly ash together with alumina than adding fly ash alone. Chappex and Scrivener (2012a) found that only 3.9 mmol/L aluminum in the pore solution was sufficient to significantly reduce the aggregate deterioration caused by ASR.

Generally, two mechanisms were proposed to explain the beneficial effects of aluminum on ASR expansions:

(1) aluminum was incorporated into C-S-H forming C-A-S-H, which has higher alkali binding capability, thus reducing the alkalinity of pore solution (Hong and Glasser, 2002).
(2) the presence of aluminum in pore solution can suppress the silica dissolution rate from aggregates by aluminum incorporation into the silica surface (Chappex and Scrivener, 2012b, 2013; Krivenko et al., 2014; Leemann et al., 2015).

It has been recognized that aluminum can substitute the bridging silicon tetrahedra in C-S-H forming C-A-S-H (Andersen et al., 2003; Stade and Müller, 1987; Sun et al., 2006). Hong and Glasser (2002) showed that incorporation of Al into C-S-H remarkably enhances the alkali binding capability of the binder especially when Ca/Si ratio is low (0.85 in the study). It is believed that the pH of the pore solution is reduced with the presence of aluminum, accounting for the lower ASR expansion.

However, Chappex and Scrivener (2012a) found that the alkali fixation capacity of the binder did not exhibit distinct difference as higher content of aluminum incorporated and the pore solution showed similar alkalinity correspondingly. It was explained that the aluminum incorporation increases alkali fixation capacity very slightly in real cementitious system with high Ca/Si (1.5 in the study). The following works by Chappex and Scrivener (2012b, 2013) suggested that the beneficial effect of aluminum on ASR is attributed to the incorporation of aluminum into the silica structure on the aggregate surface, resulting in a reduction of the silica dissolution rate, which was further supported by Leemann's work (Leemann et al., 2015) based on a model system simulating the real cementitious system with aluminum source. Krivenko et al. (2014) also reported that a dense zeolitic shell ($Na_2O \bullet Al_2O_3 \bullet mSiO_2 \bullet nH_2O$) was observed around the aggregate grains in the presence of active alumina, thus preventing the further reaction between the alkalis and aggregates.

2.2.5 Laboratory testing for evaluating ASR expansion in concrete

Numerous test methods have been developed and used to assess the potential for aggregates to produce ASR-induced damage and to evaluate the efficiency of preventive measures to control the ASR expansion. Field performance in concrete structure has been claimed as the best method of evaluating the susceptibility of an aggregate to ASR. However, due to the limited availability of structures and its limitation on parameter study influencing ASR damage (Thomas et al., 2006), laboratory tests are usually performed instead to predict the behavior of the materials under field conditions. Several standard laboratory test methods have been established to test the potential reactivity of aggregates or evaluate preventive measures, among which the Accelerated Mortar-Bar Test (ASTM C 1260) and Concrete Prism Test (ASTM C 1293) are the most commonly used two methods.

The Accelerated Mortar-Bar Test (AMBT) offers a relatively rapid test for evaluating the ASR expansion behavior of the mortar bars. The mortar bars with sample aggregates are prepared and stored in a strong alkaline solution (1 mol/L NaOH) at an elevated temperature (80 °C) for 16 days. According to the expansion at 16 days, aggregates can be classified into three categories: expansion less than 0.10% are

indicative of innocuous behavior; expansion more than 0.20% are indicative of potentially deleterious behavior; between 0.10% and 0.20%, aggregates may exhibit either innocuous or deleterious behavior in field performance.

Despite the wide use of the test, it is generally considered that the testing environment is overly severe as the aggregates showing good performance in the field and in concrete prism expansion tests were identified as reactive in the AMBT. Therefore, it is suggested that the test should only be used to accept and not reject aggregates. In addition, if an aggregate fails the test, the concrete prism test should be used to confirm the results before an aggregate is rejected (Thomas et al., 1997).

The Concrete Prism Test (CPT) involves the expansion measurement of concrete prisms made of Type I Portland cement with augmented alkali content of 1.25% by mass of cement. All prisms are stored in a sealed container over water at 38°C. Length measurements are taken routinely at 7, 28, and 56 days, and 3, 6, 9, and 12 months. Potentially deleterious behavior is indicated in the standard if the one-year expansion is greater than or equal to 0.04% and it is reasonable to conclude that the preventive measure is effective in controlling ASR expansion if the average expansion is less than 0.04% at two years. The comparison of the test regime of AMBT and CPT is shown in Table 2.2.

Table 2.2 The comparison of the test regime of AMBT and CPT

ASTM test	Specimen type	Specimen size	Test condition	Duration	Comment
C 1260 AMBT	Mortar	25×25×285 mm	Immersed in 1 M NaOH at 80 °C	16 d	Over severe; Used to accept not reject aggregates; fast evaluation
C 1293 CPT	Concrete (added NaOH)	75×75×285 mm	Stored over water at 38 °C	1, 2 y	Most reliable; Best correlation to field performance; long-term test.

The CPT is currently considered the most representative test method when compared to the filed performance of structures. The test has been continuously calibrated against field performance over years and no aggregates cause concrete deterioration after passing the test (Thomas et al., 1997). The main shortcomings of the CPT for

evaluating aggregates reactivity and preventive measures are the long duration of the test (1-2 year).

2.3 An overview of alkali-activated binders

The cement industry significantly contributes to global carbon dioxide (CO_2) emissions through the calcination of limestone and the combustion of fossil fuels during the cement production (Worrell et al., 2001). With the increased imperative to reduce the environmental impact of cement industry, the development of low-CO_2 alternative binders to ordinary Portland cement (OPC) has obtained enormous research interest at present. Alkali-activated binder is one of the promising alternatives when suitable raw materials and proper formulation are adopted (Provis, 2018). The hardened binder is produced by the reaction of an alkali activator and a solid aluminosilicate precursor. The precursor dissolves under alkaline conditions and the soluble components then rearrange through solution and condense to form a dense binding gel (Duxson et al., 2007; Glukhovsky et al., 1980).

A wide range of industrial by-products, natural raw materials and synthetic aluminosilicate sources could be used as alkali-activated precursors, like blast furnace slag, fly ash, metakaolin, kaolinitic clays and glass waste (Duxson and Provis, 2008). Depending on the composition of the precursors used, the alkali-activated binder could be classified into the following two main categories (Krivenko, 1997; Krivenko, 1994):

- **High-calcium system, $(Na,K)_2O$-CaO-Al_2O_3-SiO_2-H_2O**: It is produced by activation of calcium and silicon rich precursors such as blast furnace slag (SiO_2 + CaO > 70%) using relatively moderate alkaline solutions. The main reaction product is a C-S-H gel incorporating aluminum in its structure, usually accompanied by the formation of hydrotalcite and AFm type phases like strätlingite (Haha et al., 2011; Shi et al., 2011; Wang and Scrivener, 1995).
- **Low-calcium system, $(Na,K)_2O$-Al_2O_3-SiO_2-H_2O**: The precursor used primarily consist of aluminum and silicon such as metakaolin and fly ash with low CaO content. The reaction product is a three-dimensional alkali aluminosilicate hydrate (N-A-S-H) gel (Duxson, et al., 2007). The

terminology “geopolymer” is often used to describe this low-calcium alkali-activated binder (Davidovits, 1991).

The following covers the significant features and the chemistry of the alkali activation reactions in each of the systems.

2.3.1 Alkali-activation of high-calcium system

The development and investigation of the alkali-activated binder by using calcium-rich precursors such blast furnace slag have been conducted for over a century (Kuehl, 1908; Purdon, 1940; Shi et al., 2006). In the past decade, intensive research interest were in the understanding of the binder microstructure and the activation reactions with the aim to scientifically optimize the performance of the alkali-activated concrete, while achieving acceptable workability and reduced environmental footprint (Bernal et al., 2014; Provis and van Deventer, 2014).

Glukhovsky and Krivenko (Glukhowsky, 1967; Krivenko, 1994) proposed a general model to describe the mechanism that governs the alkali activation of the Ca-rich precursors and it was divided into three main stages: dissolution of the glassy precursor particles, coagulation of the disaggregated products, condensation and precipitation of the solid products.

The dissolution of the precursor takes place when hydroxyl ions attack the covalent Si-O-Si and Al-O-Si bonds the starting precursors and initiate the rupture of the bonds:

$$\equiv Si–O–Si\equiv + OH^- \Rightarrow \equiv Si(OH^-)–O–Si\equiv \Rightarrow \equiv Si–OH + {}^-O–Si\equiv$$

The alkaline metal cations in the solution neutralizes the resulting negative charge forming $\equiv Si\text{-}O^-\text{-}Na^+$ bonds. These alkaline silicates may also participate in ion exchange reactions with divalent ions to form ≡Si-O-Ca-OH type complexes. The hydroxyl groups attack the Si-O-Al bond in the same way, forming aluminate complexes in the alkaline solution, predominately $Al(OH)_4^-$.

The accumulation of silicate and aluminate species enhances contact among the disaggregated products, forming a coagulated structure where polycondensation

takes place forming new Si–O–Si and Si–O–Al bonds. The cluster formed by the polymerization of the aluminosilicate dimers and oligomers, generating colloidal particles and the presence of particles in the initial solid phase prompts the precipitation of binder materials.

Burciaga et al. (2013) have illustrated the alkali-activation of slag by starting with hydrolysis and dissolution of blast furnace slag under alkaline condition. It involves the breaking of slag bonds (Ca-O, Mg-O and Al-O-Al) and covalent bonds (Si-O-Si and Al-O-Si) on the glassy slag surfaces under alkaline condition. Next, ionic species such as Ca^{2+}, Al^{3+}, Mg^{2+}, $Si(OH)_4$ and $Al(OH)_4^-$ will be released from depolymerized glass network of slag and dissolved into pore solution, and then followed by the establishment of Si-Al layer with tetrahedrally coordinated with oxygen on the slag surface. Once the dissolved ions have reached their solubility limit, coagulation and precipitation will take place, and then leads to the development of hydration products with Si-Al layer on the slag surface (Glukhovsky et al., 1980; Krizan and Zivanovic, 2002; Li et al., 2010; Puertas et al., 2004). However, blast furnace slag also contains minority crystalline phase such as gehlenite ($2CaO.Al_2O_3.SiO_2$), akermanite ($2CaO.MgO.2SiO_2$) and merwinite which are inert to the alkali activation process.

C-A-S-H gel is generally recognized as the main hydration product of alkali-activated blast furnace slag. In Fig. 2.3b, C-A-S-H structure is illustrated by chains of tetrahedrally coordinated silicate ions (SiO_4^-) with dreierketten structure which linked alternately with an intralayer of Ca-O double sheet. Similar structure is also found in the C-S-H formed within OPC based on Fig. 2.3a. However, the main difference is the involvement of aluminum into C-A-S-H gel to substitute the silicon from the bridging sites (Fernández-Jiménez et al., 2003; Puertas et al., 2011). This replacement mechanism has been supported by sharp peak of $Q^2(1Al)$ and tetrahedral aluminum under the ^{29}Si and ^{27}Al magic-angle spinning nuclear magnetic resonance (MAS-NMR) spectra (Wang and Scrivener, 2003). Moreover, C-A-S-H in alkali-activated slag has lower Ca/Si ratio as compared to C-S-H in OPC (Garcia-Lodeiro et al., 2015).

Secondary reaction products are also formed accompanied with the formation of C-A-S-H gel, such as AFm type phases (like strätlingite), hydrotalcite, and zeolite (like gismondine and garronite) (Haha et al., 2011; Shi et al., 2011; Wang and Scrivener,

1995). Hydrotalcite has been identified in alkali-activated blast furnace slag with relatively high contents of MgO. It is commonly detected in alkali-activated slag activated by NaOH or water glass (Haha et al., 2011). Hydrotalcite consists of a layer of brucite with interlayering of water molecules and balancing anions such as CO_3^{2-}, and closely mixed with C-A-S-H within alkali-activated slag binder (Chen and Brouwers, 2007). AFm type phases such as tetra-calcium aluminate hydrate (C_4AH_{13}) or stratlingite (C_2ASH_8) might also be formed in alkali-activated slag binder and the formation of AFm phases are greatly dependent on the composition of slag especially calcium, aluminum and magnesium content (Chen and Brouwers, 2007). Usually no calcium hydroxide was identified in the binder activated by alkali silicate or hydroxide (Shi et al., 2011; Shi et al., 2015).

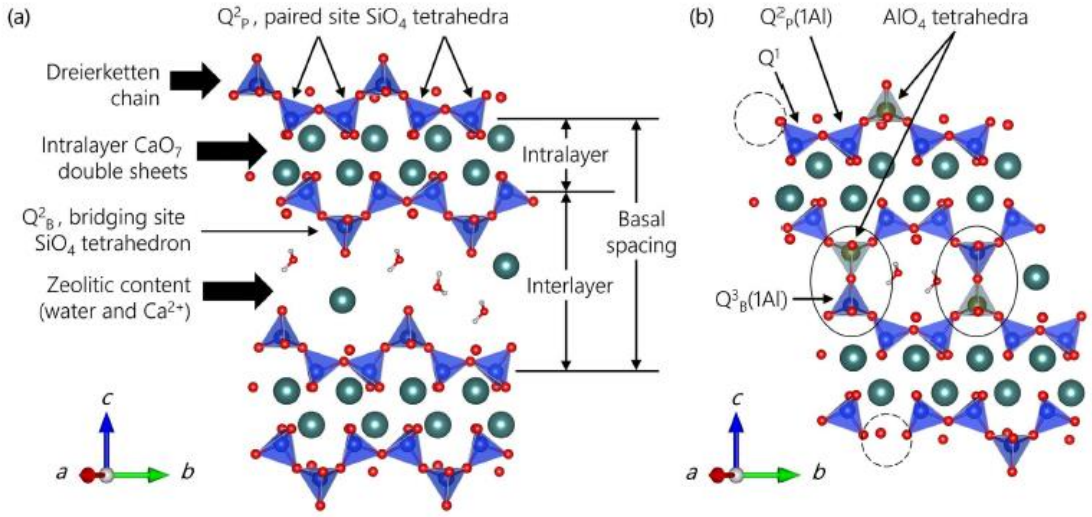

Fig. 2.3 Schematics diagram of main hydration product of OPC and AAS (Geng et al., 2017). (a): Crystalline C-S-H formed in OPC. (b): Amorphous C-A-S-H with cross-linked by Al (solid circles) formed in AAS. Si, Al, Ca, O and H atoms have been indicated by blue, grey, green, red and white color respectively.

2.3.2 Alkali-activation of low-calcium (geopolymer) system

The alkali-activation of low-calcium aluminosilicate precursors such as low-Ca fly ash or metakaolin forms an amorphous three-dimensional aluminosilicate products, which is also known as geopolymers. It has been shown to be an efficient alternative

to ordinary Portland cement in a range of applications, exhibiting high mechanical strength, good fire and acid resistance (Davidovits, 1994).

Fig. 2.4 presents a simplified reaction mechanism for geopolymerization process (Duxson et al., 2007). The solid aluminosilicate source dissolved by alkaline hydrolysis producing aluminate and silicate species into solution. As a result, a complex mixture of silicate, aluminate and aluminosilicate species is formed in the system to reach equilibrium. The continuing dissolution of amorphous aluminosilicate results in a supersaturated solution, within which the aqueous phases start networking by condensation and form a gel. As the connectivity of the gel network increases, the continuing reorganization in the system results in the formation of the three-dimensional aluminosilicate networks, which is what we named the geopolymers. It should be noted that these processes are largely coupled and occur simultaneously, even though they are successively presented in Fig. 2.4.

The geopolymerization process is summarized as two successive and controlling stages (Duxson et al., 2007):

- Nucleation: It includes the dissolution of aluminosilicate materials and the formation of polymeric species, highly depending on thermodynamic and kinetic parameters.
- Growth: In this stage, nuclei reach a critical size and crystals begin to develop, determining the microstructures and pore distribution of the material, which are the critical factors dominating physical properties.

The structure of the reaction product of a sodium-based geopolymer is shown in Fig. 2.5. The reaction products is a three-dimensional aluminosilicate gel formed by connection of tetrahedrally coordinated Si^{4+} and Al^{3+} cations bridged by oxygen (Provis et al., 2005). The negative charge of AlO_4^- group is balanced by alkali cations, typically Na^+ and/or K^+. Some hydroxyl groups are presented at the surface of the gel although it is insignificant in the context of the structure of the material.

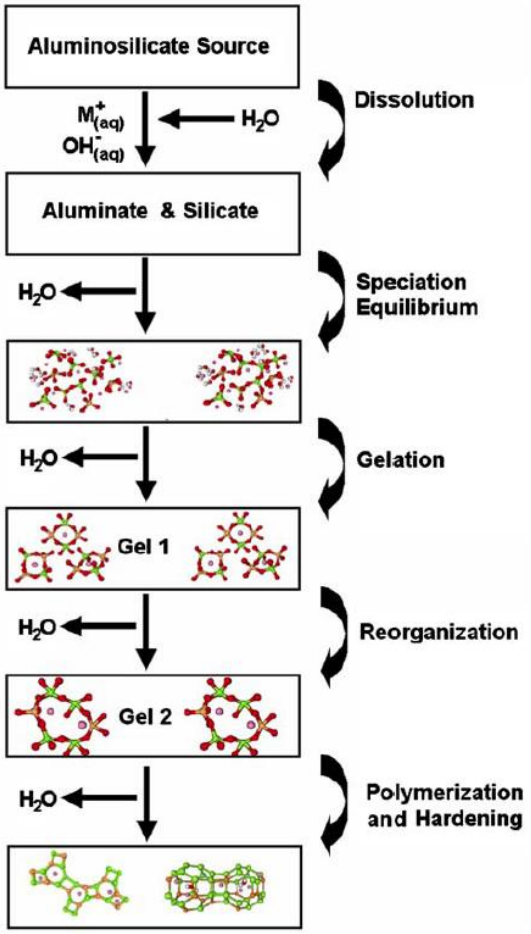

Fig. 2.4 Conception model for geopolymerization (Duxson et al, 2007)

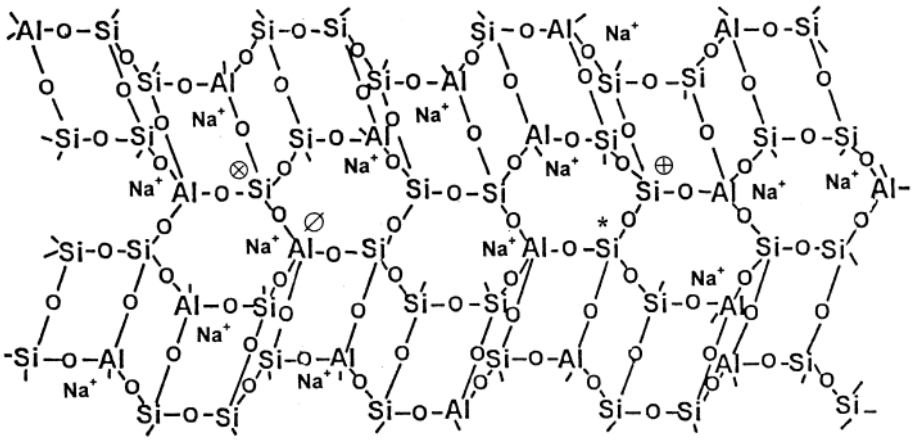

Fig. 2.5 Conceptual model of three-dimensional framework structure of a sodium geopolymer (Barbosa et al., 2000)

2.3.3 Alkali-activated binder produced by natural mineral resources

Over the past two decades, tremendous development has been made on the alkali-activated binders using traditional precursors, such as the industry by-products like blast furnace slag or coal fly ash, and the synthetic precursors like metakaolin (Duxson et al., 2007; Provis and van Deventer, 2014; Shi et al., 2019). With the aim to expand the alkali activation technology to utilize more industrial wastes and also search for more alternatives with ecological benefits, low costs and prime material availability, more types of wastes as well as natural resources have been studied as the potential alkali-activated precursors as shown in Fig. 2.6 (Payá et al., 2019; van Deventer et al., 2007).

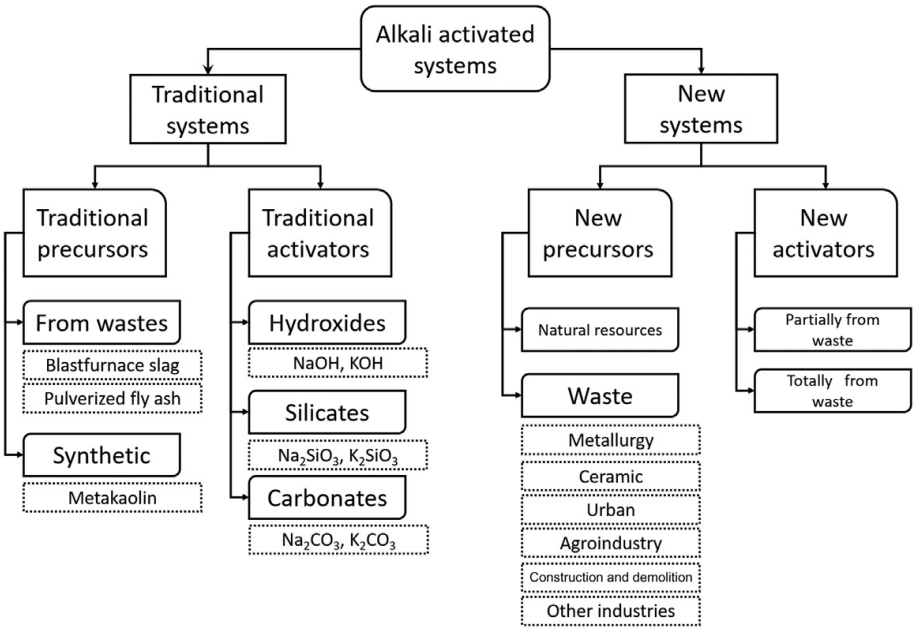

Fig. 2.6 Traditional and new alkali-activated precursors and activators (Payá et al., 2019)

Natural mineral resources includes non-kaolinite clay and feldspars are of interest to researchers in producing alkali-activation binders recently. Buchwald et al. (2009) showed that illite/smecite clays can be used for alkali activation after thermal treatment and the calcination temperature should be carefully selected to ensure the full dehydroxylation of the clay minerals and prevent the formation of new stable phases. Ruiz-Santaquiteria et al. (2013) showed that the reactive SiO_2/Al_2O_3 ratio in the dehydroxylated clays has large impacts on the compressive strength of the produced AAM. Valentini et al. (2018) produced alkali-activated binder by using the

local thermal-treated smectite clay with moderate addition of waste calcium carbonates and the binder exhibited appealing mechanical property without high temperature curing. Dietel et al. (2017) concluded that specific surface area and the amount of soluble Si and Al are the key factors determining the strength of the alkali-activated binder by using local illitic clays.

Feldspars are the most widespread mineral group accounting for around 40% of the Earth's crust and contain silica and alumina, which are an appealing natural sources for the alkali-activated precursors. Feng et al. (2012) synthesized geopolymer precursors by thermal activation of albite feldspars with sodium hydroxide and sodium carbonate. The crystalline albite structure broke down and an amorphous geopolymer precursor was formed with the addition of alkali source and thermal treatment at 1000℃. The geopolymer binder with acceptable compressive strength was formed just by mixing water with the synthesized precursors.

2.4 Alkali-silica reaction in geopolymer concrete

Several studies have been conducted on the ASR behavior of geopolymer concrete in the presence of reactive aggregates (García-Lodeiro et al., 2007; Kupwade and Allouche, 2012; Pouhet and Cyr, 2015; Williamson and Juenger, 2016) and it was generally suggested that geopolymer concrete has higher resistance to ASR compared with conventional OPC concrete.

García-Lodeiro et al (2007) found that the ASR-induced expansion in fly ash geopolymer concrete was much smaller than that of OPC concrete based on the accelerated mortar bar test and the expansion of geopolymer was below the limit (0.1%) prescribed in the standard. Typical ASR map cracking could be observed on the OPC specimens, while the geopolymer mortar exhibited no surface cracking. It was found that substantial amount of zeolitic phases were formed in fly ash geopolymer and little volumes of expansive ASR gel was also observed. It was explained that the lack of calcium in the geopolymer system limited the formation of ASR products and the tiny amount of ASR gel formed was non-expansive also due to the low calcium content of the gel.

Kupwade and Allouche (2012a) conducted a similar study but with different types of fly ash. It was shown that ASR reaction product was observed in the geopolymer speciman made with Class C fly ash, while the sample made with Class F fly ash exhibited no indication of ASR gel formation. But all the geopolymer specimens had only small expansions below the expansion threshold.

Pouhet and Cyr (2015a) also found that the incorporation of reactive silica with particle size between 0.16 and 2 mm did not lead to the ASR expansion in metakaolin-based geopolymer even though a small amount of ASR gel was found on the surface of the reactive aggregates. The pH value of the geopolymer pore solution was measured and found a high pH of 14 in the initial pore solution but with a rapid reduction in the following 180 days. The pH of the pore solution was less than 12 at only 14 days and the fast reduction was suggested to be attributed to the carbonation of the pore solution. One hypothesis was therefore proposed that the rapid reduction of the pore solution alkalinity did not allow the hydroxyls to break the silica network within aggregates, thus reducing the formation of ASR gel. The deficiency of calcium in the system was another possible reason proposed by the authors.

The recent work by William and Juenger (2016) studied the influence of activating solution concentration on the ASR behavior of fly ash geopolymer. The results showed that the geopolymer concrete has little expansion although the alkali ion concentration of pore solution within the sample at 7 days was found 3-4 times higher than the previously suggested expansion thresholds in OPC concrete. It was therefore believed that sufficient alkalis existed in the geopolymer pore solution to attack the reactive silica. The deficiency of calcium in geopolymer is suggested as the most likely reason for the low expansion observed for geopolymer concrete.

In summary, it is generally suggested that the geopolymer concrete is less vulnerable than OPC concrete based on the results reported in limited studies. However, the underlying mechanism is still unclear even though several hypotheses have been proposed. Further studies are required to further understand the fundamental mechanisms of the resistance of geopolymer concrete to alkali-silica reaction.

Chapter 3 Pore Solution Chemistry and Alkali-silica Reaction Resistance of Low-Calcium Fly Ash Geopolymer

3.1 Overview

The previous literature generally reported that the geopolymer concrete is less vulnerable to alkali-silica reaction than conventional ordinary Portland cement concrete. However, the lack of understanding on the pore solution chemistry of the geopolymer binders limits the investigation on the underlying mechanisms for low ASR-induced expansion of these binders. The study displayed in this chapter aims to systematically investigate the composition and alkalinity of the pore solution in a low-calcium fly ash-based geopolymer, providing information for the analysis on the ASR behavior of the geopolymer concrete.

3.2 Materials and methods

3.2.1 Materials

The class F fly ash with compositions shown in Table 3.1 was used for geopolymer synthesis. Silica and alumina constitute 58.6% and 30.4% by mass, respectively, of the fly ash, giving a SiO_2/Al_2O_3 molar ratio of 1.9. Activating solution of sodium hydroxide with concentration of 10 mol/L was prepared by dissolving analytical reagent (AR) grade NaOH pellets (purity $\geq$ 96%) into deionized water. After full dissolution, the solution was cooled down for 24 h to room temperature before mixing with fly ash to synthesis geopolymer. Type I Portland cement with Na_2O_{eq} of 0.66% (Table 3.1) was used for the OPC specimens. The alkali-silica reactive aggregates used in this work are the local sedimentary rocks extracted from Jurong Rock Caverns, Singapore. The main crystal phases of the rocks are quartz and albite (Lahoti et al., 2017).

Table 3.1 Chemical compositions of the raw materials (% by mass)

	SiO_2	Al_2O_3	Fe_2O_3	CaO	MgO	K_2O	Na_2O	P_2O_5	SO_3	TiO_2
Cement	17.6	3.2	3.1	62.5	3.6	0.4	0.4	0.1	3.6	0.6
Fly ash	58.6	30.4	4.7	1.2	0.8	1.5	-	0.5	0.1	2.0
Reactive aggregates	63.7	13.3	3.8	2.2	0.5	4.1	3.5	0.1	2.1	0.4

3.2.2 Methods

3.2.2.1 Concrete prism test (CPT)

The OPC concrete prisms with dimension of 75 mm × 75 mm × 285 mm and a water-to-cement ratio of 0.45 were prepared in accordance with ASTM C1293. The alkali content of the OPC was increased to 1.25% Na_2O_{eq} by adding NaOH pellets into the mixing water. The fly ash geopolymer concrete prisms were prepared in the same procedure with the only exception that fly ash was substituted for cement and 10 mol/L NaOH activating solution was substituted for mixing water. While silicates are usually contained in alkaline activators to control the composition of fly ash geopolymer, only NaOH solution is used as the activator in the present work for simplicity. The local ASR reactive aggregates with grading shown in Fig.3.1 were used in both the OPC and the geopolymer concrete prisms with an aggregate-to-binder ratio of 2.3, by mass.

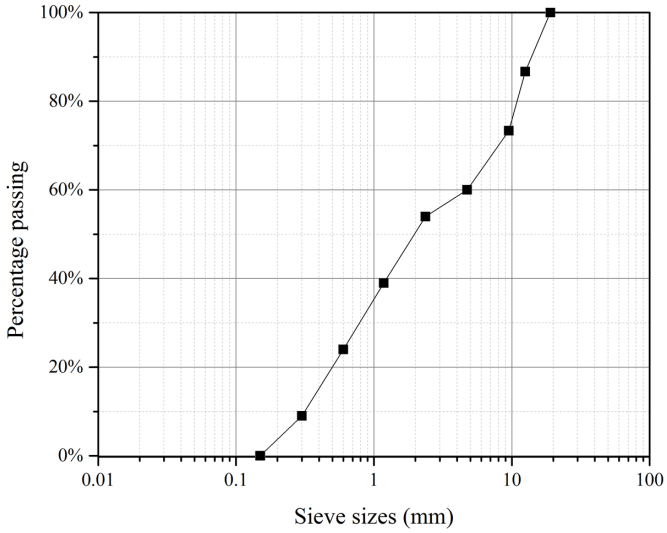

Fig. 3.1 Grading curve of the reactive aggregates

After casting, the OPC concrete prisms were cured at 23 °C for 24 h and the fly ash geopolymer concrete prisms were cured at 80 °C for the same duration (*i.e.,* 24 h), which is commonly applied for fly ash-based geopolymer to facilitate the polymerization in the early age due to the relatively low reactivity of fly ash. All the specimens were cured in an environmental chamber with 98% RH to prevent moisture loss. After curing for 24 h, the prisms were de-molded and stored over water in a sealed container with absorbent material covering the sides. The containers are 19 L polyethylene buckets with diameter of 310 mm and height of 370 mm. The buckets were covered with airtight lids to prevent the loss of enclosed moisture due to evaporation. A perforated rack was placed in the bottom of the container so that the concrete prisms were 30 mm above the bottom and the container was filled with water to a depth of 20 mm above the bottom. The absorbent material made of polypropylene geotextile was placed around the inside wall of the container from the top into the water at the bottom. The bucket was then placed in an oven at 38°C. The lengths of the specimens were measured routinely for 12 months and the average expansion readings of three prisms for each type of specimen together with its standard deviation were reported.

Optical and electron microscopic analyses were carried out on the samples taken from the prism specimens immediately after the 12-month test. Concrete blocks with dimension of 25 × 25 × 10 mm was cut and removed from the concrete prisms. One of the concrete block surfaces was glued to an object glass. The concrete block was then cut approximately 1 mm above the object glass and the concrete slice bonded to the object glass was ground down to a thickness of 100 μm. Then it was polished using a polishing wheel rotating at 100 rpm with 1 μm diamond paste applied to a silk polishing cloth that was fixed to the rotating wheel. The thickness of the concrete slice was polished to around 20 μm to make the slice translucent. Then the resulted sample was examined in a polarized light microscope (Olympus BX51). After that, secondary electron (SE) imaging and energy-dispersive X-ray spectroscopy (EDX) analysis were carried out on the same sample by using a field emission scanning electron microscope (FESEM, JEOL JSM-7600F). The specimens were freeze-dried under vacuum for 72 h and coated with a platinum layer to prevent charging before the SEM/EDX analysis.

3.2.2.2 Pore solution chemistry of fly ash geopolymer

Geopolymer and OPC paste specimens with a diameter of 45 mm and a height of 85 mm were prepared for the pore solution extraction. The paste has the same mix design as the concrete used in the CPT, except that aggregates were omitted in preparing the paste sample. The paste specimens were then stored in the same condition as specified in the CPT. The pore solution of the pastes at different ages was extracted following the method described by Barneyback and Diamond (1981) by using a high-pressure extraction setup which is similar to that described by Cyr et al. (2008). An additional air circulation system was equipped to the setup to drive the extracted solution into the collection bottle and the CO_2 in the circulating air was removed by aerating it through 1 mol/L NaOH solution in order to minimize carbonation of pore solution during the extraction process. The extraction was carried out on a 3000 kN servo-hydraulic compression testing machine (MTS YAW-3000L) with a loading rate of 1.2 kN/s and loaded up to 1200 kN.

Immediately after the extraction, the pore solution was filtered by using a syringe filter with pore sizes of 0.45 μm to remove particles in the solution. After that, the pH of the solution was measured using a standard pH meter (Mettler Toledo SevenCompact) and the ion concentrations of Na, K, Si, Al and Ca in the solution diluted into 100 times were measured by using an inductively coupled plasma-optical emission spectrometer (ICP-OES, PerkinElmer Optima 8000).

In addition, the solution was analyzed by Fourier transform infrared spectroscopy (FTIR, PerkinElmer Spectrum) and solution-state nuclear magnetic resonance (NMR, Bruker Avance 400 MHz). FTIR spectra were obtained from 4000 to 400 cm^{-1} in attenuated total reflectance (ATR) mode. ^{29}Si NMR spectra were obtained at 79.49 MHz by using 90° pulses of 14.5 μs and 5-s recycle delays with number of scans of 256. ^{27}Al spectra were obtained at 104.26 MHz by using 90° pulses of 10 μs and 1-s recycle delays with number of scans of 64. All the spectra were obtained under the same condition at ambient temperature on 400 μL of pore solution sample with 10% of $^{2}H_2O$ for NMR locking. Chemical shifts of ^{29}Si and ^{27}Al were reported in parts per million referenced to tetraethoxysilane and $AlCl_3$ solution, respectively.

3.3 Results and discussion

3.3.1 Concrete prism test

Expansion results of the OPC and fly ash geopolymer concrete prisms are shown in Fig. 3.2. The dash line in the figure represents the acceptable expansion limit of 0.04% at one year as prescribed in ASTM C1293. As can be seen, the OPC concrete prisms showed a rapid expansion within the first two months and continued expanding afterwards with a lower expansion rate. The average expansion of OPC prisms exceeded the one-year expansion limit in 9 months, reaching 0.06% in one year. While the fly ash geopolymer prisms showed almost no signs of expansion (0.006%) after 12 months, it suggested the higher resistance of fly ash geopolymer concrete to ASR, which is consistent with published literature (García-Lodeiro et al., 2007; Kupwade‐Patil and Allouche, 2012; Williamson and Juenger, 2016).

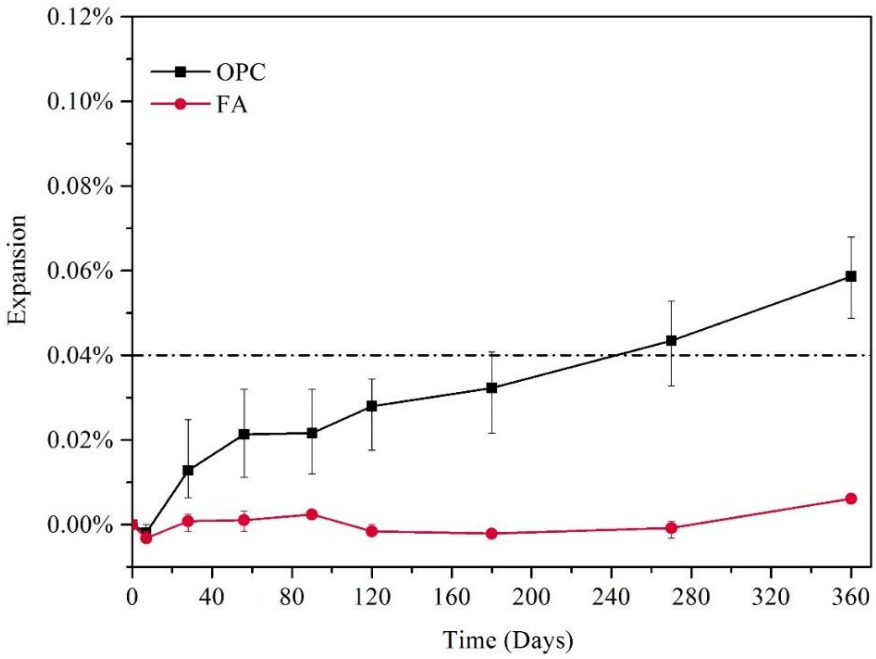

Fig. 3.2 Expansion results of OPC and fly ash geopolymer concrete prisms in CPT.

In general, numerous microcracks were observed along the aggregate-matrix interfaces and extended through aggregates in the OPC concrete prism specimens after 1-year CPT. Fig. 3.3(a) shows the typical polarized light microscopic images of the OPC concrete prism specimens after 1-year CPT. As can be seen, a layer of gel-like phase with thickness around 10 μm was observed at the interface between an

aggregate and surrounding OPC paste matrix, and a microcrack (about 10 μm) filled with gel extending from the interface and cut through several aggregates. The SE image on the same location (Fig. 3.3b) showed the morphology of the gel-like phase and the average chemical composition determined by EDX confirmed it is a typical ASR product with $(Na_2O+K_2O)/SiO_2$ molar ratio of 0.15 and $(CaO+MgO)/SiO_2$ molar ratio of 0.33 (Hou et al., 2005).

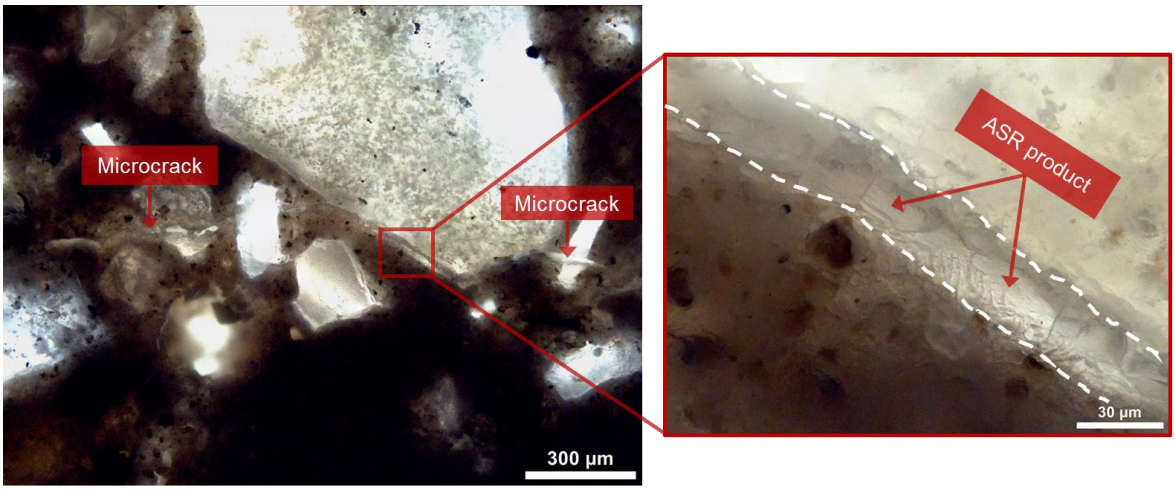

(a)

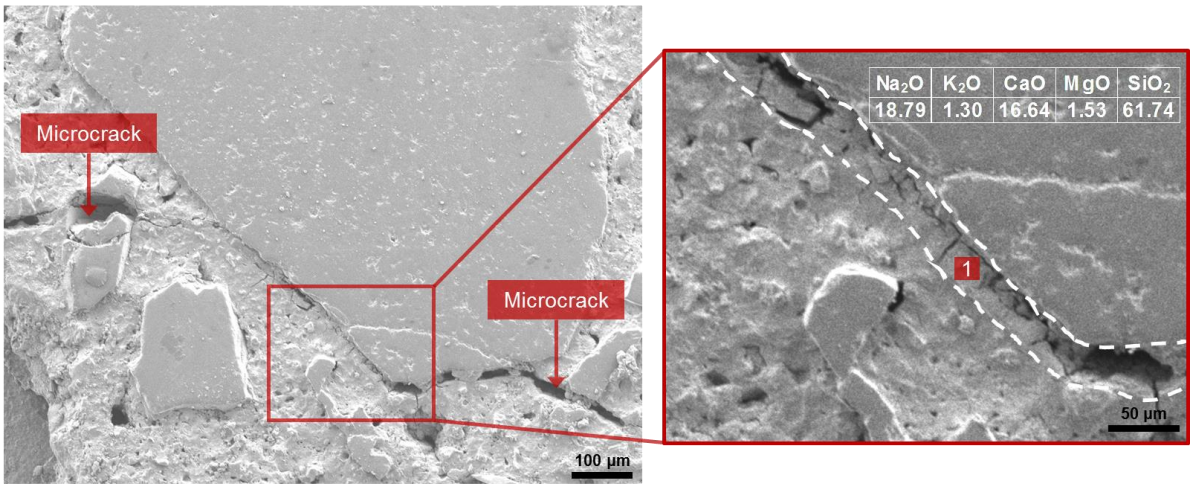

(b)

Fig. 3.3 (a) Typical polarized light microscopic image of the microcracks and ASR products formed in the OPC concrete prism specimens after 1-year CPT. (b) SE image on the same location with chemical composition (wt. %) of ASR product (site 1) detected by SEM/EDX.

Fig. 3.4 illustrates the typical SE image of aggregate-matrix interface of the fly ash geopolymer concrete prism specimens after 1-year CPT. Generally, no typical morphology of ASR product was observed in geopolymer concrete prism specimens and good bonding between the reactive aggregates and the surrounding geopolymer paste matrix was observed without additional phases at the interface. Few tiny microcracks (less than 1 μm) were observed in the geopolymer matrix, which were most likely introduced due to sample preparation.

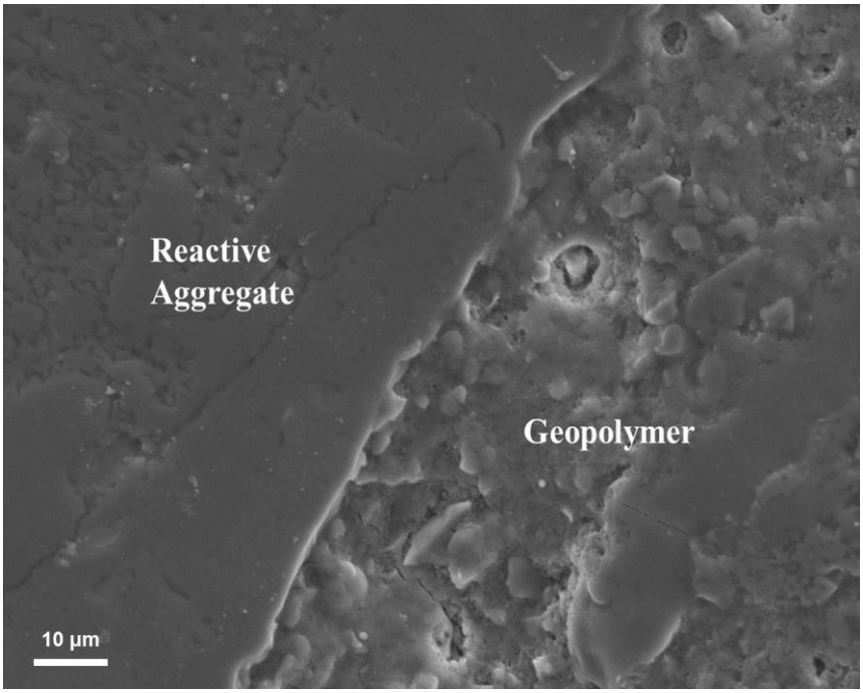

Fig. 3.4 Typical SE image of aggregate-matrix interface of the fly ash geopolymer concrete prism specimens after 1-year CPT.

3.3.2 Pore solution chemistry of fly ash geopolymer

The pore solution of the fly ash geopolymer paste samples with the same mix design as the fly ash geopolymer concrete prisms and stored in the same condition as specified in the CPT was extracted and analyzed. The concentrations of major ions (Na, K, Si, Al, Ca) and the pH value of the pore solution in the fly ash geopolymer paste at different ages were plotted in Fig. 3.5. The pore solution results of fresh paste were also obtained from the extraction of the fluid paste immediately after mixing, indicated as hollow markers in Fig. 3.5. For comparison, the pH level of the pore solution in the OPC pastes was also reported in Fig. 3.5(d). It has been reported that

the pore solution of OPC pastes reached an equilibrium state at age of one month and the further change of the pH is negligible (Diamond, 1989). Thus, the pH of the OPC pore solution was measured only up to age of 28 d and it is assumed that the pH would remain stable afterwards.

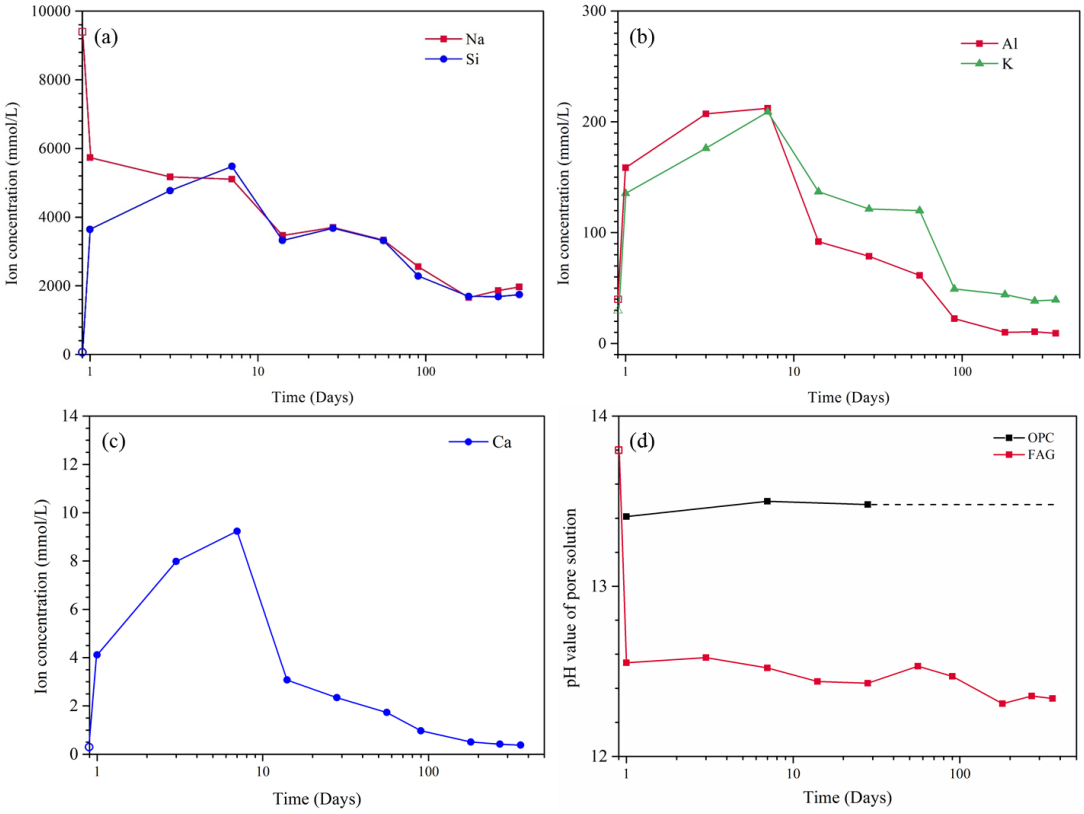

Fig. 3.5 The concentrations of (a) Na, Si, (b) Al, K and (c) Ca in the fly ash geopolymer pore solution as a function of time. (d) The pH of the geopolymer and OPC pore solution as a function of time. Hollow markers are the results of the fresh paste.

As can be seen in Fig. 3.5(a), the sodium concentration with a high initial value of 9.4 mol/L immediately after the mixing reduced rapidly within the first day, continued to reduce gradually in the following 6 months and stabilized afterwards at around 1.6-2.0 mol/L. The reduction of sodium content was most likely due to the participation of sodium into the geopolymer frameworks and parts of them were involved to balance the negative charge on the tetrahedral aluminum (Duxson et al., 2005). Unlike sodium ions that were mainly from activating solutions, the other ions (K, Si, Al, Ca) in the pore solution were released from the dissolution of the fly ash.

Their concentrations kept increasing initially, indicating that the dissolution of fly ash was dominant in the first 7 days to provide soluble silicate and aluminate species into the solution. Then the dissolution rate gradually reduced with time and the condensation was dominant to form geopolymer gel reducing the soluble species. The concentrations of the ion species (Na, K, Si, Al, Ca) in the pore solution maintained stable after 6 months, indicating the completion of the polymerization process and the pore solution was at equilibrium with the geopolymer binders.

The pH value of the pore solution is shown in Fig. 3.5(d). As can be seen, the pH level of the OPC pore solution increased slightly in the first seven days due to the cement hydration and stabilized at 13.5. In comparison, the pH value of the geopolymer pore solution reduced significantly from 13.8 to 12.6 in only one day and stabilized afterwards. This remarkable reduction in the first day is mainly due to the rapid dissolution of fly ash in the activating solution with high alkalinity and accelerated in the curing condition at 80°C. The hydroxide ions in the activating solution were largely consumed in the dissolution process to rapture the Si-O-Si and Si-O-Al bonds in the fly ash (Buchwald et al., 2011).

Fig. 3.6 shows the infrared spectrum between 2000 and 800 cm^{-1} for pore solution extracted from geopolymer paste specimens at ages between 1 day and 1 year. Significant bands at 1637 cm^{-1} are associated with the bending vibration of H-O-H in water molecules (Bernal et al., 2010). Major bands at 993-1003 cm^{-1} are corresponding to the asymmetric stretching vibration of Si-O-T bonds, where T is tetrahedral silicon or aluminum (Bernal et al., 2010), indicating the presence of silicon or aluminum tetrahedra in connected units. The shoulder at 1100 cm^{-1} is assigned to the asymmetric stretch of Si-O-Si bonds in a relatively pure silicate phase without incorporation of aluminum tetrahedra (Bakharev, 2005). A slight band shift is observed from 993 cm^{-1} gradually to 1003 cm^{-1} with the increase of the sample age, most probably due to the reduced amount of aluminum, leading the peak shift to higher wavenumbers (Bakharev, 2005).

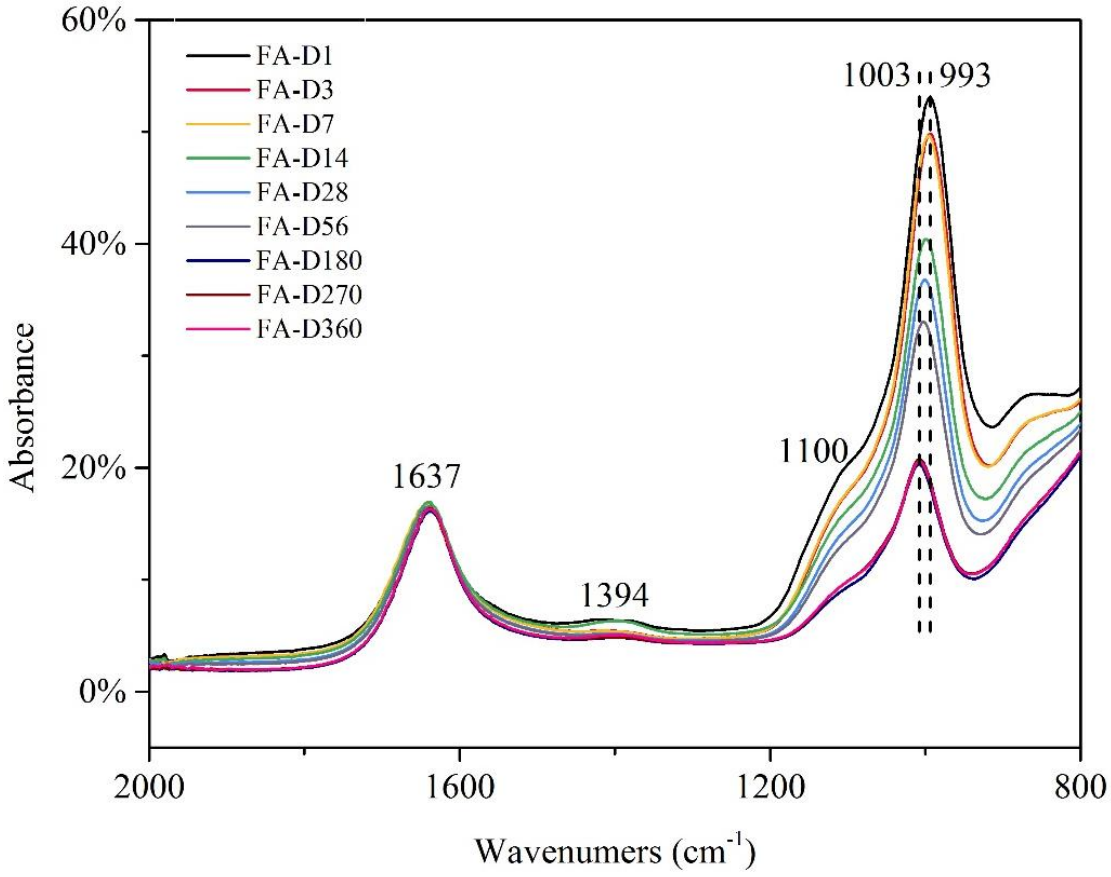

Fig. 3.6 FTIR spectra (800-2000 cm^{-1}) of the geopolymer pore solutions at ages between 1 day and 1 year.

The vibration band at 1394 cm^{-1} is associated with the stretching vibration of O-C-O bonds in the carbonate group (Bernal et al., 2010). Very weak vibration is observed at 1394 cm^{-1} only for the pore solution at 1 and 14 d and no obvious peak is present for the pore solution at other ages. It suggests that the carbonation on the geopolymer pore solution in the presented curing condition was very limited and the slight carbonation on the 1 d and 14 d pore solutions most probably occurred during the extraction process.

Further information on the short-range order of the aluminum and silicon in the pore solution is given by the solution-state NMR spectroscopy. The ^{27}Al NMR spectra of the geopolymer pore solutions at ages between 1 day and 1 year are shown in Fig. 3.7. As can be seen, all spectra reveal a broad and asymmetrical band with a range of 45-80 ppm, indicating all the aluminum were tetrahedrally coordinated in the solutions (Martineau et al., 2016). The line-broadening of ^{27}Al NMR spectra is always

observed due to the second-order quadrupolar line shifts (Lippmaa et al., 2005). The asymmetrical band indicates it consists of signals at least from two environments. Thus, a deconvolution of the ^{27}Al NMR spectra was conducted based on the peak assignments of the q^n site aluminum in the previous NMR studies on alkali aluminosilicate solutions (Azizi and Ehsani-Tilami, 2009; Samadi-Maybodi et al., 2001), where q refers to tetrahedrally coordinated aluminum and the superscripts indicate the number of bridges to silicon. The spectra were fitted by Gaussian-Lorentzian Sum function with about 50% Gaussian shape. Peak positions and widths for each identified species were maintained constant throughout the deconvolution process.

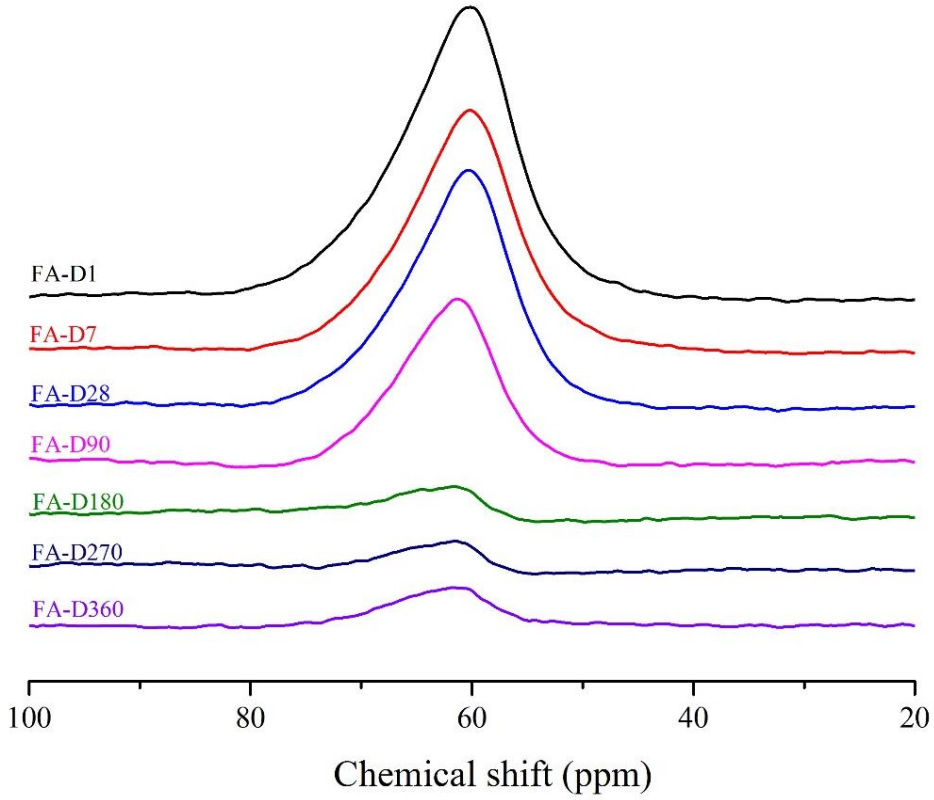

Fig. 3.7 ^{27}Al NMR spectra of the geopolymer pore solutions at ages between 1 day and 1 year.

The deconvolution results of the pore solution at day 1 is shown in Fig. 3.8 and a summary of the deconvolution results are presented in Table 3.2. It shows that all the spectra consist of three bands, *i.e.*, q^4, q^3 and q^2, indicating the aluminum tetrahedra are bonded with silicones and are present in aluminosilicate oligomers. The

monomeric $Al(OH)_4^-$ (q^0) is reported as the predominant aluminate species in the dissolution process. However, no signal of q^0 was detected at chemical shift of 80 ppm (Engelhardt et al., 1983) in pore solution at all ages, suggesting the monomeric $Al(OH)_4^-$ was incorporated into aluminosilicate oligomers after dissolution within 1 day. It has been reported that $Al(OH)_4^-$ monomers are more readily to combine with long-chain silicate oligomers rather than silicate monomers (Glasser and Harvey, 1984), which agrees with the observations here that q^1 sites were absent and q^4 sites were the majority in the solution at early ages followed by q^3 sites (Table 3.2). The variation of the amount of the q^4 sites Al (Fig. 3.9) agrees well with the variation of the silicon and aluminum concentration in the pore solutions discussed earlier (Fig. 3.5), both of which are governed by the kinetics of the dissolution-condensation in the geopolymerization process. The amount of the q^4 sites Al slightly increased from day 1 to day 7 due to the aluminum liberated from the dissolved fly ash incorporated into the silicate oligomers. After that, the condensation of the aluminosilicates dominated, leading to the reduction of the q^4 sites. An equilibrium state was reached within the pore solution after 6 months.

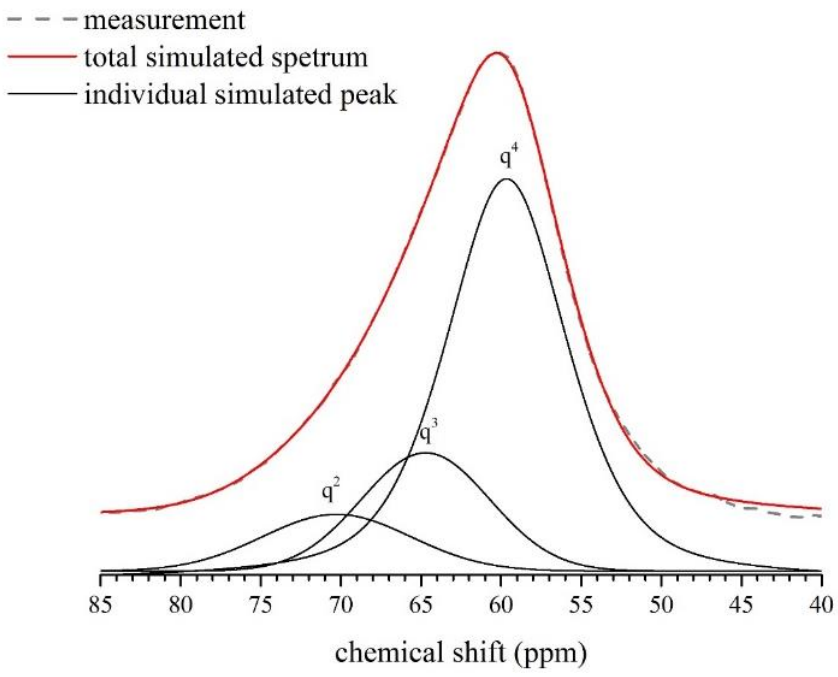

Fig. 3.8 Deconvolution of the ^{27}Al NMR spectra of the pore solution with age of 1 day.

Table 3.2 ^{27}Al NMR chemical shifts and relative integrated intensities of q^n site Al from deconvolution of the ^{27}Al NMR spectra for pore solution

Samples	Relative integrated peak intensities, %		
	q^4 (59.7 ppm)	q^3 (64.7 ppm)	q^2 (70.3 ppm)
D1	72.0	18.0	10.0
D7	78.5	16.9	4.6
D28	70.4	22.9	6.7
D90	68.5	22.8	8.7
D180	45.6	43.6	10.8
D270	45.0	46.0	9.0
D360	46.2	41.9	11.9

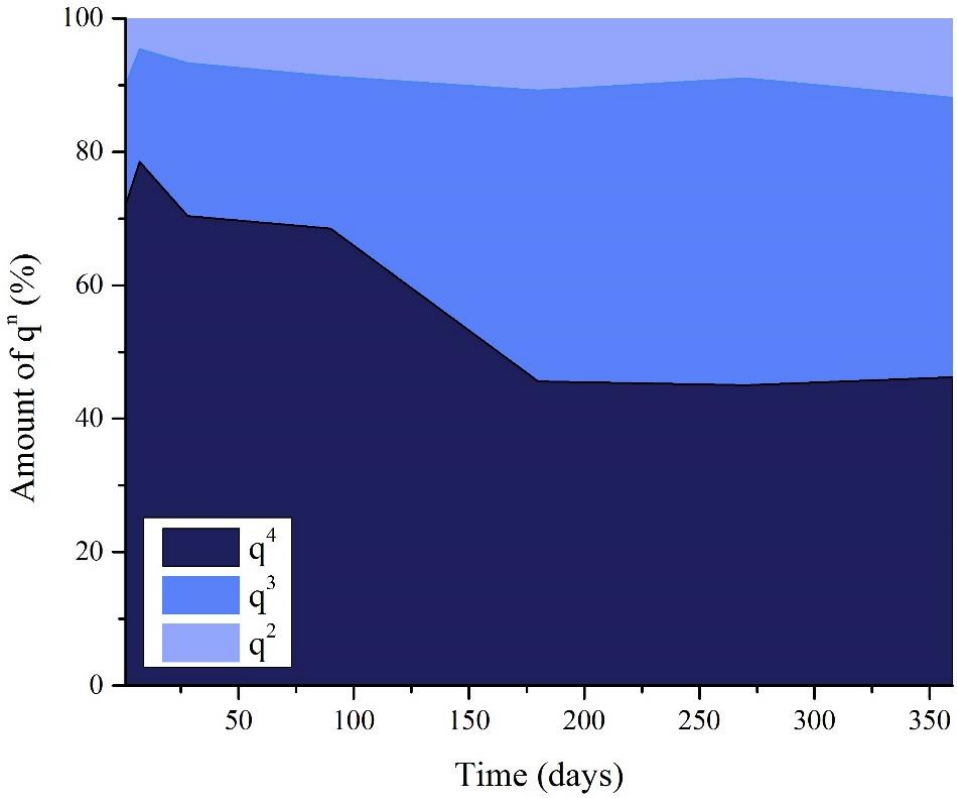

Fig. 3.9 The amount of q^2, q^3 and q^4 sites aluminum present in the pore solution at ages between 1 day and 1 year

^{29}Si NMR spectra of the geopolymer pore solutions at ages between 1 day and 1 year are shown in Fig. 3.10. All the spectra consist of five distinct bands which can be assigned to Q^0, Q^1, Q^2_Δ, Q^2 and Q^3 sites silicon as indicated in Fig. 3.10 (Bass and Turner, 2002), where Q refers to tetrahedrally coordinated silicon, the superscripts

represent the number of siloxane bridges and the subscript Δ designates the silicon in three-membered rings. These are the typical features commonly observed in the spectra of alkali silicate solutions (Bass and Turner, 2002). The observed line boarding of the peaks is attributed to the high viscosity of the solution, which makes distinguishing of the separate species within each Q region difficult (Phair and van Deventer, 2002). Additionally, a broad hump was detected on the shielding side of Q^3 band in the spectra of pore solutions at ages between 1 day and 180 days, which is also observed in the spectra of concentrated alkali silicate solutions (Bass and Turner, 2002), representing polymerized Q^4 sites silicon. The asymmetrical shape of the hump indicates the incorporation of aluminum into the silicates (Brus et al., 2016; Lippmaa et al., 1981), which agrees with the ^{27}Al NMR results. It is observed that the peak of the Q^4 band shifted in the direction of increased shielding from 7 days to 6 months and were less overlapping with the Q^3 band, which may be attributed to the decreasing amount of aluminum in the oligomers, as the ^{29}Si resonance frequency increases when the neighboring silicon is replaced by aluminum tetrahedra (Kinrade and Swaddle, 1989). After 6 months, the Q^4 band became non-obvious indicating most of the aluminosilicate oligomers were condensed into geopolymer binders. The continuous condensation of the aluminosilicate oligomers observed here could further densify the microstructure of the geopolymer pastes after hardening, which supports the observations by other researchers (Gunasekara et al., 2016; Wardhono, 2014) that the permeability of the fly ash geopolymer concrete reduced and the compressive strength increased from 90 to 360 days.

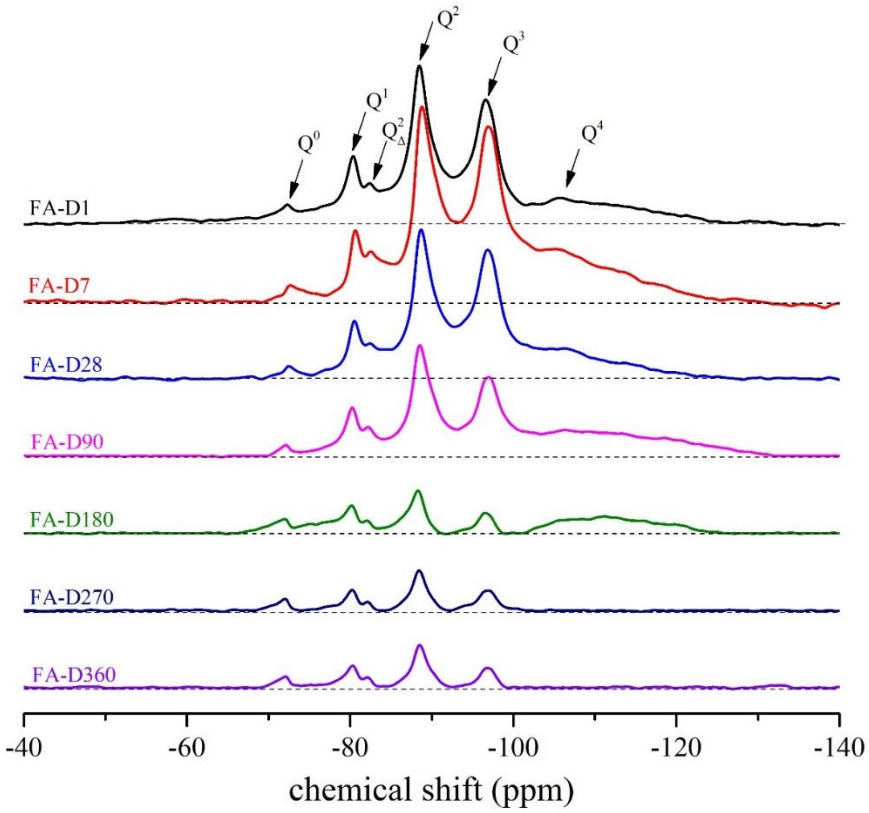

Fig. 3.10 ^{29}Si NMR spectra of the geopolymer pore solutions at ages between 1 day and 1 year.

3.3.3 Relation of the pore solution to ASR resistance of the fly ash geopolymer

It has been reported that sufficient alkalinity in concrete pore solution is required to sustain the alkali-silica reaction at a certain rate that could lead to significant ASR expansion (Vayghan et al., 2016; Shehata and Thomas, 2006). Several minimum hydroxide ion concentrations of pore solution have been proposed for deleterious expansion to occur in OPC concrete (Diamond, 1983a; Duchesne and Bérubé, 1994; Kollek et al., 1986; Struble, 1988; Thomas et al., 2006). Several researchers (Diamond, 1983a; Kollek et al., 1986; Thomas et al., 2006) reported a minimum value of hydroxide ion concentration in pore solution between 0.2 to 0.3 mol/L under which deleterious ASR expansion is unlikely to occur, while Duchesne and Bérubé (Duchesne and Bérubé, 1994) proposed a relatively higher threshold in hydroxide concentration around 0.65 mol/L and Struble (Struble, 1988) suggested a pH threshold between 13.65 and 13.83.

In the present study, the pH value of the pore solution in the fly ash geopolymer was stabilized at around 12.5, which is much lower than the thresholds proposed in the previous studies. Thus, the dissolution rate of the reactive silica in the pore solution here is unlikely to sustain the ASR due to the insufficient alkalinity of the pore solution (Vayghan et al., 2016; Rajabipour et al., 2015), which most likely accounts for the low expansion of the geopolymer concrete prisms.

Pouhet and Cyr (2015) reported a rapid reduction of the pH value of geopolymer pore solution and explained that it was probably due to the carbonation of the pore solution. However, infrared spectra in Fig. 3.6 exhibit limited carbonation of the geopolymer pore solution in the present study, probably because the high humidity of the storage condition in concrete prism test largely inhibited the carbonation of the pore solution (Saetta et al., 1993). We thus concluded the rapid reduction of pH initially was mainly attributed to the consumption of the hydroxide ions for the fly ash dissolution. It should be noted that in a natural condition, carbonation of the geopolymer pore solution would happen (Cyr and Pouhet, 2016) and further reduce its alkalinity, which could make geopolymer concrete even less vulnerable to ASR.

Pore solution of OPC concrete was mainly composed of highly concentrated alkali hydroxide with minor amount of calcium hydroxide and sulfates (Diamond, 1989; Swamy, 1992). In the studies of pore solution in OPC concrete, the hydroxide ion concentration was generally assumed to be equal to the concentration of alkali ions due to the electrical neutrality of the solution and other ionic species were insignificant in the solution compared to alkali ions (Duchesne and Bérubé, 1994; Swamy, 1992). Thus, concentration of alkali ions is often measured and used as an indication of the alkalinity of pore solution in OPC concrete. However, this assumption may not be applicable to the geopolymer pore solution, as both alkali ions and silicates were identified as the major components in the geopolymer pore solution and the silicates were the major anions balancing the alkali ions. Thus, high alkali content does not necessarily mean high hydroxide ion content or high pH value in the geopolymer pore solution. Using the alkali content to represent the pore solution alkalinity in geopolymer system could be misleading and result in wrong interpretation of results.

It is known that the pore solution of normal OPC concrete is saturated with calcium and the calcium content in the pore solution was typically ranged from 0.6 to 2.5 mmol/L (Helmuth et al., 1993) due to the low solubility of calcium hydroxide in the alkaline pore solution with pH level typically in a range of 13.2-13.8 (Struble, 1988). The majority of calcium hydroxide from cement hydration are present in solid states in OPC. In the present study, the geopolymer synthesized by using the fly ash with calcium content of 1.2% is much lower compared to that in cement (62.5%). Although the dissolution of fly ash lead to increase of the calcium content up to 9.2 mmol/L at 7 days, the concentration is still much below the solubility of calcium hydroxide (~12 mmol/L (Yuan et al., 2010)) in the pore solution with pH of 12.5. It indicates no soluble calcium source is available to further release calcium into the pore solution. With the condensation of the geopolymer, the calcium content is continued to reduce to 0.4 mmol/L, which is negligible when considering the effects of calcium on ASR expansions.

Calcium is believed to playing an important role on ASR expansion in OPC concrete. It has been suggested that calcium could facilitate the dissolution of reactive silica by promoting the gelation of silicates species in the pore solution to form poly-metal-silicates (Glasser and Kataoka, 1982; Gaboriaud et al., 1999). Thus, in addition to the insufficient alkalinity, the deficiency of calcium in the geopolymer pore solution could also contribute to the reduction of the dissolution rate of the reactive silica and the gelation process might also be hindered due to the lack of polyvalent metal ions to link silica ions (Iler, 1979).

Moreover, it has been reported that calcium could free up alkalis back into pore solution by exchanging the alkalis from ASR gel, which is known as “alkali recycling”. Once the calcium in pore solution is consumed and incorporated into the gel, further dissolution of solid portlandite could compensate the deficiency of the calcium as well as hydroxide ions, to maintain the alkalinity in the pore solution. Thus, as the deficiency of calcium hydroxide acting as a “pH buffer” in geopolymer concrete, it can be reasonably expected that even though the ASR expansion occurs in the geopolymer concrete with sufficiently high alkalinity in the pore solution, the

reaction cannot be sustained due to the consumption of hydroxide ions by ASR without compensating by calcium hydroxide.

It has shown that the presence of soluble aluminum could help to mitigate the ASR expansion in OPC concrete. Chappex and Scrivener (2012b) found that only 3.9 mmol/L soluble alumina in the OPC pore solution was sufficient to significantly reduce the aggregate deterioration caused by ASR. It was suggested that the mitigation was mainly attributed to the incorporation of aluminum into the reactive silica structure, resulting in reduction of the silica dissolution rate. In the geopolymer pore solution, as shown in the current study, the aluminum was mainly present in the aluminosilicate oligomers. Further studies are necessary to reveal the influences of the presence of this type of aluminosilicate species in the pore solution on the ASR expansion of geopolymer concrete.

3.4 Summary

This study evaluated the ASR expansion behaviors of the OPC and fly ash-based geopolymer concrete containing alkali-silica reactive aggregates by using the concrete prism test. Pore solution analyses, in terms of ion concentrations, pH, chemical bonds, and short-range order of the silicon and aluminum were conducted on the fly ash geopolymer paste at different ages up to one year.

The results showed that the pore solution of the fly ash geopolymer in the current study was mainly composed of alkali ions, silicates and aluminosilicates species. The geopolymer pore solution composition was different from the OPC pore solution, where high concentration of alkali hydroxide is the dominating component. Q^0-Q^4 sites silicon were detected in the geopolymer pore solution and all the aluminum in the pore solution were tetrahedrally coordinated, mainly presented in the form of aluminosilicate oligomers.

The CPT results suggested much higher ASR resistance of the fly ash geopolymer concrete compared to the OPC concrete. The lower expansion of the geopolymer concrete was most probably due to the insufficient alkalinity in the geopolymer pore solution in the present study. The pH of the pore solution reduced dramatically to 12.6 in only one day due to the consumption of hydroxide ions for the fly ash

dissolution. Moreover, the deficiency of calcium and the presence of aluminum in the geopolymer pore solution might also contribute to enhancing the ASR resistance of geopolymer concrete. Further studies are necessary to understand of these effects on the ASR in geopolymer concrete.

Chapter 4 Effect of Pore Solution Alkalinity on ASR Expansion of Metakaolin Geopolymer Concrete

4.1 Overview

In the chapter three, the low ASR-induced expansion of fly-ash-based geopolymer was observed and the pore solution analysis showed that it is mainly due to the insufficient alkalinity of the geopolymer pore solution. The reduction of the alkalinity was likely due to the consumption of the hydroxyl ions for the fly ash dissolution, providing soluble aluminates and silicates for geopolymerization. The alkalinity of the pore solution is mainly dependent on the activating solution concentration and it was reported that once the activating solution concentration was beyond a certain level, the dissolution and formation of the reaction products were maximized and the remaining alkali solution was unused in the pore solution (Abdullah et al., 2011). The study in this chapter thus aims to investigate the effect of the pore solution alkalinity on the ASR expansion behavior of the geopolymer concrete. Metakaolin was adopted as the geopolymer precursor instead of fly ash in this study due to the high reactivity and purity of the metakaolin. It allows a control of the pore solution alkalinity by adjusting the mix design. In addition, the impact of aluminum in the geopolymer pore solution on the ASR expansion is also discussed.

4.2 Materials and methods

4.2.1 Materials

Metakaolin (Metamax, BASF) with composition shown in Table 4.1 was used for geopolymer synthesis. Silica and alumina constitute 53.0% and 43.8% by mass, respectively, of the metakaolin, giving a SiO_2/Al_2O_3 molar ratio of 1.2. Sodium silicate solution (catalog no. 105621, Merck Millipore) with 8 wt. % of Na_2O and 27 wt. % of SiO_2 and NaOH pellets (AR grade, catalog no. 106469, Merck Millipore) were used to prepare the activating solution. Type I Portland Cement from Lafarge with an Na_2O_{equiv} of 0.66% (Table 4.1) was used for the OPC specimens. The reactive aggregates used in the concrete were novaculite, a sedimentary rock mainly consisting of silica in forms of chert and flint, which have been known as highly alkali-silica reactive mineral components within aggregates (Swamy, 1992). The

granite was used as non-reactive aggregates in the control concrete specimens. The grading of the aggregates is shown in Fig. 4.1.

Table 4.1 Chemical composition of the raw materials (% by mass)

	SiO_2	Al_2O_3	Fe_2O_3	CaO	MgO	K_2O	Na_2O	P_2O_5	SO_3	TiO_2
Cement	17.6	3.2	3.1	62.5	3.6	0.4	0.4	0.1	3.6	0.6
Metakaolin	53.0	43.8	0.4	<0.1	<0.1	0.2	0.2	<0.1	0.0	1.7
Reactive aggregate	98.9	0.7	0.2	-	<0.1	0.1	-	-	-	<0.1

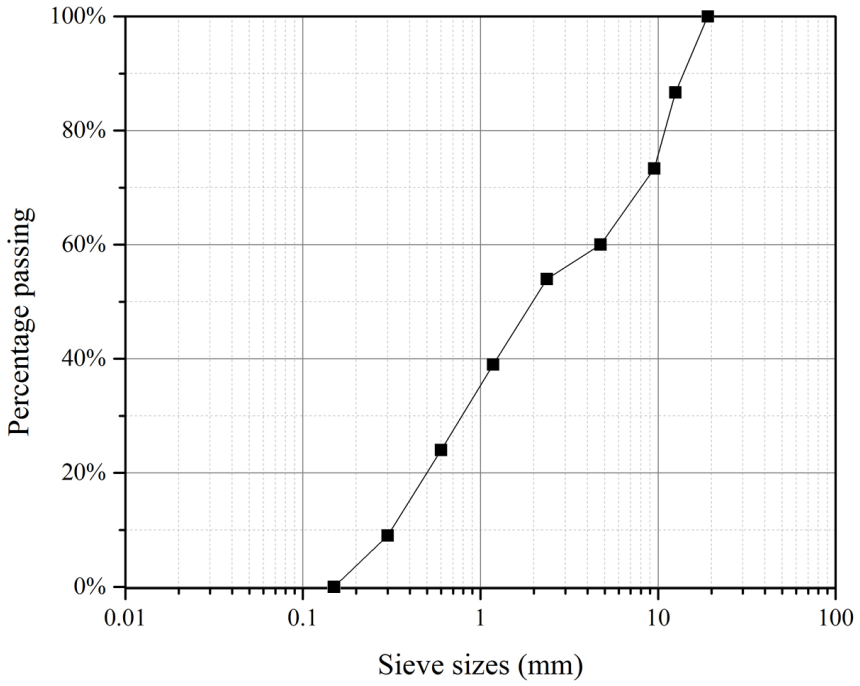

Fig. 4.1 Grading curve of the aggregates

4.2.2 Methods

4.2.2.1 Concrete prism test (CPT)

The OPC concrete prisms with dimension of 75 mm × 75 mm × 285 mm and a water-to-cement ratio of 0.45 were prepared in accordance with ASTM C1293. The alkali content of the OPC was increased to 1.25% Na_2O_{eq} by adding NaOH pellets into the mixing water. Graded reactive and non-reactive aggregates were used, respectively, to prepare the OPC concrete prisms (*i.e.*, OPC_r and OPC_nr) with an aggregate-to-

binder ratio of 2.3, by mass. The metakaolin geopolymer concrete prisms were prepared in the same procedure with the mix design showing in Table 4.2. The SiO_2/Al_2O_3 molar ratio of all the mixtures was kept constant at 3.6, while the Na_2O/Al_2O_3 molar ratio of the MK_0.9_r (nr) and MK_1.5_r (nr) was 0.9 and 1.5, respectively. The aggregate-to-binder ratio of the all the mixtures was 2.3, by mass.

Table 4.2 Mix design (by mass) of the geopolymer concrete prisms

Sample	Metakaolin	Activating solution			Aggregates (types)
		Sodium silicate solution	NaOH pellet	Milli-Q water	
MK_0.9_nr	11.6	17	1.8	1	26.7 (non-reactive)
MK_0.9_r	11.6	17	1.8	1	26.7 (reactive)
MK_1.5_nr	11.6	17	4.2	1	26.7 (non-reactive)
MK_1.5_r	11.6	17	4.2	1	26.7 (reactive)

After casting, all the concrete prisms were cured at 23°C and 98% RH for 24 h. Then the prisms were de-molded and stored over water in sealed containers with absorbent material covering the sides. The containers are 19 L polyethylene buckets with diameter of 310 mm and height of 370 mm. The buckets were covered with airtight lids to prevent the loss of enclosed moisture due to evaporation. A perforated rack was placed in the bottom of the container so that the concrete prisms were 30 mm above the bottom and the container was filled with water to a depth of 20 mm above the bottom. The absorbent material made of polypropylene geotextile was placed around the inside wall of the container from the top into the water at the bottom. The bucket was then placed in an oven at 38°C. The lengths of the specimens were measured routinely for 12 months and the average expansion readings of three prisms for each type of specimen together with its standard deviation were reported.

Scanning electron microscopic (SEM) and energy-dispersive X-ray spectroscopy (EDX) analyses were carried out on the concrete prisms after the test by using a field emission scanning electron microscope (FESEM, JEOL JSM-7600F). The specimens were fractured to expose the aggregate-binder interfaces for examination. No polishing was conducted on the samples to preserve the full morphology of the ASR

products and aggregate surface. The fractured samples were freeze-dried at -50℃ under vacuum for 72 h and coated with a platinum layer prior to the analysis.

4.2.2.2 Pore solution analysis

The paste specimens with a diameter of 45 mm and a height of 85 mm were prepared for the pore solution extraction. The paste has the same mix design as the concrete used in the CPT, except that aggregates were omitted in preparing the paste sample. The specimens were then stored in the same condition as specified in the CPT. The pore solution of the pastes at different ages was extracted followed the method described by Barneyback and Diamond (1981) by using a high-pressure extraction setup which is similar to that described by Cyr et al. (2008). An additional air circulation system was equipped to the setup to drive the extracted solution into the collection bottle and the CO_2 in the circulating air was removed by aerating it through 1 mol/L NaOH solution in order to minimize carbonation of pore solution during the extraction process. The extraction was carried out on a 3000 kN servo-hydraulic compression testing machine (MTS YAW-3000L) with a loading rate of 1.2 kN/s and loaded up to 1200 kN.

Immediately after the extraction, the pore solution was filtered by using a syringe filter with pore sizes of 0.45 μm to remove particles in the solution. After that, the pH of the solution was measured using a standard pH meter (Mettler Toledo SevenCompact) and the ion concentrations of Na, K, Si, Al and Ca in the solution were measured by using an inductively coupled plasma-optical emission spectrometry (ICP-OES, PerkinElmer Optima 8000).

In addition, the solution was analyzed by the solution-state nuclear magnetic resonance (NMR, Bruker Avance 400 MHz). ^{29}Si NMR spectra were obtained at 79.49 MHz by using 90° pulses of 14.5 μs and 5-s recycle delays with number of scans of 256. The pore solution extracted from MK_1.5 paste at 28 d was also analyzed by ^{27}Al solution-state NMR. The spectra were obtained at 104.26 MHz by using 90° pulses of 10 μs and 1-s recycle delays with number of scans of 64. All the spectra were obtained under the same condition at ambient temperature on 400 μL of pore solution sample with 10% of $^{2}H_2O$ for NMR locking. Chemical shifts of ^{29}Si and

^{27}Al were reported in parts per million referenced to tetraethoxysilane and $AlCl_3$ solution, respectively.

4.2.2.3 ^{27}Al MAS NMR on geopolymer pastes

The geopolymer pastes MK_0.9 and MK_1.5 at age of 1 d and 7 d were analyzed by ^{27}Al MAS NMR to investigate the amount of unreacted metakaolin within the geopolymer. The tests were conducted by using a Bruker Avance III HD 600 spectrometer (14.1 T), with a spinning speed of 13 kHz. ^{27}Al spectra were acquired at 156.39 MHz with a 90° pulse of 3 μs, recycle delay of 2 s and 100 scans. The chemical shifts of ^{27}Al were externally referenced to the $AlCl_3$ solution at 0 ppm.

4.2.2.4 Reaction of the pore solution with the aggregates

In order to understand the reaction of aggregates and the geopolymer pore solution, the reactive and non-reactive aggregates sample of 10 g with particle size of 300-600 μm were exposed to 10 mL pore solution extracted from the MK_1.5 paste specimens at age of 28 d.

The reactants were put in a sealed plastic bottle for 14 d at 80°C to accelerate the reaction. The pH of the pore solution was measured at 3, 7 and 14 d of the reaction and the solution was cooled down to room temperature prior to the measurement.

After 14 d, the solid phases including aggregates and the reaction products in the pore solution were extracted from the solution separately based on their different densities. The remaining solution was filtered with a 0.45 μm filter and the concentrations of the remaining ions (Na, Si, Al) in the filtrate were measured by using ICP-OES.

The extracted reaction products and the aggregates were washed, respectively, in distilled water with a minimum agitation of 100 rpm for 1 min and filtered with a 0.45 μm filter. The washing process was repeated until no sodium and silicate ion was detected by ICP-OES in the filtrate to make sure that the pore solution on the solid surface has been entirely removed. Then the reaction products and the aggregates were freeze-dried and analyzed by ^{29}Si and ^{27}Al MAS NMR. The tests were conducted by using a Bruker Avance III HD 600 spectrometer (14.1 T), with a spinning speed of 10 kHz. ^{29}Si spectra were acquired at 119.24 MHz with a 90° pulse

of 4 μs, recycle delay of 60 s and 700 scans. ^{27}Al spectra were acquired at 156.39 MHz with a 90° pulse of 3 μs, recycle delay of 2 s and 800 scans. The chemical shifts of ^{29}Si and ^{27}Al were externally referenced to tetraethoxysilane (TEOS) and $AlCl_3$ at -82.04 ppm and 0 ppm, respectively.

The reaction products were also analyzed by X-ray diffraction (XRD) using a Brucker D8 Powder XRD diffractometer with an incident beam of CuKα (λ = 1.5418 Å) radiation and a 2θ scanning range of 10° to 70°. SEM/EDX analysis was also carried out on the reaction products by using a field emission scanning electron microscope (FESEM, JEOL JSM-7600F).

4.3 Results

4.3.1. Concrete prism test

Fig. 4.2 shows the expansion results of the OPC and the metakaolin geopolymer concrete prisms with reactive and non-reactive aggregates. As can be seen, the OPC concrete prisms with reactive aggregates expanded substantially, exceeding the one-year expansion limit (0.04%) prescribed in ASTM C1293 in only two months, which confirms that the aggregates used are highly alkali-silica reactive. As expected, the OPC prisms with non-reactive aggregates showed almost no expansion. In contrast, no deleterious ASR expansions were observed for both MK_0.9_r and MK_0.9_nr concrete prisms, indicating that these binders had higher resistance to ASR than OPC. While for the concrete activated by the alkaline solution with elevated sodium hydroxide content, *i.e.*, MK_1.5_r and MK_1.5_nr, obvious expansions were observed after 28 d, reaching the expansion limit at around two months and remaining almost stable afterwards. The possible reason for the expansion is discussed in detail in the following section.

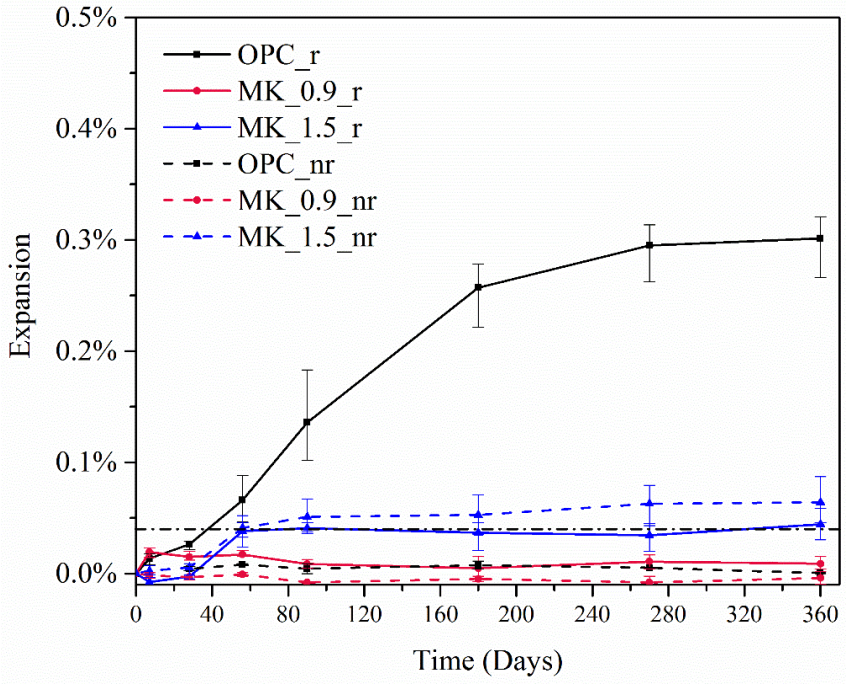

Fig. 4.2 Expansion results of OPC and metakaolin geopolymer concrete prisms in CPT

The SE images of the surfaces of the reactive aggregates within the OPC, MK_1.5 and MK_0.9 concrete after CPT are shown in Fig. 4.3. The ASR products with typical "rosette-type" morphology (Davies and Oberholster, 1988; García-Lodeiro et al., 2007) were observed (in red circles in Fig. 4.3b) on the aggregate surface in OPC concrete and the EDX results showed that they are typical Na(K)-Ca-silicate ASR gel with (Na+K)/Si molar ratio of 0.2 and Ca/Si molar ratio of 0.1. Additionally, no typical morphology of ASR was observed on the aggregate surfaces in the geopolymer concrete prisms (Fig. 4.3b and c). The morphology of the rock surface in MK_0.9_r after CPT remains similar to that before the test (Fig. 4.3a). While numerous voids were observed on the surface of reactive aggregates in MK_1.5_r concrete (Fig. 4.3c), it indicated that the reactive aggregates were seriously corroded by the alkaline pore solution. Despite that, no additional phase was obviously observed on the surface of the aggregates in MK_1.5_r, suggesting that the aggregates was simply dissolved into the pore solution with no additional gel formed on the aggregate surface in MK_1.5_r.

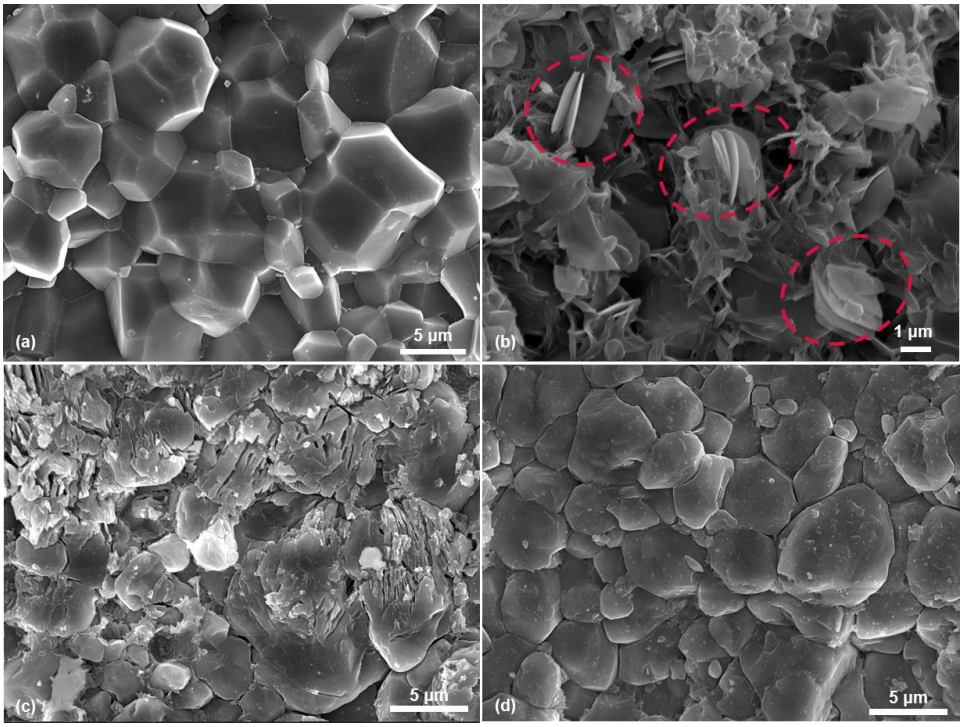

Fig. 4.3 Secondary electron (SE) images of the surface of reactive aggregate (a) before CPT, (b) in OPC prism after CPT, (c) MK_1.5_r and (d) in MK_0.9_r after CPT.

4.3.2. Analysis of geopolymer pore solution and pastes

The compositions of the pore solution in metakaolin geopolymer pastes at different ages are plotted in Fig. 4.4. In the pore solution of MK_0.9 paste, a reduction of the concentration of Na, Si and Al is observed from 1 d to 3 d, which is attributed to the polycondensation of the silicate and aluminate species as well as the incorporation of the sodium into the aluminosilicate gel. After three days, the ion concentrations remained almost stable, indicating that the condensation process has almost finished within the first three days for MK_0.9 paste. The trend of the Na concentration over time was consistent with that in the fly ash geopolymer as shown in Fig. 3.5 as the sodium in both geopolymer system was gradually incorporated into the geopolymer binder. The concentration of the Si and Al was increased initially in the pore solution of the fly ash geopolymer (Fig. 3.5), while Si and Al concentration in MK_0.9 kept reducing since age of 1 d. The different trends are most probably due to the lower reactivity of the fly ash so that the continuous dissolution of the fly ash in the first 7

days kept releasing soluble aluminates and silicates species, while the dissolution of metakaolin was almost finished within one day.

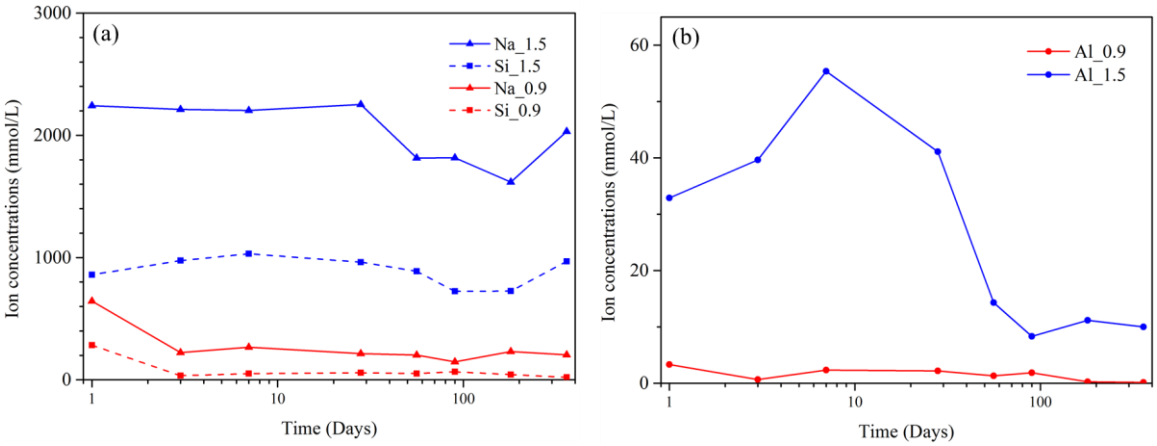

Fig. 4.4 The concentration of (a) Na, Si and (b) Al in the pore solution of geopolymer paste MK_1.5_r and MK_0.9_r as a function of time.

In the pore solution of MK_1.5 paste, the concentration of Si and Al in the MK_1.5 pore solution increased slightly in the first seven days, suggesting that the releasing rate of soluble Si and Al by metakaolin dissolution are over the condensation rate of these species. After seven days, the concentrations of Si and Al continue to reduce until three months, indicating the condensation gradually dominated. An increase of the concentration of silicon and sodium was observed from 6 to 12 months, probably due to the evaporation of the water during that 6 months. Further investigations are required in the future works.

Fig. 4.5 showed ^{27}Al MAS NMR spectra of MK_0.9 and MK_1.5 pastes at age of 1 d and 7 d. Metakaolin is known to contain Al(IV) (~60 ppm), Al(V) (~30 ppm) and Al(IV) (~0 ppm) (Duxson et al., 2005). During alkali activation of metakaolin, Al(V) and Al(VI) will be converted to tetrahedral sites and the speciation of aluminum in the alkaline solution is restricted to Al(IV). Therefore, any remaining Al(V) and Al(VI) in the geopolymer pastes are attributed to the unreacted metakaolin and the appearance of Al(V) and Al(VI) has been used as an quantitative indication of the amount of unreacted metakaolin in geopolymers. As can be seen in Fig. 4.4, mall peaks of Al(V) and Al(VI) were observed in the spectra of MK_0.9 at age of 1 d, while the spectra of MK_1.5_D1 exhibited a lower peak of Al(VI) and the peak of

Al(V) disappeared. It showed that the less amount of unreacted metakaolin existed in the MK_1.5 paste at 1 d, suggesting that the dissolution of metakaolin was facilitated due to the activating solution with elevated alkalinity was used in the MK_1.5 geopolymer. At age of 7 d, the peaks of Al(V) and Al(VI) in MK_0.9 pastes were further reduced, while almost identical spectra of MK_1.5 were observed at the age of 1 d and 7 d. It suggested the dissolution metakaolin in MK_1.5 was almost finished within one day.

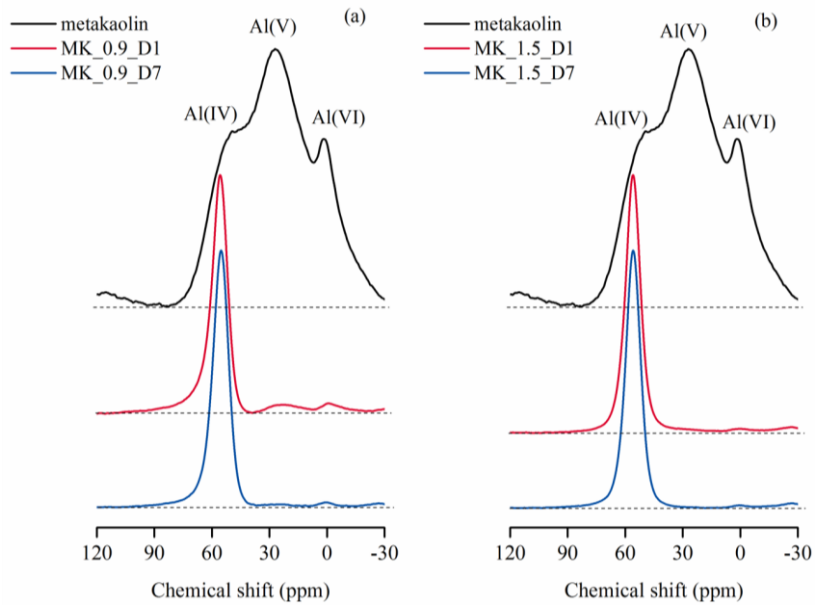

Fig. 4.5 ^{27}Al MAS NMR spectra of the metakaolin, (a) MK_0.9 and (b) MK_1.5 paste at age of 1 d and 7 d.

Fig. 4.6 showed ^{29}Si NMR spectra of the pore solutions of MK_0.9 and MK_1.5 geopolymer pastes at ages between 1 d and 90 d. As can be seen, at the age of 1 d, both the MK_0.9 and MK_1.5 pore solutions consisted of Q^0, Q^1, Q^2, Q^3 and Q^4 sites silicon (Bass and Turner, 2002) as indicated in the figure. After one day, the peaks assigned to Q^0, Q^1, Q^2, Q^3 sites silicon were almost disappeared with only the Q^4 site silicon presented in the MK_0.9 pore solution, suggesting that the silicon condensed forming polymerized silicates in the MK_0.9 pore solution after one day. In contrast, the Q^0 to Q^3 peaks remained in the MK_1.5 pore solution until the age of 28 d indicating that the condensation of silicon in the pore solution was retarded compared to that of the MK_0.9 pore solution. It is most probably due to the high alkalinity of the pore solution of MK_1.5 as the silicate species under high pH conditions tended

to form small dimers and trimers rather than the larger polymers (Garcia-Lodeiro et al., 2015; Sagoe-Crentsil and Weng, 2007; Weng and Sagoe-Crentsil, 2007). In the spectra of MK_1.5 pore solution at age of 90 d, the Q^1 to Q^3 peaks were almost disappeared suggesting the silicon was further condensed in the MK_1.5 pore solution from 28 d to 90 d.

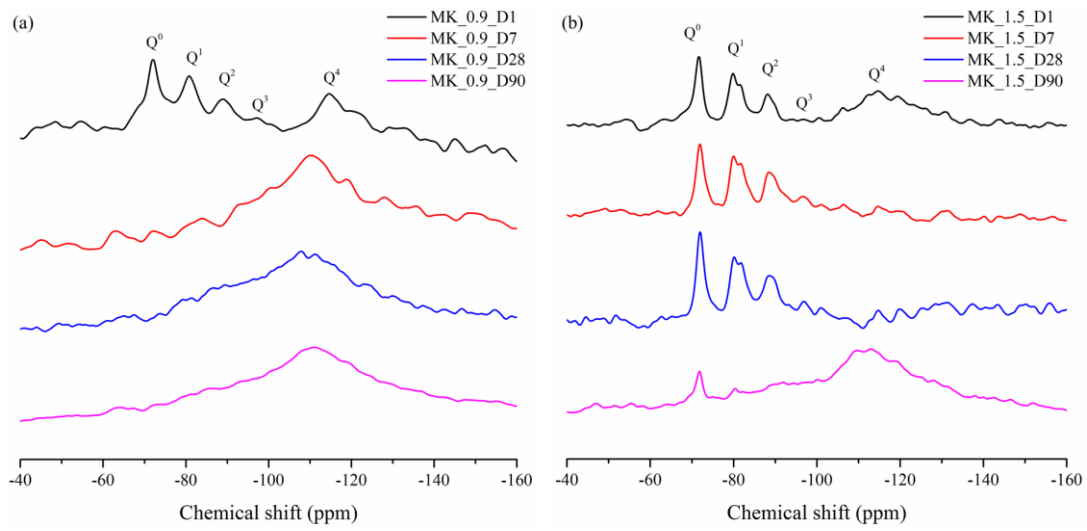

Fig. 4.6 ^{29}Si NMR spectra of the pore solution of (a) MK_0.9 and (b) MK_1.5 geopolymer pastes at ages between 1 d and 90 d.

Fig. 4.7 shows the pH level of the pore solution in OPC and metakaolin geopolymer pastes at different ages. The pH of the activating solution of the geopolymer was measured and indicated as hollow markers in the figure. The pH level of the OPC pore solution increased slightly in the first seven days due to the cement hydration and stabilized at 13.5 afterwards. The pH of the OPC pore solution was measured only up to age of 28 days and it is believed that the further change of the pH is negligible as the OPC pore solution was reported to reach an equilibrium after nearly one month (Diamond, 1989).

Despite the activating solution with high alkalinity, the pH level of the geopolymer pore solution (12.9 for MK_0.9 and 13.3 for MK_1.5) ended up below that of the OPC pastes (13.4) in only one day. The rapid reduction of the pH value was attributed to the consumption of the hydroxide for the dissolution of the metakaolin precursor. After a significant reduction of the pH of the MK_0.9 pore solution within the first day, a continuous reduction was observed until 28 days, suggesting that the

dissolution of the metakaolin continued in a slower rate. Then the pH was stabilized at around 12.2.

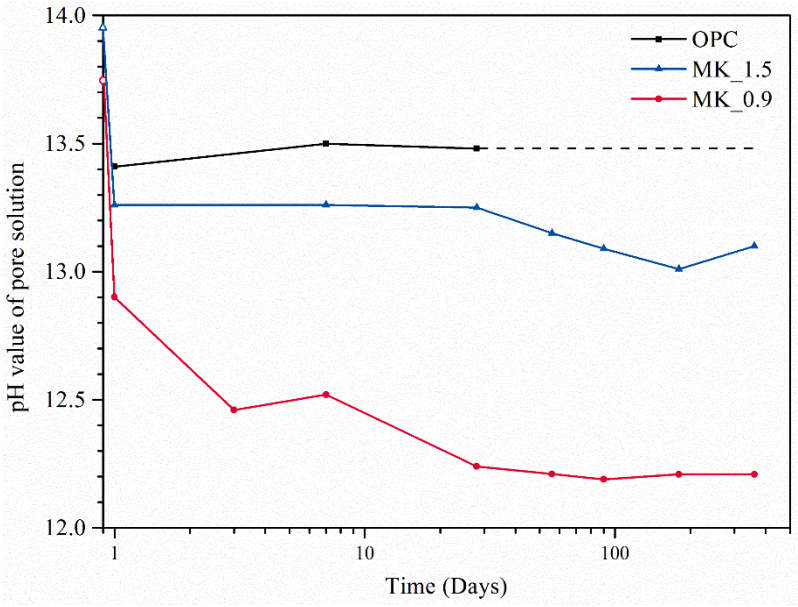

Fig. 4.7 The pH of the pore solution in the OPC and geopolymer paste as a function of time.

For the MK_1.5 pore solution, the significantly higher pH level compared to that of MK_0.9 shows that the increase of alkalinity of the activating solution did increase the pH of the pore solution. The pH of MK_1.5 pore solution remained stable after one day, indicating that the dissolution of the metakaolin is almost completed due to the high alkalinity in the solution significantly increases the kinetics of the metakaolin dissolution. It is consistent with the MAS NMR results shown in Fig. 4.5. The pH of the pore solution started to reduce after 28 days, which is probably to be due to the alkali leaching from the specimens. As the specimens were stored over water in a sealed container as prescribed in the standard ASTM C1293, it was reported that the condensing water on the specimen surface resulted in the diffusion of the alkali and hydroxide ions from the pore solution to the sample surface (Thomas et al., 2006).

4.3.3. Reaction of the pore solution with the aggregates

The extracted pore solution from sample MK_1.5 paste at age of 28 days was directly mixed with reactive and non-reactive aggregates, respectively. Fig. 4.8 shows the pH of the pore solution during the reaction for 14 days. As can be seen, a slight reduction

of the pH was observed in the first three days in the pore solution that reacted with non-reactive aggregates (MK_1.5_nr). The pH then remained stable at 13.1. For the solution reacted with reactive aggregate (MK_1.5_r), the pH of the pore solution reduced rapidly within the first seven days and then stabilized at 12.3, suggesting the dissolution of the reactive aggregates consumed hydroxyl ions in the solution and then pore solution alkalinity became too low to attack the aggregates after the reaction for 7 days. The pH of the MK_0.9 pore solution was found to stabilize at only 12.2 as shown in Fig. 4.7, thus it could be expected that the attack on the reactive aggregates by the hydroxyl ions in the pore solution was negligible in the MK_0.9_r concrete prisms.

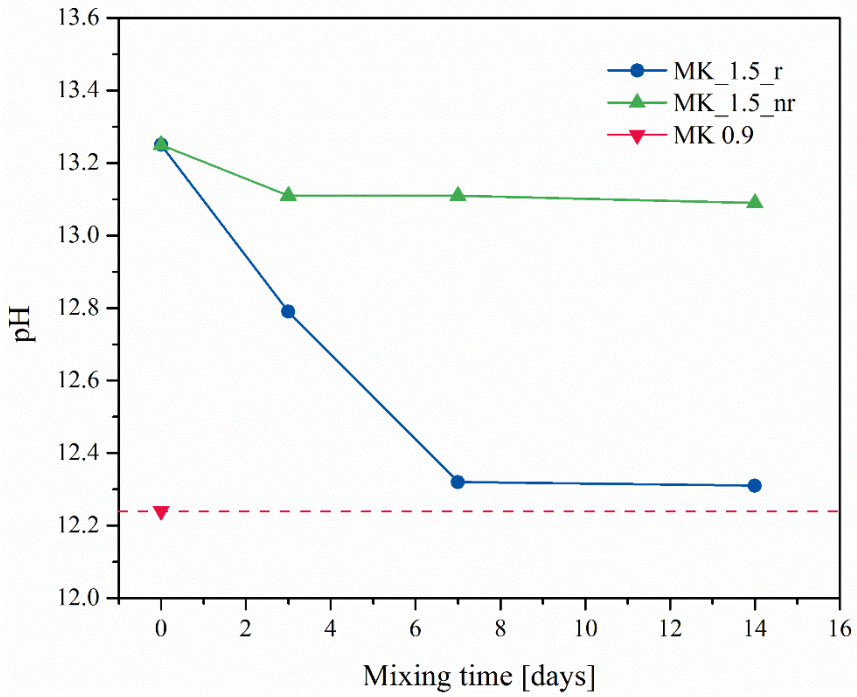

Fig. 4.8 The pH of the pore solution during reaction with aggregates as a function of time.

The compositions of pore solution before and after the reaction with aggregates are plotted in Fig. 4.9. As can be seen, the concentration of Si is largely increased in the pore solution after the reaction with reactive aggregates, suggesting siliceous aggregates were dissolved into the pore solution. Due to the low reactivity of the non-reactive aggregates, the concentration of Si in the pore solution is slightly increased after the reaction. The concentrations of Na reduced to a similar level in both the

solutions that mixed reactive and non-reactive aggregates and the concentrations of Al reduced to round only 1 mmol in both the solutions after the reaction.

After the reaction for 14 d, a white solid phase distinct from the aggregates was formed and observed in both solutions reacted with reactive and non-reactive aggregates. The XRD analysis of the solid phases (Fig. 4.10) showed that zeolite was formed in both the solution mixed with reactive and non-reactive aggregates. The EDX showed that the zeolitic phases had the similar Na/Al ratio at around 1.2 but different Si/Al molar ratios of 3.0 and 2.0, respectively, in the pore solution that mixed with reactive and non-reactive aggregates. The peaks of quartz observed in the XRD pattern is attributed to the aggregates mixed in as it was difficult to separate the new-formed phase and aggregates entirely.

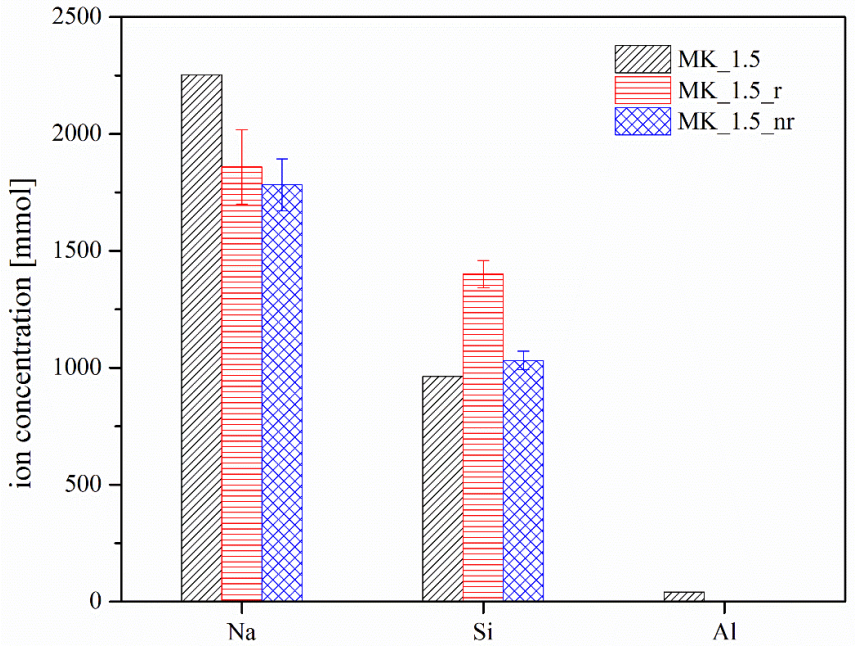

Fig. 4.9 Comparison of pore solution composition of MK_1.5 paste before the reaction with aggregates (MK_1.5) and after the reaction with reactive (MK_1.5_r) and non-reactive aggregates (MK_1.5_nr) for 14 days.

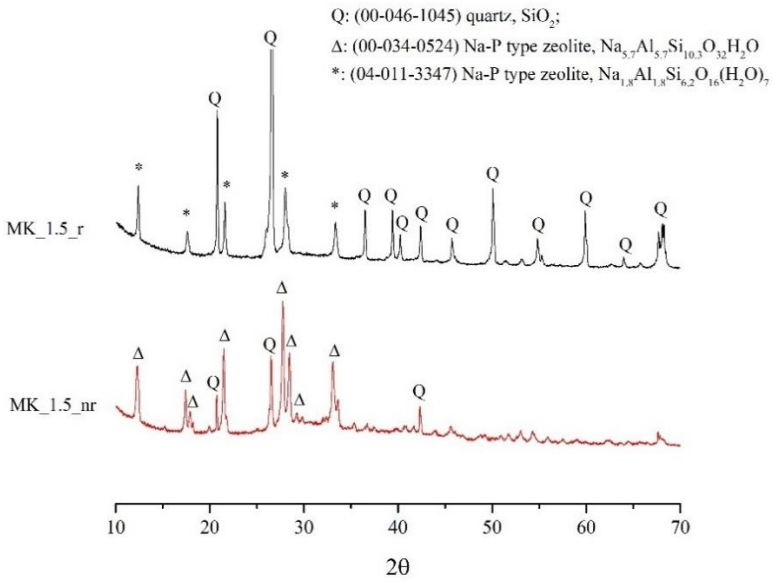

Fig. 4.10 XRD of the solid phase after the mixing of the pore solution and aggregates for 14 days.

The ^{29}Si and ^{27}Al NMR spectra of the extracted solid phase from the pore solution reacted with aggregates are shown in Fig. 4.11 and Fig. 4.12, respectively. The ^{29}Si spectra of both the zeolitic phases consist of $Q^4(4Al)$, $Q^4(3Al)$, $Q^4(2Al)$, $Q^4(1Al)$ and $Q^4(0Al)$ silicon sites as indicated in Fig. 4.11, which is usually observed in Na-P zeolite (Bell, 1999). $Q^4(0Al)$ peak is attributed to the silicon in the zeolite as well as the silicon in the quartz of the aggregates.

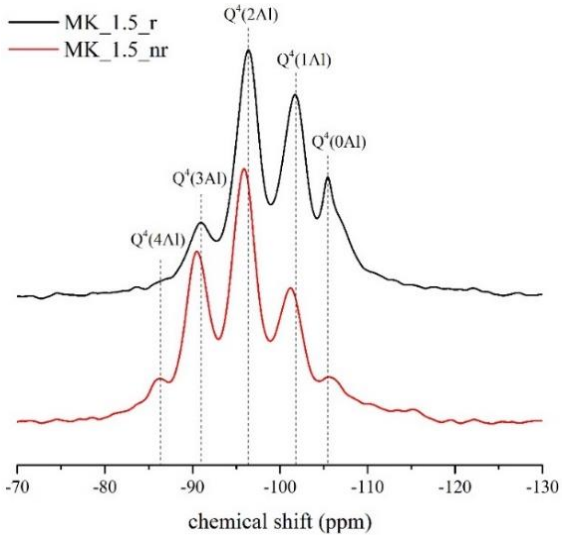

Fig. 4.11 ^{29}Si MAS NMR spectra of the extracted solid phase from the pore solution mixed with reactive and non-reactive aggregates.

The ^{27}Al spectra (Fig. 4.12) exhibited a significant peak at 60 ppm, indicating that the all the aluminum was incorporated in a silicate network surrounded by four silicate tetrahedra (Buchwald et al., 2011). The small peak in a range of 5-10 ppm is attributed to the small amount of six-coordinated Al presented in the aggregates (Martineau et al., 2016).

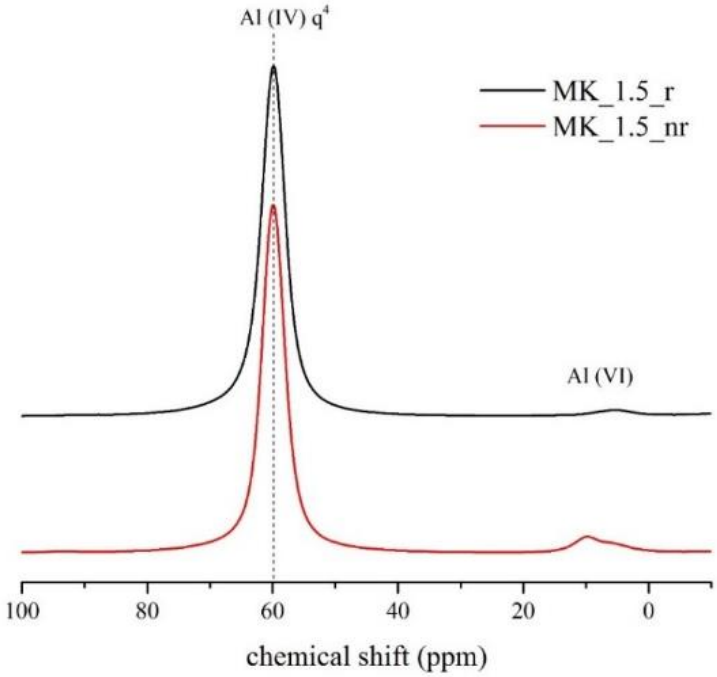

Fig. 4.12 ^{27}Al MAS NMR spectra of the extracted solid phase from the pore solution mixed with reactive and non-reactive aggregates.

4.4 Discussion

4.4.1 Expansion of MK_1.5 geopolymer concrete prisms

Obvious expansion of the MK_1.5_r and MK_1.5_nr concrete prisms was observed after 28 days in the concrete prism tests (Fig. 4.2). The similar expansion behaviors between the concrete prisms with reactive and non-reactive aggregates suggests that the expansion is not attributed to the ASR but most likely due to the volume changes of the geopolymer binder.

The ^{29}Si MAS NMR analysis on the MK_1.5 geopolymer pore solution (Fig. 4.6) showed that the condensation of silicon in the pore solution was retarded compared to that of the MK_0.9 pore solution. most probably due to the high alkalinity of the

pore solution of MK_1.5 as the silicate species under high pH conditions tended to form small dimers and trimers rather than the larger polymers (Garcia-Lodeiro et al., 2015; Sagoe-Crentsil and Weng, 2007; Weng et al., 2007). It was also observed in Fig. 4.4 that the concentrations of Si and Al in MK_1.5 pore solution are significantly higher than that in MK_0.9 pore solution even though the initial amount of Si and Al in both systems are identical. The observation confirms that the condensation of the dissolved silicate and aluminate species within MK_1.5 paste was greatly hindered.

After seven days, the concentrations of Si and Al within MK_1.5 pore solution started to reduce (Fig. 4.4), suggesting that the dissolution rate of the metakaolin reduced and the condensation gradually dominated. As shown in the Fig. 4.6, degree of polymerization of the silicon in MK_1.5 pore solution increased from 28 d to 90 d, suggesting the silicon in the pore solution was further condensed. Especially, the pH of the MK_1.5 pore solution reduced probably due the alkali leaching after 28 d, which may further promote the formation of the larger silicate oligomers and thus the condensation of the polymeric aluminosilicates.

Volume expansion of the fly ash and metakaolin geopolymer at early ages was observed previously by some researchers when the samples were cured in humid conditions (Dang et al., 2005; Mobili et al., 2016; Zuhua et al., 2009). It is thus believed that the further condensation of the aluminosilicate species in the pore solution after the hardening at 28 d in this study is most likely the reason for the expansion of the MK_1.5 concrete prisms observed in the concrete prism test.

4.4.2 Effect of pore solution alkalinity on ASR-induced expansion in geopolymer concrete

Sufficient alkalinity in the concrete pore solution is required for the aggregates being attacked to a degree that will lead to significant ASR expansion (Vayghan et al., 2016; Shehata and Thomas, 2006). As previously mentioned in the third chapter, several minimum hydroxide ion concentrations of pore solution have been proposed for deleterious expansion to occur in OPC concrete depending on the reactivity of the aggregates (Diamond, 1983a; Duchesne and Bérubé, 1994; Kollek et al., 1986;

Struble, 1988; Thomas et al., 2006). In general, the minimum pH value of the pore solution is above 13.

The pH value of the MK_0.9 paste was reduced below 13 in only one day and continued to reduce, reaching stable at around 12.2. The pore solution alkalinity is not sufficient for the ASR to occur, resulting in the negligible expansion of the MK_0.9_r concrete prisms in the concrete prism test.

As a result of the elevated alkalinity in the activating solution, the pH of the pore solution in MK_1.5 paste was remarkably increased compared to that of MK_0.9 paste. The pH of the pore solution in MK_1.5 paste was maintained at 13.2 throughout 28 days. Despite the leaching of the alkalis, the pH was still above 13.0. However, there is still almost no ASR-induced expansion observed for the MK_1.5_r concrete prisms. As previously mentioned, the expansion of MK_1.5_r concrete prisms observed after 28 days was most probably due to the further condensation of the aluminosilicate species in the pore solution rather than the ASR.

The reaction of the reactive aggregates with the extracted pore solution from MK_1.5 paste showed that the dissolution of the reactive aggregates by pore solution resulted in the increase of the Si concentration and the reduction of the pH of the pore solution. The dissolution of the reactive aggregates agrees with the observation of the reactive aggregates surface in the MK_1.5_r concrete prism in SEM (Fig 4.3c), which shows serious corrosion of the aggregates. Non-reactive aggregates were mixed with pore solution as a control and only a slight reduction of the pore solution of pH was observed, indicating that the reaction of the non-reactive aggregates with the pore solution was limited due to the low reactivity of the aggregates.

The formation of zeolite was observed both in the pore solution regardless of whether reactive or non-reactive aggregate was used, suggesting that the formation of the zeolite was mainly due to the condensation of the silicate and aluminate species within original pore solution. The use of the reactive aggregate only contributed more soluble silica to the pore solution, resulting in the formation of zeolite with higher Si/Al ratio.

Despite the significant dissolution of the reactive aggregates in the pore solution with elevated alkalinity, no ASR gel was observed in the solution and accordingly no ASR-induced expansion was observed in the MK_1.5_r concrete prisms. The results suggested that the pore solution alkalinity was not the only controlling factor for the ASR expansion in the geopolymer concrete.

4.4.3 The role of aluminum on the reaction of pore solution and aggregates

It has been reported that the presence of aluminate ions in the OPC pore solution contributed to mitigating the ASR expansion as the aluminum was incorporated into the silica structure on the aggregate surfaces, resulting in a reduction of the silica dissolution rate (Chappex and Scrivener, 2012b, 2013; Leemann et al., 2015).

Chappex and Scrivener (2013) showed that only 3.9 mmol/L aluminum in the pore solution was sufficient to significantly reduce the aggregate deterioration caused by ASR. In the present study, the aluminum concentration in the pore solution of MK_1.5 paste at age of 28 d was much higher (41 mmol/L). In the OPC pore solution, which consists primarily of alkali hydroxide, the monomeric $Al(OH)_4^-$ should be the dominate aluminate phase (Sagoe-Crentsil and Weng, 2007). In the current study the aluminum in the geopolymer are presented as q^1, q^2, q^3 and q^4 species in the pore solution, as shown in Fig. 4.13, suggesting all aluminum was connected with silicon and presented as aluminosilicate species. No signal of q^0 (i.e., chemical shift at 80 ppm) was detected, indicating that no monomeric $Al(OH)_4^-$ was present in the pore solution due to the rapid condensation of the monomeric $Al(OH)_4^-$ with silicate species (Sagoe-Crentsil and Weng, 2007; Weng and Sagoe-Crentsil, 2007).

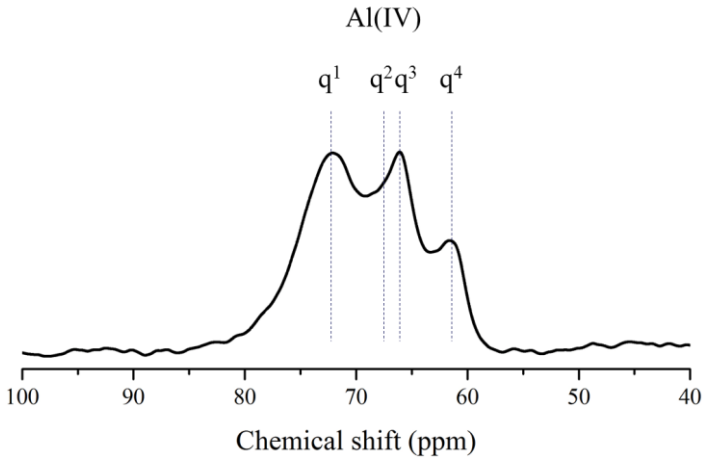

Fig 4.13 ^{27}Al NMR spectra of the pore solution extracted from MK_1.5 paste at 28 d.

After the reaction between the pore solution and reactive aggregates, the ^{27}Al MAS NMR spectra (Fig. 4.14) showed no difference between the reactive aggregates before and after the reaction, suggesting that the aluminum that presented as aluminosilicate species in the geopolymer pore solution was not incorporated into the aggregate surfaces. Instead, almost all the aluminum in the pore solution was condensed and precipitated forming zeolitic phases.

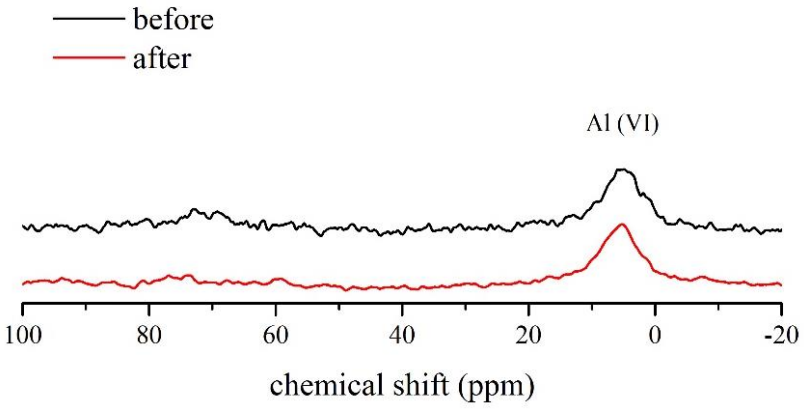

Fig 4.14 ^{27}Al MAS NMR spectra of the reactive aggregates before and after the reaction with pore solution.

Therefore, despite the higher concentration of aluminum in the geopolymer pore solution compared to that in OPC pore solution, the aluminum, which was presented as aluminosilicate species, is unlikely to be incorporated into the aggregates surfaces

and mitigate the dissolution of the aggregates, which was observed in the OPC pore solution.

4.5 Summary

This study investigated the effect of pore solution alkalinity on the ASR expansion of metakaolin geopolymer concrete. The results showed that geopolymer concrete prisms with elevated pore solution alkalinity exhibited no ASR-induced expansions. The reactive aggregates within these samples were seriously corroded by the pore solution but no ASR gel was detected. Further study by using the extracted pore solution to directly react with the aggregates showed that the reactive aggregates are simply dissolved into the pore solution and the aluminosilicate species within the pore solution was condensed into the zeolite regardless of the type of aggregate used. The results suggest that the pore solution alkalinity was not the only controlling factor for the ASR expansion in the geopolymer concrete.

The influence of the aluminum on the ASR mitigation in OPC concrete was likely due to the incorporation of aluminum into the silica structure on the aggregate surfaces, resulting a reduction of the silica dissolution rate. While due to the aluminum in the geopolymer pore solution was presented in the aluminosilicate species, the incorporation of aluminum into aggregates was not detected in the reaction between the geopolymer pore solution with reactive aggregates, suggesting the ASR resistance of geopolymer concrete was not attributed to the aluminum presented in the pore solution.

Chapter 5 Effect of Calcium Hydroxide on ASR Expansion of Alkali-activated Slag Mortars

5.1 Overview

The absence of calcium hydroxide has been proposed to account for the lower ASR expansion in geopolymer concrete as calcium hydroxide is believed to play an important role in the ASR in OPC concrete, but its role is controversial. Firstly, it was proposed that calcium hydroxide provide a large reservoir of hydroxide ions to maintain the pH level of the pore solution, thus sustaining the attack on the reactive aggregates (Rajabipour et al., 2015). Secondly, a number of studies concluded that the presence of calcium influences the gelation process (Glasser and Kataoka, 1982; Gaboriaud et al., 1999). In the absence of calcium, it was reported that the reactive silica simply dissolved in the alkali hydroxide solution without forming any gel (Diamond, 1989; Leemann et al., 2011; Struble, 1987). In addition, it was also proposed that calcium increases the viscosity of the ASR gel, thus increasing the ASR expansion of the concrete (Bleszynski and Thomas, 1998; Gholizadeh et al., 2016), while some researchers concluded that the presence of calcium does not noticeably influence the swelling pressure and the expansive property (Struble and Diamond 1981). As the calcium that directly added into geopolymer system would be incorporated into the geopolymer structure forming C-A-S-H gel, which is similar to the structure of alkali-activated slag system, the study in this chapter is thus to investigate the effect of calcium hydroxide on the ASR expansion of the alkali-activated slag mortar and to understand the role of calcium hydroxide in the ASR in alkali-activated system. The information provided by the study is believed to contribute to understanding whether the absence of calcium in the geopolymer system is responsible for the low ASR expansion.

5.2 Materials and methods

5.2.1 Materials

The GGBFS was sourced from Engro Corporation Ltd. and its chemical composition is summarized in Table 5.1. The basicity coefficient $K_b = (CaO + MgO)/(SiO_2 + Al_2O_3)$ of the slag is 1.25 and its Blaine fineness is 436 m^2/kg. The alkali activator

used was a sodium hydroxide solution prepared by dissolving NaOH pellets (AR grade, purity ≥ 96%) into deionized water. The solution was cooled down for 24 h to room temperature before mixing with GGBFS. Calcium hydroxide powder used in the current study was of AR grade with a purity more than 96%. Type I Portland cement with Na_2O_{eq} of 0.66% (Table 5.1) was used for preparation of the control OPC specimens. The aggregates used were novaculite, a sedimentary rock mainly consisting of silica in forms of chert and flint, which have been known as highly alkali-silica reactive mineral components within aggregates (Swamy, 1992). The graded aggregates were prepared with a standard gradation prescribed in ASTM C1260 as shown in Table 5.2.

Table 5.1 Chemical compositions of the raw materials (wt. %)

	SiO_2	Al_2O_3	Fe_2O_3	CaO	MgO	K_2O	Na_2O	P_2O_5	SO_3	TiO_2
Cement	17.6	3.2	3.1	62.5	3.6	0.4	0.4	0.1	3.6	0.6
GGBFS	27.4	14.7	0.3	43.4	9.3	0.4	0.4	-	1.9	1.5
Reactive aggregate	98.9	0.7	0.2	-	<0.1	0.1	-	-	-	<0.1

Table 5.2 Gradation of the aggregates

Sieve Size		Mass, %
Passing	Retained on	
4.75 mm (No. 4)	2.36 mm (No. 8)	10
2.36 mm (No. 8)	1.18 mm (No. 8)	25
1.18 mm (No. 8)	600 µm (No. 30)	25
600 µm (No. 30)	300 µm (No. 50)	25
300 µm (No. 50)	150 µm (No. 100)	15

5.2.2 Methods

5.2.2.1 Accelerated mortar bar test (AMBT)

The accelerated mortar bar tests on OPC and AAS mortar specimens were conducted in accordance with ASTM C1260 (2014). The mix designs of the mortar specimens

were summarized in Table 5.3. The OPC mixture is a standard mix design of the OPC binder prescribed in ASTM C1260 to evaluate the reactivity the aggregates, which is usually adopted as the control OPC samples in the comparison of ASR behavior with AAS samples (Puertas et al., 2009; Shi et al., 2015). All the OPC and AAS mortar bars with dimensions of 25 mm × 25 mm × 285 mm were prepared with 1 part of binder (*i.e.*, cement or GGBFS) and 2.25 parts of the graded reactive aggregates. Three mortar bars were prepared for each mixture. For AAS mortar specimens, the slag was dry-mixed with different content of $Ca(OH)_2$ powder (*i.e.*, 2, 4, 10, 25 wt.% by mass of slag) for 10 min and then mixed with sodium hydroxide solution with the same alkali content (*i.e.*, 5 wt.% Na_2O by mass of the slag) and water-to-slag ratio of 0.4. The control AAS mortars (AAS-C) without addition of $Ca(OH)_2$ were also prepared following the same procedures.

Table 5.3 Mix design of the OPC and AAS mortars

Sample	Water/binder ratio	Aggregate/binder ratio	Na_2O (wt.% by GGBFS)	$Ca(OH)_2$ (wt.% by GGBFS)
OPC	0.47	2.25	-	-
AAS-C	0.4	2.25	5	0
AAS-2%CH	0.4	2.25	5	2
AAS-4%CH	0.4	2.25	5	4
AAS-10%CH	0.4	2.25	5	10
AAS-25%CH	0.4	2.25	5	25

After casting, all the mortar specimens were sealed and initially cured in ambient condition (23±2℃, 6±5% RH) for 24 h. The specimens were de-molded and subsequently stored in water in sealed containers in an oven at 80℃ for another 24 h. Immediately after the 24 h curing, the initial lengths of the mortar specimens were measured by using a digital length comparator with accuracy of 1μm. The specimens were then immersed in 1 mol/L NaOH solutions in sealed containers in an oven at 80℃ for 14 d. The lengths of the specimens were routinely measured and the average expansions of three mortar bars for each mix were reported.

5.2.2.2 Pore solution analysis

OPC and AAS paste specimens with diameter of 45 mm and height of 85 mm were prepared for the pore solution extraction. The paste has the same mix design as shown in Table 5.3, except the aggregates were omitted. All the paste specimens were cured in ambient condition with temperature of 23±2℃ and 65±5% RH. The pore solution of the paste was extracted after curing for 7 d. The pore solution extraction was conducted by using a high-pressure extraction setup following the method described by Barneyback and Diamond (1981). The setup is similar to that described by Cyr et al. (2008) and it was equipped with an additional air circulation system to drive the extracted pore solution into the collection bottle. The CO_2 in the circulating air was removed by aerating it through a 1 mol/L NaOH solution during extraction process to minimize carbonation of pore solution. The extraction was conducted by using a 3000 kN servo-hydraulic compression testing machine (MTS YAW-3000L) with a loading rate of 1.2 kN/s and loaded up to 1200 kN. For each mix, two pore solution samples were extracted and analyzed. The extracted pore solution was immediately filtered by using a syringe filter with a pore sizes of 0.45 μm to remove the particles in the solution. The concentrations of Na, K, Al, Si and Ca in the pore solution were measured by using an inductively coupled plasma-optical emission spectrometer (ICP-OES, PerkinElmer Optima 8000).

5.2.2.3 SEM/EDX examination

Secondary electron (SE) imaging and energy-dispersive X-ray spectroscopy (EDX) analysis were carried out on the mortar samples after the AMBT tests by using a field emission scanning electron microscope (FESEM, JEOL JSM-7600F). The mortar specimens were fractured to expose the aggregate-binder interfaces for examination. No polishing was conducted on the samples to preserve the full morphology of the ASR products. The fractured samples were freeze-dried at -50℃ under vacuum for 72 h and coated with a platinum layer prior to the analysis.

5.2.2.4 XRD and TGA

After pore solution extraction, the fracture paste samples were crushed and ground to a grain size smaller than 150 μm. The samples were then freeze-dried at -50℃ under

vacuum for 72 h prior to X-ray diffraction (XRD) and thermogravimetric analysis (TGA). The XRD powder diffractograms were obtained by using a Brucker D8 Powder XRD diffractometer with an incident beam of CuKα (λ = 1.5418 Å) radiation and a 2θ scanning range of 10° to 60°. A thermogravimetric analyzer (PerkinElmer TGA 4000) was used to perform qualitative and quantitative analysis of the hydration products and the portlandite content with a heating rate of 10℃/min from 30℃ to 900℃ with N_2 gas flux of 100 ml/min.

5.3 Results

5.3.1 Accelerated mortar bar test

Fig. 5.1 shows the ASR expansions of the OPC and AAS mortar bars in AMBT. The black dotted line represents the acceptable expansion limit (0.1%) of mortar bars stored in alkaline solution for 14 d as prescribed in ASTM C1260. As can be seen, the OPC mortars exhibited a large expansion exceeding the expansion limit in around only 4 d, reaching 0.3% after 14 d. It confirmed that the aggregates used are alkali-silica reactive.

For AAS mortar bars, the results show that the expansion increased with the increasing contents of the additional calcium hydroxide. The control AAS mortars (AAS-C) expands slightly below 0.1% after 14 d, whereas the expansions of all the other AAS mortar samples exceeded the expansion limit. Especially for AAS-10%CH and AAS-25%CH specimens, the length increased substantially in the first 3 d and reached 0.4% and 0.8%, respectively, after 14 d.

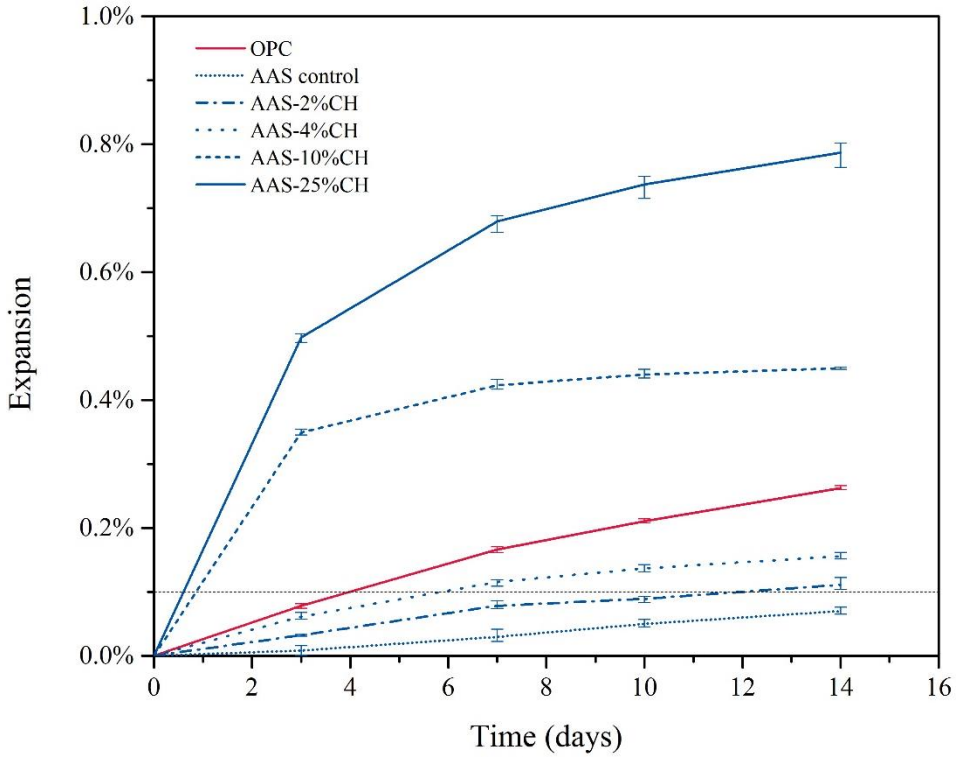

Fig. 5.1 ASR expansion of the OPC and AAS mortar bars in AMBT.

5.3.2 SEM/EDX

The SE images of the ASR products in the mortar samples after alkaline exposure for 14 d are shown in Fig. 5.2. As can be seen, the ASR products with typical "rosette-type" morphology as reported in literature (Davies and Oberholster, 1988; García-Lodeiro et al., 2007) were observed at the aggregate-binder interfaces in the mortars. The morphology of the ASR gel was similar among all the OPC and AAS mortars with different calcium hydroxide dosage.

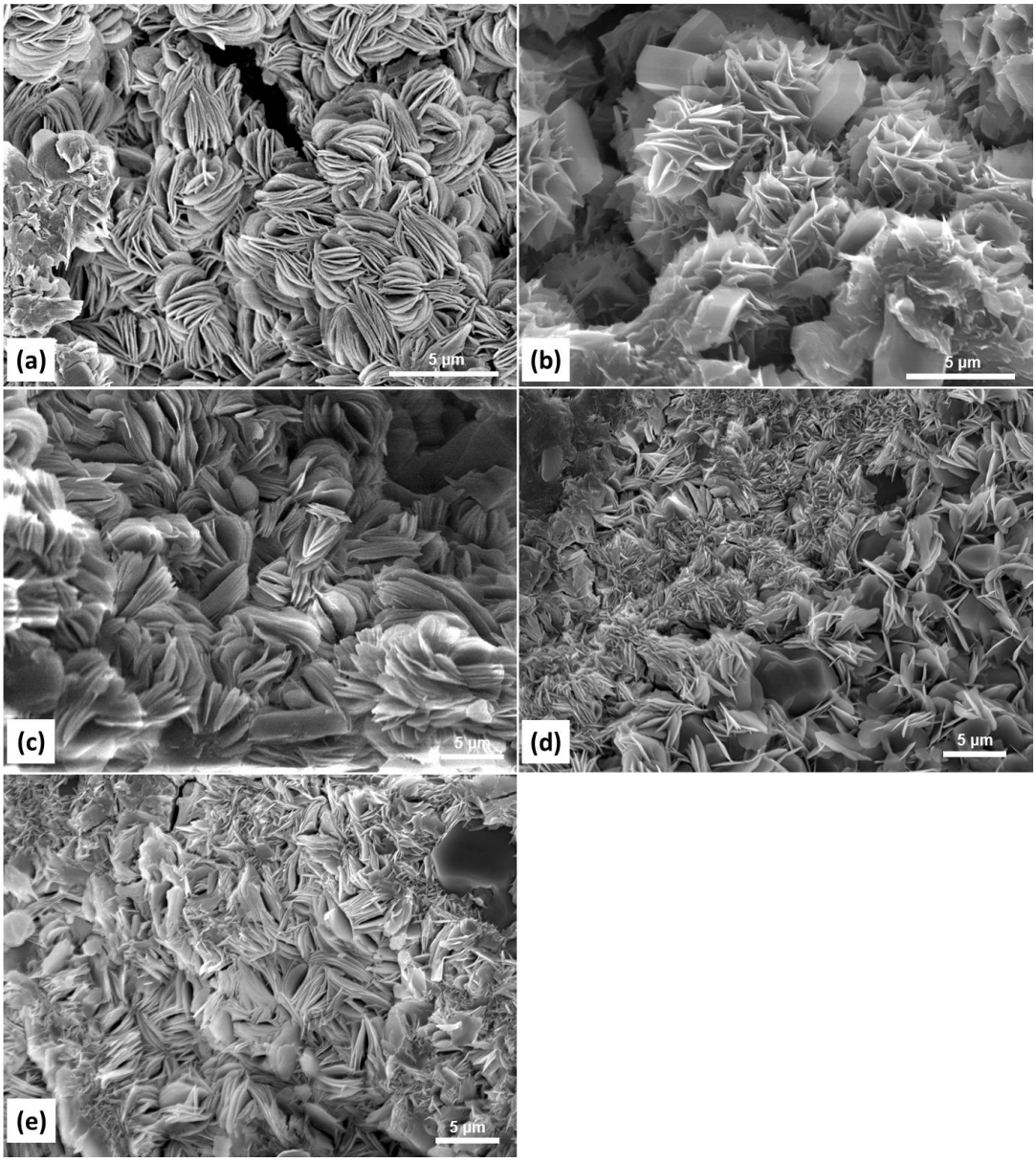

Fig. 5.2 SE images of the ASR products in (a) OPC, (b) AAS-C, (c) AAS-2%CH, (d) AAS-4%CH, and (e) AAS-25%CH mortars after AMBT.

The chemical compositions of these ASR products determined by EDX (Table 5.4) confirmed that these products are typical Na(K)-Ca-silicate ASR gel with similar (Na+K)/Si and Ca/Si molar ratios. Especially, the Ca/Si molar ratio remained stable around 0.2, despite of different calcium hydroxide content within the samples.

Table 5.4 Composition of the ASR products determined by EDX (molar ratio)

Samples	No. of measured points	(Na+K)/Si	Ca/Si
		Average ± errors	
OPC	15	0.39 ± 0.15	0.18 ± 0.03
AAS-C	23	0.43 ± 0.24	0.19 ± 0.10
AAS-2%CH	22	0.66 ± 0.13	0.17 ± 0.05
AAS-4%CH	13	0.44 ± 0.05	0.20 ± 0.03
AAS-25%CH	18	0.40 ± 0.13	0.22 ± 0.02

5.3.3 Pore solution composition

The concentrations of Na, K, Si, Al and Ca in the pore solution of the OPC and AAS pastes at age of 7 d are plotted in Fig. 5.3. The results show that the pore solution of the OPC pastes mainly consists of alkali (sodium, potassium) ions with minor amount of calcium and silicate ions, which is consistent with the pore solution results reported in other literature (Struble, 1988).

In AAS pastes, the pore solution also predominantly contains concentrated alkalis with small amount of calcium and silicates, and the alkali concentrations are one order higher than that of OPC mortars as the concentrated alkali activators used for the slag activation. In contrast to the OPC paste that Al is negligible in the pore solution, the concentration of Al in AAS pore solution is much higher, in the range of 17-28 mmol/L. In general, it is observed that the concentrations of Si and Al in the AAS pore solution reduced with the increased amount of calcium hydroxide added into the mixtures, probably because the additional calcium hydroxide enhanced the formation of C-A-S-H, resulting in the condensation of more Si and Al from the pore solution. Despite the different amount of calcium hydroxide added into the AAS mixture, the concentration of Ca remained almost constant in the AAS pore solution, which is attributed to the low solubility of calcium hydroxide in the highly alkaline pore solution and all the pore solutions have saturated with calcium.

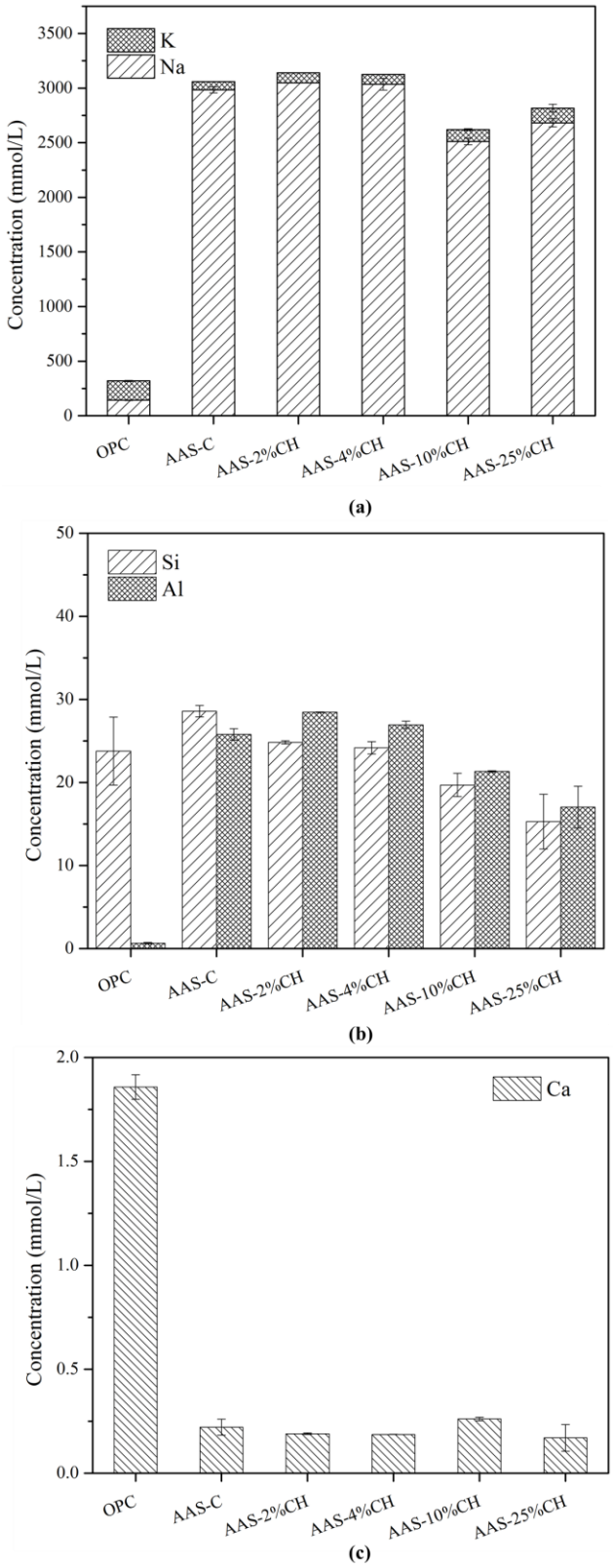

Fig. 5.3 Concentrations of (a) alkalis (Na, K) (b) Si, Al and (c) Ca in the pore solution of OPC and AAS pastes at age of 7 d.

5.3.4 X-ray diffraction

The XRD patterns of OPC and AAS pastes are shown in Fig. 5.4. For OPC pastes, the presence of cement hydration products (*i.e.,* C-S-H and calcium hydroxide) and unreacted cement (*i.e.,* C_3S, C_2S) are prominent in the XRD diagram.

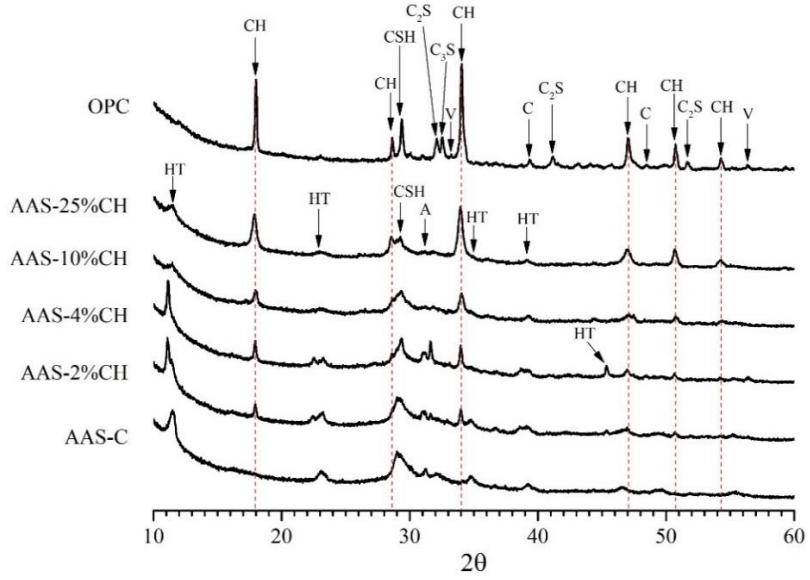

Fig. 5.4 XRD patterns of the OPC and AAS pastes at age of 7 d. (CH: portlandite; CSH: calcium silicate hydrate; Ht: hydrotalcite; C_3S: alite; C_2S: belite; C: calcite; V: vaterite; A: akermanite).

In AAS pastes, the broadened peak at 2θ = 29.5° indicates the poorly crystalline C-S-H in all the pastes, which is the main reaction product in AAS (Duxson and Provis, 2008; Ravikumar and Neithalath, 2012; Wang and Scrivener, 1995). Akermenite ($Ca_2MgSi_2O_7$) and hydrotalcite ($Mg_6Al_2CO_3(OH)_{16}\cdot H_2O$) are also observed in all the pastes. Akermenite is a crystal phase that exists in the unreacted GGBFS (Duxson and Provis, 2008) and hydrotalcite is often observed as one of the products in AAS when Mg content is relatively high in slags (Brough and Atkinson, 2002). It should be noted that no calcium hydroxide was detected in the AAS control paste and the peaks of calcium hydroxide were prominent in all the other AAS pastes. In addition, calcite and vaterite were observed in all the samples, suggesting some of the calcium hydroxide have been carbonated and the carbonation occurred most likely during the crushing the grinding of the samples prior to test.

5.3.5 Thermogravimetric analysis

Fig. 5.5 shows the derivative thermogravimetric (DTG) curves of the OPC and AAS pastes at age of 7 d. The broad peak in a temperature range of 30-230℃ is attributed to the loss of interlayer water of C-S-H, indicating the presence of C-S-H in all the OPC and AAS samples (Taylor, 1997). Three peaks at 200-250℃, 250-300℃ and 300-400℃ are associated with the decomposition of the hydrotalcite or hydrotalcite-like phases (Kim et al., 2013; Wang and Scrivener, 1995), which have also been identified using XRD. The peaks located between 420 and 480℃ indicated the dehydroxylation of the portlandite (Scrivener et al., 2018). Carbonation is also observed in the OPC pastes and the AAS pastes with additional calcium hydroxide. More than one peak was observed in the OPC pastes, AAS-10%CH and AAS-25%CH, as the exact carbonation peaks are strongly dependent on the presence of hemi- and mono-carbonates and the amount and the fineness of the carbonates (Scrivener et al., 2018).

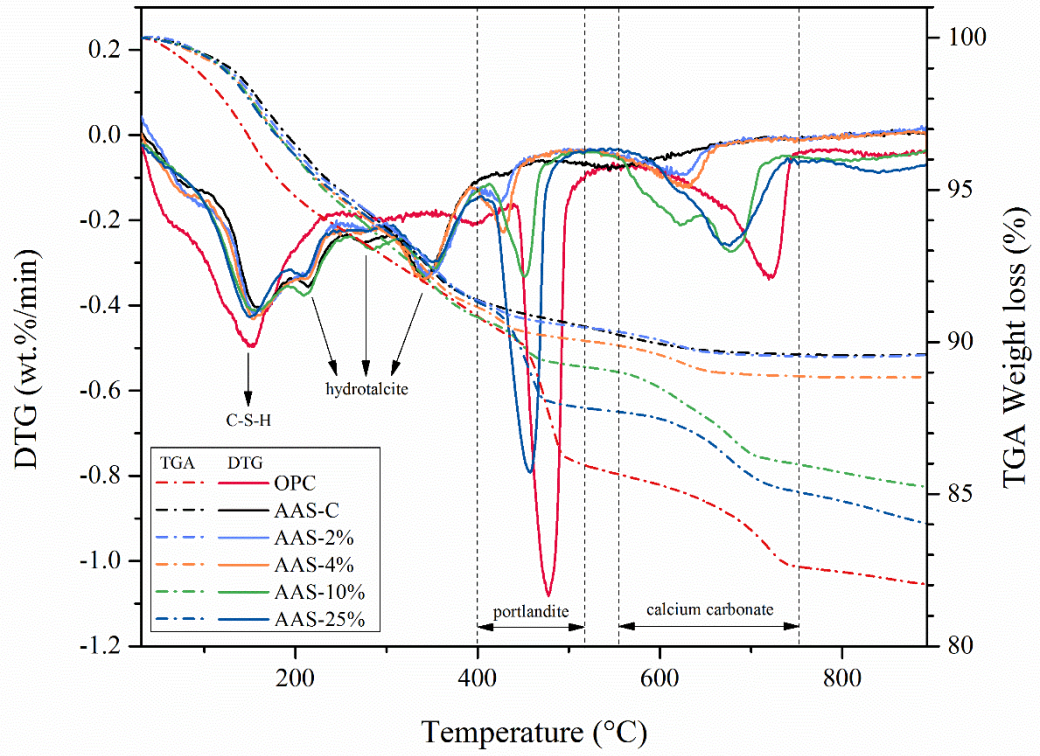

Fig. 5.5 Thermogravimetric results of the OPC and AAS pastes at age of 7 d.

5.4 Discussion

Considering the alkali concentrations in the pore solution of the OPC and AAS pastes are one to two orders higher than the concentrations of the silicate and aluminate counter-ions, it could be concluded that the electrical neutrality in the solution is maintained primarily by hydroxide ions. In this study, thus, the hydroxide ion concentration is assumed to be equal to the alkali concentration as the other ionic species are insignificant compared to alkali ions. This assumption has also been made in other studies (Duchesne and Bérubé, 1994; Swamy, 1992) to estimate the alkalinity of OPC pore solution due to the difficulties to measure the alkalinity of a concentrated solution (Swamy, 1992). Therefore, the alkali concentration as presented in Fig. 5.3a indicates the extremely high hydroxide ion concentration in the AAS pore solution in a range of 2.5-3.2 mol/L, which agrees with the concentration reported in (Lloyd et al., 2010). The estimated hydroxide ion concentration in the pore solution of OPC pastes is 0.32 mol/L, which falls within the typical range for OPC pastes (Struble, 1988).

It is known that the solubility of calcium hydroxide in OPC pore solution is very low due to the concentrated hydroxide ions in pore solution (Struble, 1988). Most of the calcium hydroxide from cement hydration are in solid pastes. The XRD and TGA results showed the presence of portlandite in the AAS pastes with additional $Ca(OH)_2$, indicating the pore solution was saturated with calcium so that the portlandite cannot further dissolve. The relationship between the concentration of calcium and hydroxide ions within the pore solution was plotted in Fig. 5.6, which agrees well with the solubility of $Ca(OH)_2$ in concentrated NaOH solution as reported by Pallagi et al (2012). As can be seen, the solubility of $Ca(OH)_2$ decreases with the increase of hydroxide ion concentration, which explains the lower concentration of calcium ions in AAS pore solution compared to that in OPC. The extremely high alkalinity in AAS pore solution largely suppresses the dissolution of the additional $Ca(OH)_2$. Thus, the majority of $Ca(OH)_2$ remained in solid forms in the AAS pastes, which could act as the reservoir of soluble calcium and hydroxide ions, albeit some of the $Ca(OH)_2$ have been carbonated as shown in the XRD and TGA results.

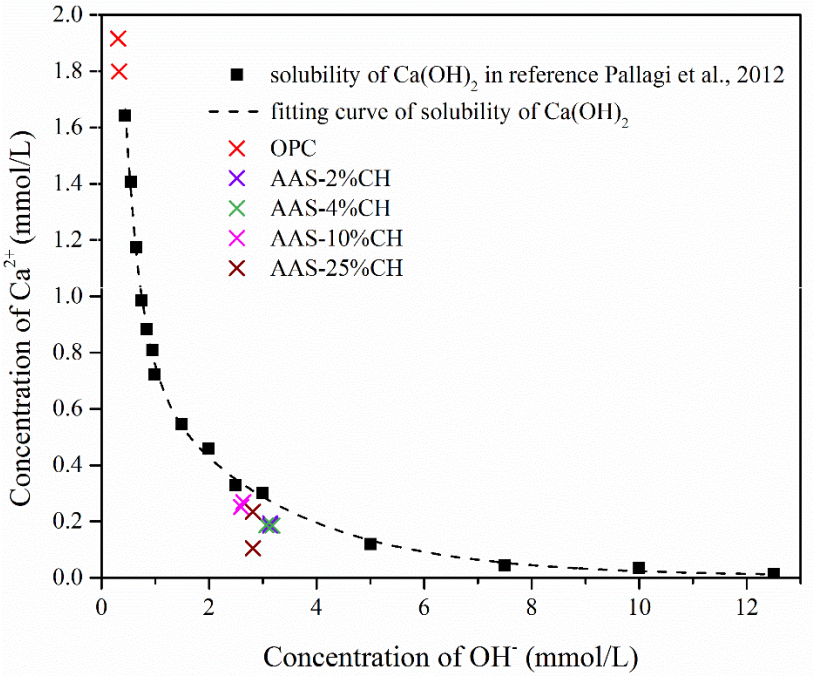

Fig. 5.6 The relationship between the concentrations of calcium and hydroxide ions within the pore solution.

The amount of portlandite in the solid pastes has been calculated according to the weight loss of the portlandite in the TGA results following:

$$\text{Mass of portlandite} = \text{portlandite weight loss} \times m_{Ca(OH)_2} / m_{H_2O},$$

where $m_{Ca(OH)_2}$ and m_{H_2O} are the molecular mass of portlandite and water, respectively. The relationship between the solid portlandite in the pastes and the expansion of the mortar at 14 d in AMBT are plotted in Fig. 5.7. It is observed that the expansion level of the AAS mortar varied significantly and highly dependent on the amount of the calcium hydroxide, despite the extremely high pore solution alkalinity in all the AAS mortars.

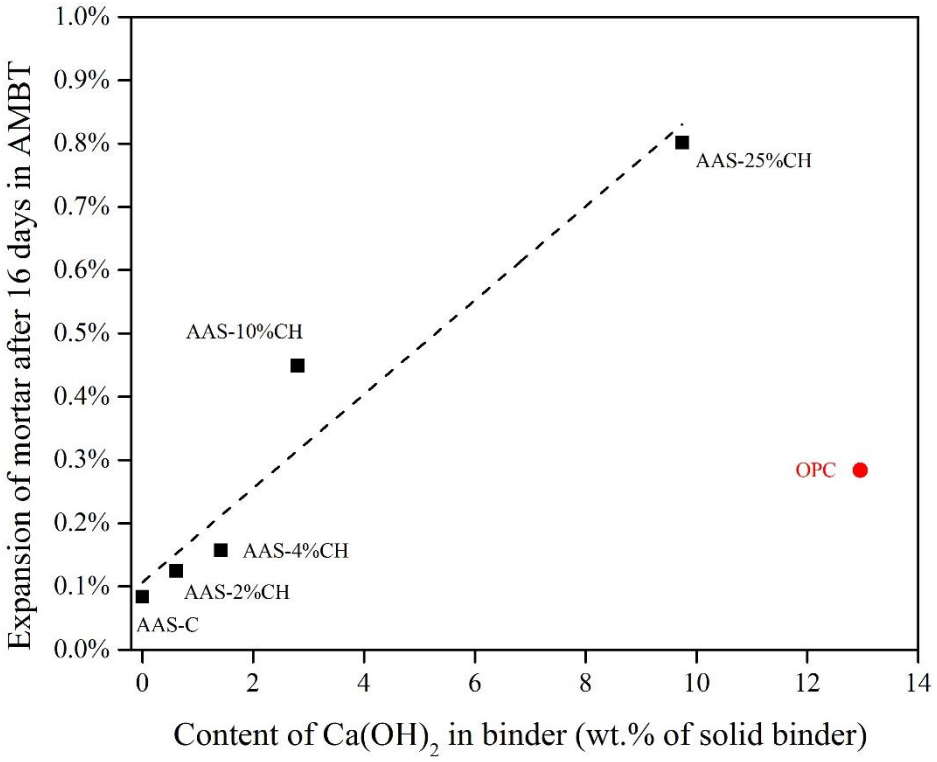

Fig. 5.7 The relationship between the expansions of mortars in AMBT and the content of $Ca(OH)_2$ within the binder.

The sufficient alkalinity in pore solution has been reported as a key prerequisite for deleterious ASR expansions (Vayghan et al., 2016; Shehata and Thomas, 2006) and several minimum hydroxide ion concentrations of pore solution have been suggested to trigger ASR in OPC concrete (Diamond, 1983a; Duchesne and Bérubé, 1994; Kollek et al., 1986; Struble, 1988; Michael Thomas et al., 2006). A minimum value of hydroxide ion concentration in a range of 0.2-0.3 mol/L has been reported in several studies (Diamond, 1983a; Kollek et al., 1986; Michael Thomas et al., 2006), while a relatively higher threshold around 0.65 mol/L was suggested by Duchesne and Bérubé (Duchesne and Bérubé, 1994). In the present study, the hydroxide ion concentration in the pore solution of AAS sample is roughly three to four times higher than the upper value of the thresholds mentioned above for OPC concrete. However, the AAS-C mortar only exhibited innocuous ASR expansion and the expansion increased with the increasing amount of additional calcium hydroxide, suggesting the insufficient pore solution alkalinity is not the only controlling factor limiting the ASR

expansion in AAS concrete. The $Ca(OH)_2$ also plays an important role in the deleterious ASR expansions.

As previously mentioned, calcium hydroxide could influence the ASR expansion of OPC mortar by acting as a "pH buffer" that maintains the pore solution alkalinity, facilitating the gelation process, or modifying the expansive property of the gel (Bleszynski and Thomas, 1998; Glasser and Kataoka, 1982; Gaboriaud et al., 1999; Vayghan et al., 2016; Rajabipour et al., 2015). The effect as a "pH buffer" is more likely to play an important role when the pore solution alkalinity is a limiting factor, such as in the OPC mortar where the hydroxide ion concentration of pore solution is around 320 mmol/L. In the AAS mortars in this study, there was no shortage of hydroxide ion concentration in the pore solution.

The SEM and EDX analysis indicate that no noticeable difference was observed in the ASR products formed in all the OPC and AAS mortars in terms of morphology as well as chemical compositions. Especially the calcium content remained stable with a Ca/Si ratio of around 0.2 in all the ASR products, which suggests the similar swelling capacity of these ASR products. The varied expansion of the mortar, thus, was most likely due to the different amount of this type of ASR products formed within the mortars.

Therefore, the increased ASR expansion resulting from the additional calcium hydroxide here was most likely because the increased amount of calcium in the system facilitated the linking of the dissolved silicate species in the pore solution to form poly-metal-silicate gel and promoted the dissolution of the reactive silica and the formation of the expansive ASR products (Glasser and Kataoka, 1982; Gaboriaud et al., 1999).

5.5 Summary

This study investigated the effect of additional calcium hydroxide on the ASR expansion of AAS mortars. The results show that the AAS mortar exhibited innocuous ASR expansion despite its high pore solution alkalinity, suggesting the insufficient alkalinity was not the only controlling factor for its low ASR expansion. Furthermore, the expansion of the AAS mortars increased with the increasing content

of the additional calcium hydroxide, indicating the presence of calcium was controlling the ASR expansion behavior.

No obvious difference was observed in the ASR products in all the mortars in terms of morphology and chemical composition. It is thus believed that the additional calcium hydroxide facilitated the gelation of the dissolved silicate species in the pore solution, resulting in the formation of larger amount of expansive ASR products. The low ASR expansion of the original AAS mortar was most probably attributed to the limited expansive ASR product formed in the mortar with deficiency of calcium.

Chapter 6 Production of ASR-Free Geopolymer Concrete by Using Local Alkali-silica Reactive Rocks as Aggregates and Precursors

6.1 Overview

Industrial by-products such as fly ash are widely used nowadays as aluminosilicate precursors for geopolymer binder production, which is environmentally friendly and cost-efficient. However, the utilization of these by-products are subjected to the variability in their characteristics and the local availability. The local availability of the precursors does not only determine the likelihood of adoption of the geopolymer binder for a specific location, but also influences the environmental benefits as the transport of bulk materials can dominate the emissions footprint of the binder as a whole if long distance transportation is required (McLellan et al., 2011; Provis, 2016). In addition, the competition in demand from the use of fly ash in blends with OPC may also restrain the available raw materials for geopolymer binders. Thus, increasing research efforts have been made recently to broaden the selection of precursors, especially to seek a local solution to utilize the local available sources for geopolymer binder productions (Shi et al., 2019).

The study in this chapter provides a solution to produce locally available geopolymer precursor by using the locally abundant IRC rocks. These local rock minerals are rich in silica and alumina, which potentially are an appealing natural source for geopolymer precursors. Moreover, ASR-free geopolymer concrete was produced by using the synthesized precursors and the local alkali-silica reactive rocks. The ASR resistance of the produced geopolymer concrete was investigated as a demonstration.

6.2 Materials and methods

6.2.1 Materials

The obtained JRC rocks were washed, dried, crushed and ground into particle size less than 150 μm for thermal treatment. The chemical composition of the rock powder is shown in Table 6.1. As can be seen, silica and alumina constitute 63.7% and 13.3% by mass, respectively, of the rocks. The XRD pattern (Fig. 6.1) indicates that quartz and albite are the major crystalline components of the JRC rocks. The sodium

hydroxide and alumina powder used are of AR grade from Sigma-Aldrich with a purity more than 96%. The average particle size of the alumina powder is less than 10 μm.

Table 6.1 Chemical compositions of the JRC rock (% by mass)

	SiO_2	Al_2O_3	Fe_2O_3	CaO	MgO	K_2O	Na_2O	P_2O_5	SO_3	TiO_2
JRC rocks	63.7	13.3	3.8	2.2	0.5	4.1	3.5	0.1	2.1	0.4

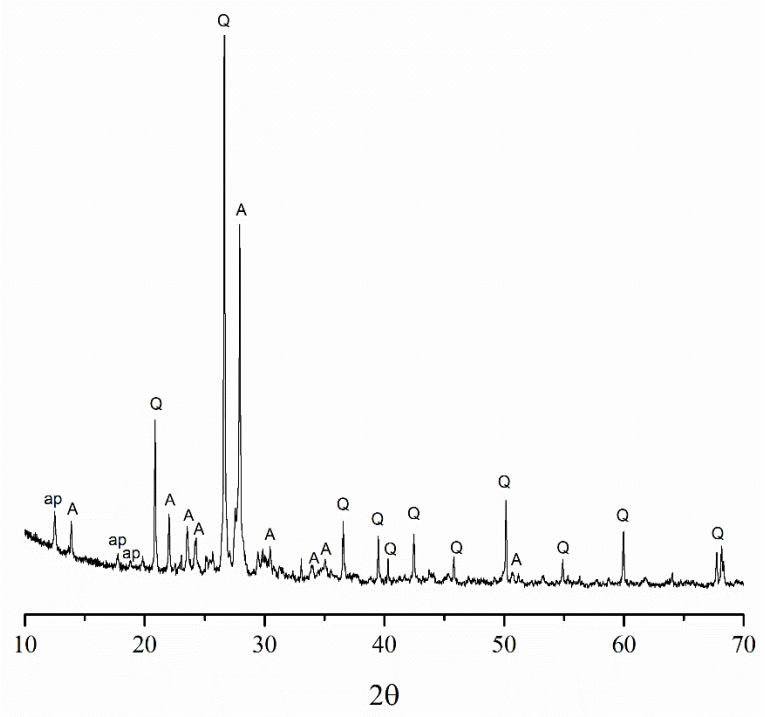

Fig. 6.1 XRD patterns of the JRC rocks (Q: quartz, A: albite, ap: aluminum phosphate, Fe: iron).

6.2.2 Thermal treatment

The JRC rocks contain a large proportion of silica and alumina, which makes them appealing as a geopolymer source material. Because the rocks mainly consist of crystalline quartz and albite, they have low reactivity for alkali-activations (Lahoti et al., 2017). Thermal treatment with sodium hydroxide was thus employed in the study to prepare glassy geopolymer precursors. Different content of alumina was added during the thermal treatment to tailor the composition of the produced aluminosilicate precursors. The JRC rock powder was dry mixed with specified amount of alumina

and sodium hydroxide powder as shown in Table 6.2. Samples 1-6 kept the same Na/Al molar ratio at 2.5 with varied Si/Al molar ratio from 1.5 to 4.1. Samples 4, 7, 8 and 9 kept the same Si/Al molar ratio at 3.0 with varied Na/Al molar ratio from 1.0 to 2.5.

Table 6.2 Mix compositions used to prepare glassy geopolymer precursors.

No.	Sample	Mix compositions by mass (g)			Molar ratio	
		JRC rock	Al_2O_3	NaOH	Si/Al	Na/Al
1	Al1.5-Na2.5	100	22.8	70.8	1.5	2.5
2	Al2.0-Na2.5	100	13.8	53.1	2.0	2.5
3	Al2.5-Na2.5	100	8.4	42.5	2.5	2.5
4	Al3.0-Na2.5	100	4.7	35.4	3.0	2.5
5	Al3.5-Na2.5	100	2.2	30.3	3.5	2.5
6	Al4.1-Na2.5	100	0	26.1	4.1	2.5
7	Al3.0-Na2.0	100	4.7	28.3	3.0	2.0
8	Al3.0-Na1.5	100	4.7	21.2	3.0	1.5
9	Al3.0-Na1.0	100	4.7	14.2	3.0	1.0

The mixture was placed into ceramic crucibles after being mixed evenly and heated in a muffle furnace at 1250℃ for 2 h. After heating, the mixture was allowed to cool down to 800℃ in the furnace and then was taken out from the furnace, exposed to room temperature (23±2℃) for a more rapid cooling. The obtained precursor was pulverized in a planetary ball mill with rotation speed of 300 rpm and sieved to ensure the particles size was under 45 μm.

6.2.3 Alkali activation and compressive strength

The pulverized precursor was activated by a 8 mol/L NaOH solution with a solution-to-solid ratio of 0.38, by mass. The resulting paste was cast into 20 mm cubic molds and cured at 80°C and 98% RH for 48 h. After curing, the cubes were placed in ambient condition (23±2°C and 65±5% RH) for another five days until the compressive strength was measured. The average compressive strength of three cubes for each mix was reported.

6.2.4 Sample characterization

X-ray diffraction (XRD) and magic-angle spinning nuclear magnetic resonance (MAS NMR) analysis were conducted on the pulverized precursors. The XRD powder diffractograms were obtained by using a Brucker D8 Powder XRD diffractometer with an incident beam of CuKα (λ = 1.5418 Å) radiation and a 2θ scanning range of 10° to 70°. The ^{29}Si and ^{27}Al MAS NMR spectra were obtained by using a Bruker Avance III HD 600 spectrometer (14.1 T) with a spinning speed of 10 kHz. ^{29}Si spectra were acquired at 119.24 MHz with a 90° pulse of 4 μs, recycle delay of 60 s and 700 scans. ^{27}Al spectra were acquired at 156.39 MHz with a 90° pulse of 3 μs, recycle delay of 2 s and 800 scans. The chemical shifts of ^{29}Si and ^{27}Al were externally referenced to tetraethoxysilane (TEOS) and $AlCl_3$ at -82.04 ppm and 0 ppm, respectively.

6.2.5 Dissolution test

Dissolution test on the pulverized precursor in the alkaline solution was conducted to directly determine the reactive silicate and aluminate species within the precursors. 1 g of the pulverized precursor was dissolved in 1000 g of NaOH solution with concentration of 8 mol/L. The solution-to-solid mass ratio of 1000 was selected to prevent the condensation of the aluminosilicate from the soluble silicate and aluminate species (Buchwald et al., 2009; Xu and van Deventer, 2000). Solution sample of 2 ml was obtained each time at 1, 3, 5, 7, 11 and 15 d. The solution was filtered with a 0.45 μm filter and the concentrations of silicon and aluminum were measured by using an inductively coupled plasma-optical emission spectrometry (ICP-OES, PerkinElmer Optima 8000).

6.2.5 Accelerated mortar bar test (AMBT)

The geopolymer mortar bars were prepared by using the produced precursor and the JRC rocks as aggregates. The precursor was dry-mixed with the graded aggregates as shown in Table 6.3 with an aggregate-to-binder ratio of 2.25, and then mixed with 8 mol/L NaOH solution with a solution-to-binder ratio of 0.38. For comparison, OPC mortar bars contain the same JRC aggregates were prepared with the same aggregate-to-binder ratio of 2.25 and a water-to-binder ratio of 0.47.

Table 6.3 Gradation of JRC rocks used as aggregates

Sieve Size		Mass, %
Passing	Retained on	
4.75 mm (No. 4)	2.36 mm (No. 8)	10
2.36 mm (No. 8)	1.18 mm (No. 8)	25
1.18 mm (No. 8)	600 μm (No. 30)	25
600 μm (No. 30)	300 μm (No. 50)	25
300 μm (No. 50)	150 μm (No. 100)	15

All the geopolymer and OPC mortar bars were cast into the molds with a dimensions of 25 mm × 25 mm × 285 mm. After casting, the OPC mortar bars were cured at 23℃ for 48 h and the geopolymer mortar bars were cured at 80°C for the same duration (*i.e.*, 48 h). All the specimens were cured in an environmental chamber with 98% RH to prevent moisture loss. After curing, the specimens were de-molded and subsequently stored in water in sealed containers in an oven at 80℃ for 24 h. Immediately after the 24 h curing, the initial lengths of the mortar specimens were measured by using a digital length comparator with accuracy of 1μm. The specimens were then immersed in 1 mol/L NaOH solutions in sealed containers in an oven at 80℃ for 14 d. The lengths of the specimens were routinely measured and the average expansions of three mortar bars for each mix were reported.

6.3 Results and discussion

6.3.1 Geopolymer binder production by using JRC rocks

Figs 6.2 and 6.3 shows the XRD patterns of the produced precursors after thermal treatment. As can be seen, the original crystalline phases of quartz and albite within the JRC rocks (Fig. 6.1) were not detected in the precursors. Instead, all the precursors exhibit a broad hump in a range of 20-35°, suggesting that the crystalline quartz and albite were converted into amorphous phases. In addition, the sharp peaks of a crystalline aluminosilicate phase, carnegieite ($NaAlSiO_4$, PDF #96-101-0954), was detected in the precursor Al1.5-Na2.5, and small peaks of this phase were also observed in the precursor Al2.0-Na2.5 and Al2.5-Na2.5. The carnegieite phase was

formed, probably due to the recrystallization during the cooling of the melted aluminosilicate phases (Markovic et al., 2003) and it seems that the higher aluminum content added into the mixture promoted the formation of the crystalline carnegieite phase. The formation of sodium sulfate (Na_2SO_4) detected in the precursors is likely due to the decomposition of the sulfate phases within the JRC rocks (Table 6.1) during the heat treatment.

Fig 6.4 displays the ^{27}Al MAS NMR spectra of the JRC rock, Al_2O_3 and the produced precursors. The JRC rock mainly consist of four-coordinated aluminum (q^4), which is attributed to the aluminum in albite (Wang-hong and Kirkpatrick, 1989) in the JRC rocks, and a small amount of six-coordinated aluminum (q^6). The Al_2O_3 added in the mixture only consist of a single peak with an average chemical shift of 15 ppm (Choi et al., 2009). After thermal treatment, the peak attributed to the Al_2O_3 disappeared and a broad q^4 peak was observed in all the precursors, indicating that the additional Al_2O_3 was incorporated into the silicate network in the JRC rock and turned into four-coordinated aluminum. A small peak attributed to the Al_2O_3 detected in the precursor Al3.0-Na2.5, Al2.0-Na2.5 and Al3.0-Na2.5 is most likely due to the uneven mixing of the powder before thermal treatment, resulting in a small amount of Al_2O_3 remains unreacted. Moreover, it is observed that the q^4 peak width of the precursors (except Al1.5-Na2.5) after thermal treatment is increased compared to that of JRC rocks. It suggested that the aluminosilicate structure of the sample after thermal treatment is more disordered than the original JRC rock, which is consistent with the XRD results in Fig. 6.2 and 6.3. The relatively smaller peak width of the sample Al1.5-Na2.5 is due to the formation of a large amount of crystalline aluminosilicate phase as showed in Fig. 6.2.

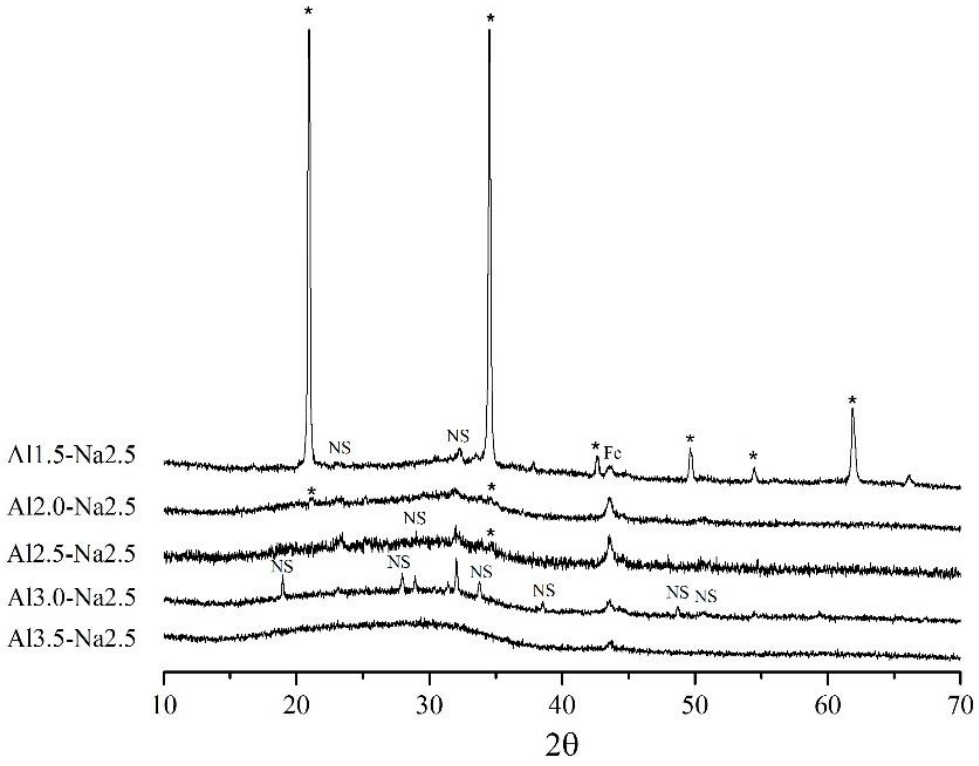

Fig. 6.2 XRD patterns of the produced precursors with Si/Al ratio from 1.5 to 3.5 and Na/Al ratio at 2.5 (NS: sodium sulfate, Fe: iron; *: carnegieite, $NaAlSiO_4$).

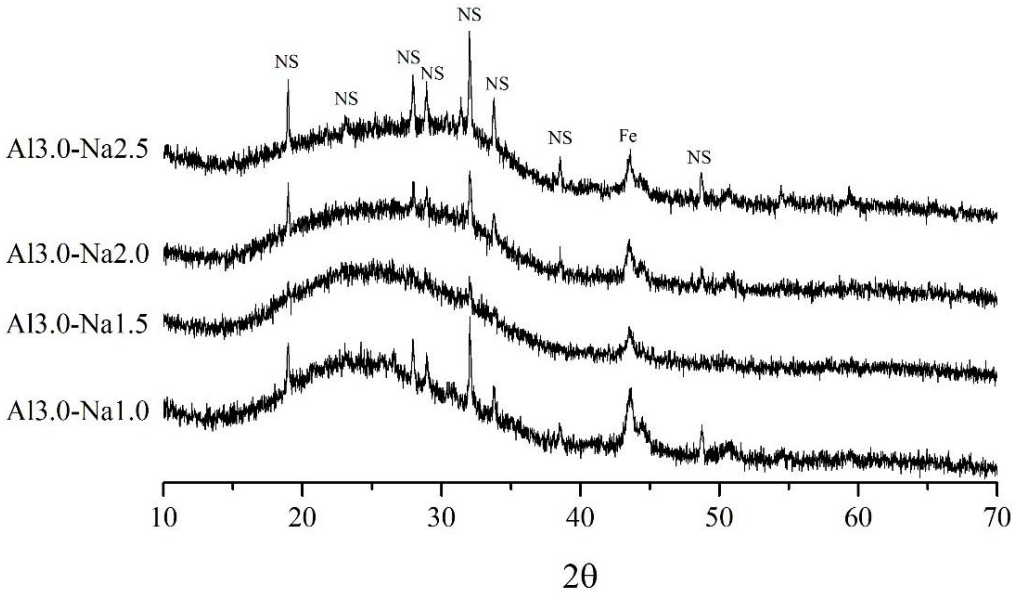

Fig. 6.3 XRD patterns of the produced precursors with Na/Al ratio from 1.0 to 2.5 and Si/Al ratio at 3.0 (NS: sodium sulfate, Fe: iron;).

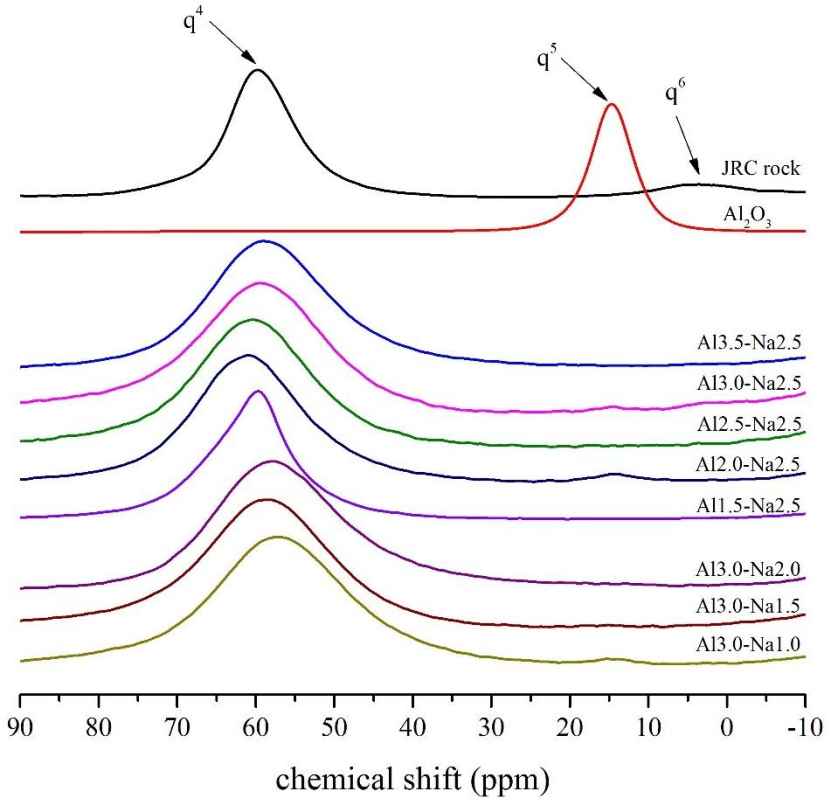

Fig. 6.4 ^{27}Al MAS NMR spectra of the JRC rock, Al_2O_3 and the produced precursors.

Fig 6.5 shows the ^{29}Si MAS NMR spectra of precursors. All the spectra exhibit a wide band in a range of chemical shift from -60 to -110 ppm, which is attributed to the signal of the combination of silicon environments Q^n(mAl), where n indicates the number of the bridges to silicon or aluminum and m is the number of Al neighbors. To obtain more information on the silicon coordination environments, deconvolution of the ^{29}Si MAS NMR spectra was conducted according to the peak assignments of Q^n(mAl) in the literature (Bass and Turner, 2002; Buchwald et al., 2011; Duxson et al., 2005; Engelhardt, 1989). The spectra were fitted by Gaussian-Lorentzian sum function. Peak positions for each identified species were maintained constant throughout the deconvolution process. The deconvolution results of the precursor Al3.0-Na2.5 are shown in Fig. 6.6 and a summary of the percentage of Q^n site silicon of each precursor is presented in Fig. 6.7. The deconvolution results of the other precursors are presented in the appendix.

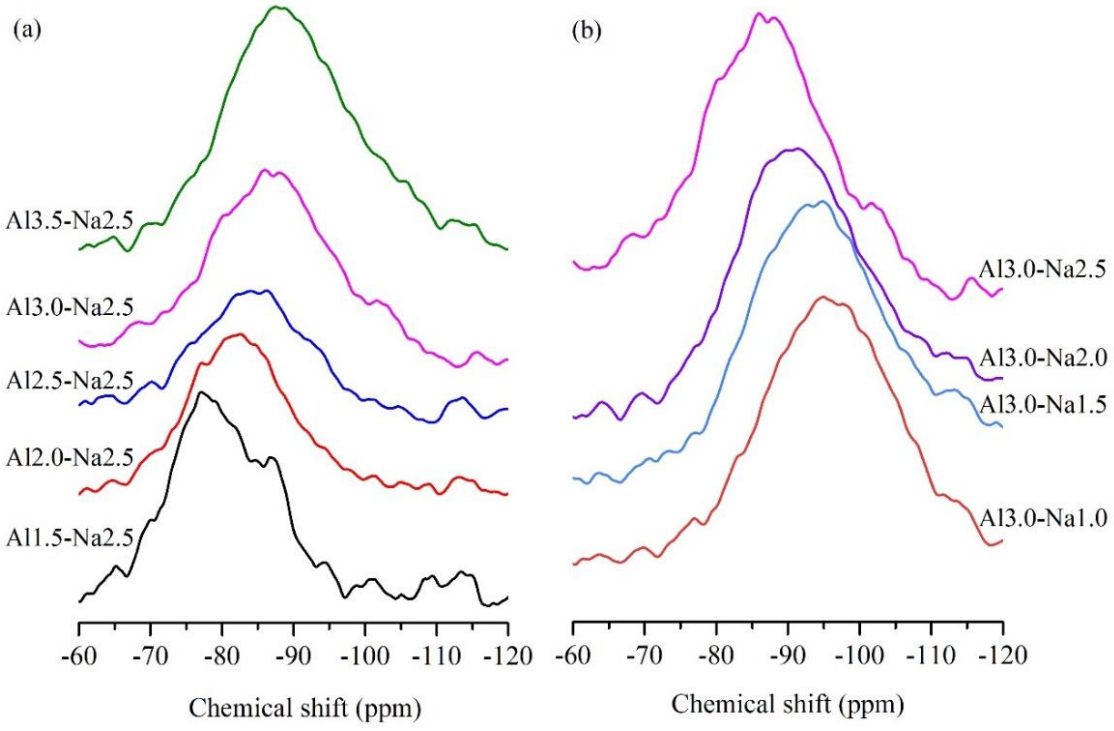

Fig. 6.5 ^{29}Si MAS NMR spectra of the precursors.

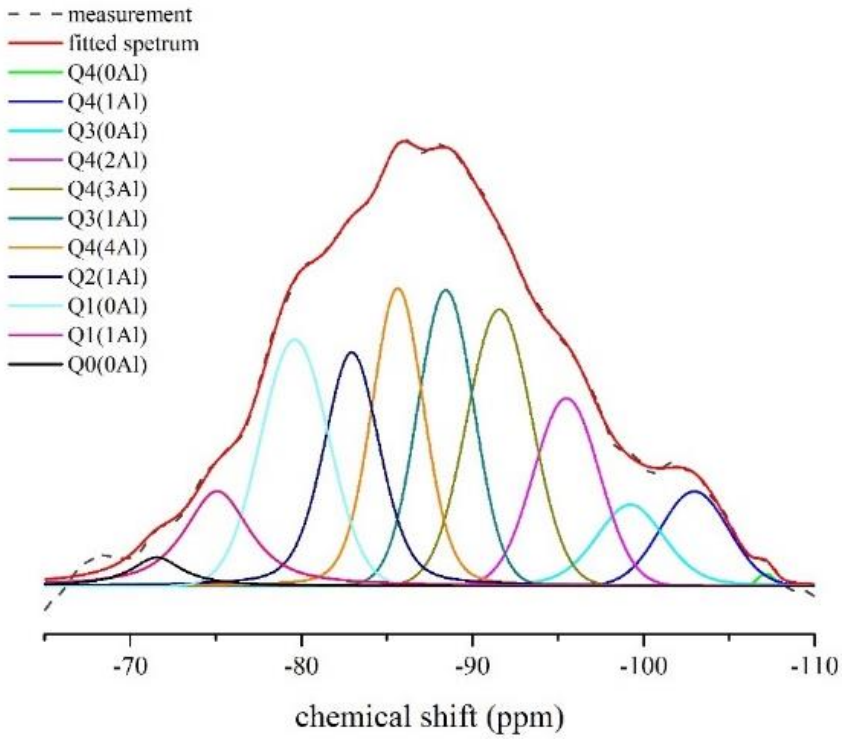

Fig. 6.6 Deconvolution of the ^{29}Si MAS NMR spectra of the precursor Al3.0-Na2.5.

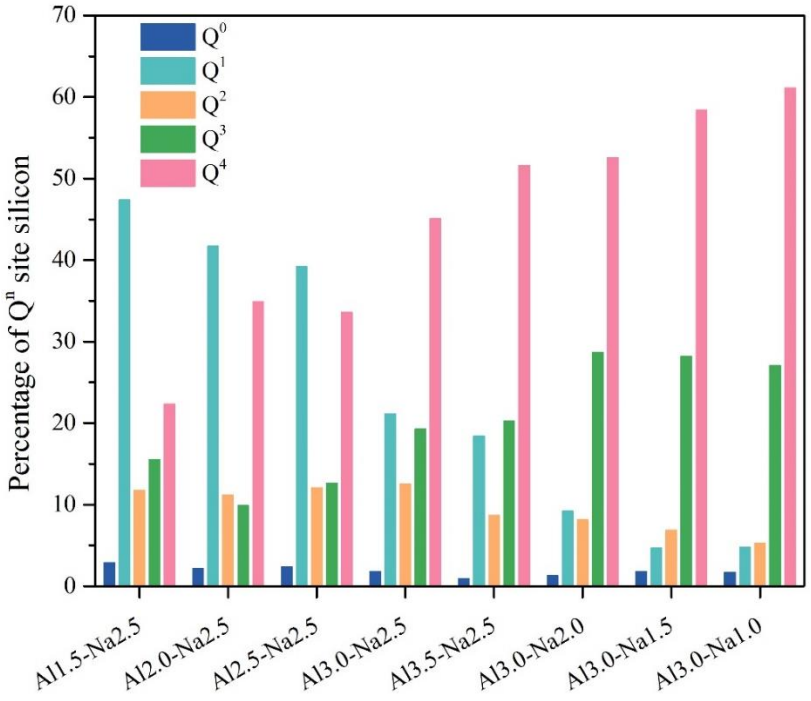

Fig. 6.7 Percentage of Q^n (n = 0, 1, 2, 3 and 4) site silicon of each precursor.

As shown in Fig. 6.7, the relative intensity of Q^4 increased and the relative intensity of Q^1 reduced with the decrease of the Si/Al ratio (*i.e.*, from precursor Al3.5-Na2.5 to Al1.5-Na2.5) and the increase of the Na/Al ratio (*i.e.*, from precursor Al3.0-Na1.0 to Al3.0-Na2.5), indicating that the degree of polymerization of the precursors decreases as the increase of the alumina and sodium hydroxide added during thermal treatment.

The concentration of the released Si and Al as a function of time in the dissolution tests on the precursors in 8 mol/L sodium hydroxide solution is shown in Fig. 6.8. As shown in Fig. 6.8a, the precursor Al1.5-Na2.5 exhibits highest initial releasing rate of silicates and the initial releasing rate was reduced with increasing Si/Al, as the aluminosilicate network is more polymerized with increasing Si/Al as shown in Fig. 6.7. Despite the fastest initial releasing rate, the dissolution of the precursor Al1.5-Na2.5 is almost stopped after only 1 day, which ends up with a lower Si concentration at 15 d compared to that of the precursors Al3.0-Na2.5, Al2.5-Na2.5 and Al2.0-Na2.5. It is mainly attributed to the formation of the crystalline carnegieite phase in the sample Al1.5-Na2.5 as shown in Fig. 6.2, which reduced the amount of soluble silicates in the precursor. A small amount of crystalline carnegieite was also detected

in the precursors Al2.5-Na2.5 and Al2.0-Na2.5 (Fig. 6.2). The formation of crystal explained the lower silicate concentration compared to that of the precursor Al3.0-Na2.5. The sample Al3.5-Na2.5, which has the lowest aluminum content, exhibited the lowest silicate concentration at equilibrium at 15 d. It suggests that the reactivity of the aluminosilicate glass is reduced as the increase of the Si/Al ratio. The relationship is consistent with the previous study on the dissolution of aluminosilicate glasses (Hamilton et al., 2001). The author proposed that the decrease of the glass reactivity with higher Si/Al ratio was attributed to that the Al-O-Si bonds are more readily broken than Si-O-Si bonds based on the thermodynamic calculations. The release of Al in the dissolution test for the sample with varied Si/Al ratio (Fig. 6.8c) showed that releasing rate of aluminate and the concentration of aluminate at equilibrium are increased with the decrease of the Si/Al ratio of the samples, indicating the aluminum content in the sample is the key factor for the release of Al.

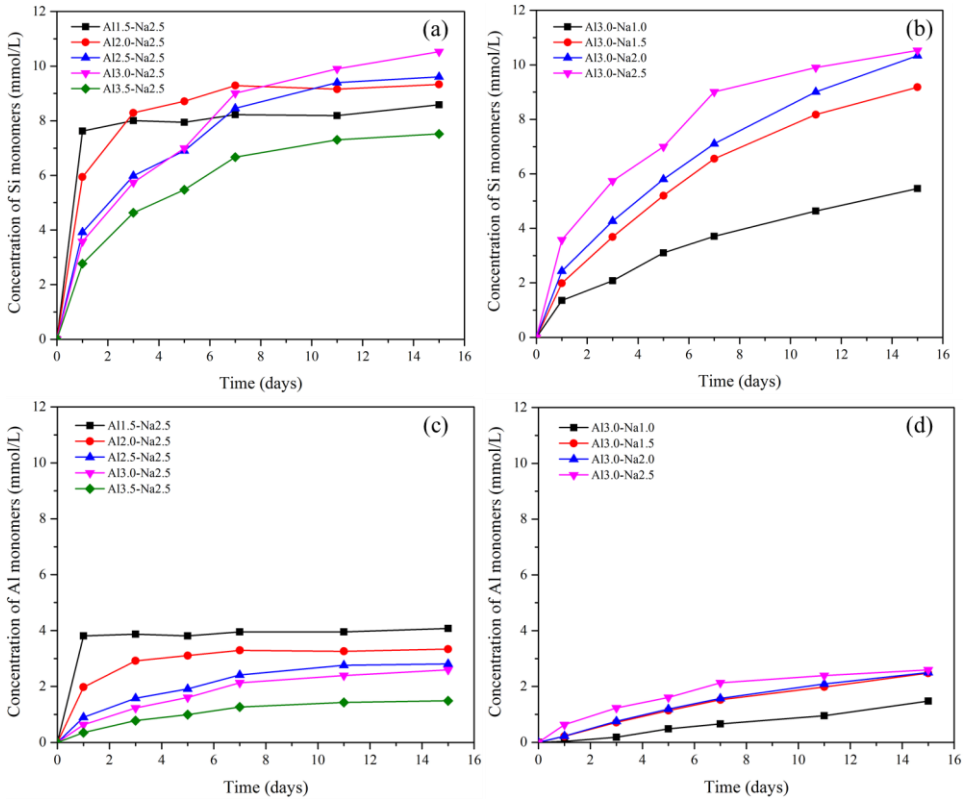

Fig 6.8 Concentration of the (a, b) Si and (c, d) Al as a function of time in the dissolution tests on the precursors in 8 mol/L sodium hydroxide solution.

For the sample with varied Na/Al ratio, the releasing rate of Si and Al is generally increased with the increase of the sodium content (Figs. 6.8b and 6.8d), as the sodium acts as a network modifier to the aluminosilicate glass. The increased sodium content resulted in less polymerized aluminosilicate network as shown in Fig. 6.7. Of particular interest is that the effect of additional sodium hydroxide on the reactivity of the aluminosilicate glass is seen to be diminished based on the concentration of the released Si at 15 d. The silicate concentration rose by 3.7 mmol/L with an increase of Na/Al ratio from 1.0 to 1.5 compared to a 1.1 mmol/L increase between the Na/Al ratio from 1.5 to 2.0, and the concentration remained in the same level when Na/Al ratio was further increased from 2.0 to 2.5. Therefore, the efficiency of the sodium hydroxide on enhancing the reactivity of the precursor should be considered during the selection of the amount of sodium hydroxide added in the mixture.

Fig. 6.9 shows the compressive strength of the alkali-activated binder at 7 d. As can be seen, for the binder produced from the precursor with Na/Al ratio of 2.5, the strength was increased with the increase of the Si/Al ratio from 1.5 to 3.0, and then decreased at the Si/Al ratio of 3.5. The trend is consistent with the concentration of the soluble silicates in the dissolution tests (Fig. 6.8a). The precursor Al3.0-Na2.5 exhibited the highest concentration of the soluble silicates, indicating the largest amount of the reactive aluminosilicates in the precursors, which is the most likely reason for the highest strength after activation. The soluble silicate species in pore solution significantly influence growth and reorganization of the aluminosilicate gel during the condensation process, which determine the microstructure and physical property of the binder (Duxson et al., 2007). The increase of soluble silicates for condensation could increase the volume of the gel and densify the microstructure, resulting in higher strength (Duxson et al., 2005).

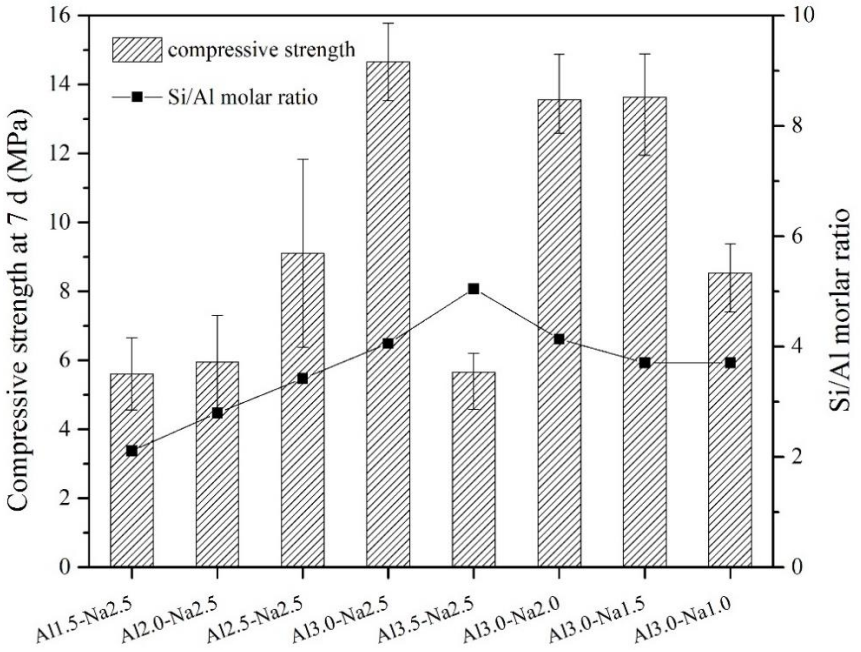

Fig. 6.9 Compressive strength of the alkali-activated binder at 7 d and the soluble Si/Al molar ratio of the corresponding precursor in dissolution test.

Many studies have reported the a range of Si/Al molar ratio of the geopolymer binder that the strength of the binder could be maximized, which generally lies to the range of 1.7-2.3 (Davidovits, 1999; Duxson et al., 2005; Fletcher et al., 2005; Pimraksa et al., 2011). In this study, according to the soluble Si and Al in the dissolution test, the maximum strength of the binder was achieved at Si/Al ratio at 4.1 (Fig. 6.9), which is significantly higher than the optimal range proposed in other studies. The strength of the binder is believed to increase by reducing the Si/Al ratio to the proposed range. However, the increase of the aluminum content in the mixture for the precursor production (like precursor Al1.5-Na2.5, Al2.0-Na2.5) promoted the formation of crystalline aluminosilicates, which decreased the amount of the reactive aluminosilicate for the geopolymerization, ending up with lower strength of the binder. Since the crystalline phase is most likely formed during the cooling process as only natural cooling was adopted, it is believed that by quenching the mixture with Na/Al ratio lies in the optimal range after thermal treatment could further enhance the strength of the produced binder.

For the binder produced from the precursor with the Si/Al ratio of 3.0, the compressive strength of the binder reached a similar level at the Na/Al ratio of 2.5,

2.0 and 1.5, and the strength was significantly reduced by around 39% at the Na/Al ratio of 1.0. The strength of the binder also agrees well with the reactivity of the corresponding precursor obtained in the dissolution test, *i.e.*, the precursor with Na/Al ratio of 2.5, 2.0 and 1.5 exhibited a similar level of soluble silicates and aluminates, which is remarkably higher than that of the precursor Al3.0-Na1.0. It confirms that the strength of the binder is highly dependent on the content of the reactive phases of the precursor produced in this study.

6.3.2 ASR expansion of the geopolymer mortar produced by using JRC rocks as aggregates and precursors.

The precursor Al3.0-Na1.5 was selected to produce the geopolymer mortar, as the corresponding binder exhibited the highest compressive strength (14-15 MPa) but consumed lowest amount of sodium hydroxide compared to the other binders with comparable strength. The reduction of the amount of sodium hydroxide used during the precursor production could significantly lower the cost as well as the environmental impacts for the geopolymer production.

The ASR expansion result of the geopolymer mortar produced by using precursor Al3.0-Na1.5 and JRC rocks as aggregates is shown in Fig. 6.10. The ASR expansion of the OPC mortar containing JRC aggregates was evaluated for a comparison. As can be seen, the OPC mortars exhibited a large expansion exceeding the expansion limit in only 7 d, reaching 0.2% at 14 d, confirming that the JRC rocks are highly reactive and the use of JRC rocks in the OPC concrete must be prohibited.

The studies in the previous chapters suggested that the lack of calcium is the controlling factor for the low ASR expansion in alkali-activated concrete. In the present study, since the geopolymer binder produced by the precursor Al3.0-Na1.5 contained limited calcium content that originally from the JRC rocks (Table 6.1), as expected, the produced geopolymer mortars only expanded slightly, far below the expansion limit, suggesting the produced geopolymer binder is innocuous to ASR.

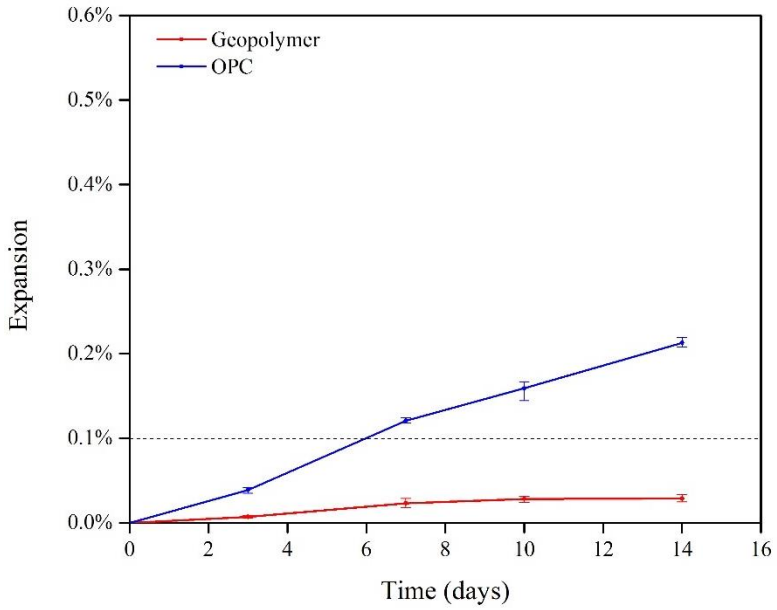

Fig. 6.10 ASR expansion of the geopolymer mortar produced from the precursor Al3.0-Na1.5 and OPC mortar containing alkali-silica reactive JRC aggregates.

6.4 Summary

Geopolymer precursor was produced by employing thermal treatment on the local alkali-silica reactive rock mixed with alumina and sodium hydroxide. After the thermal treatment, the crystalline structure of the quartz and albite within the rocks were broken down, forming a disordered, amorphous geopolymer precursor. The structure of the precursor was less polymerized as the increase of the amount of the alumina and sodium hydroxide added for the precursor production, while the increase of aluminum content promoted the formation of aluminosilicate crystal during the cooling process, which reduced the reactivity of the precursors. After alkali activation, geopolymer binder with maximum compressive strength of around 15 MPa was produced.

Moreover, the ASR-free geopolymer mortar was prepared by using the produced precursor and the local alkali-silica reactive rocks as aggregates. As a demonstration, the ASR expansion test was conducted on the geopolymer mortar. The results suggest the produced geopolymer mortar was innocuous to ASR.

Chapter 7 Conclusions and Future Work

7.1 Conclusions

The objective of the present study is to produce a reliable ASR-free geopolymer concrete by using the local ASR-suspicious rocks as both aggregates and precursors. On one hand, the influence of the geopolymer pore solution on the ASR resistance of the geopolymer concrete was investigated to understand the reason for the ASR resistance of the geopolymer concrete. The pore solution chemistry of geopolymer concrete was studied, followed by the individual investigations into the effect of pore solution alkalinity, aluminum and calcium in the pore solution on the ASR expansion behavior of the geopolymer concrete. On the other hand, the method of geopolymer precursor synthesis by using the local ASR-suspicious rocks was explored. The optimization of the binder was conducted by tailoring the composition of the produced precursor to improve the mechanical strength of the binder. Moreover, an ASR-free geopolymer concrete was produced and demonstrated by using the local ASR-suspicious rocks as both aggregates and precursors. The significant findings and main conclusions are summarized as follows.

- The pore solution of the low-calcium geopolymer binder was mainly composed of alkali ions, silicates and aluminosilicates species. The composition was different from that of OPC pore solution where high concentration of alkali hydroxide is the dominating component. Silicon with Q^0-Q^4 sites were detected in the geopolymer pore solution and all the aluminum in the pore solution were tetrahedrally coordinated, present in the form of aluminosilicate oligomers.
- Although the alkaline activators with high alkalinity was used, the pH level of the geopolymer pore solution reduced significantly after activation mainly due to the consumption of hydroxide ions for the dissolution of the precursors.
- The insufficient alkalinity usually observed in the geopolymer pore solution was one controlling factor for the ASR resistance of the geopolymer concrete. The low pore solution alkalinity could limit the dissolution of the reactive aggregates, thus the ASR was unlikely to be triggered.
- The geopolymer concrete with elevated pore solution alkalinity was still resistant to ASR, although significant dissolution of the reactive aggregates was observed.

It suggested that the insufficient alkalinity was not the only controlling factor for ASR in geopolymer concrete.

- The expansion of the AAS mortars increased with the increasing content of the additional calcium hydroxide, indicating the presence of calcium was controlling the ASR expansion behavior of AAS mortar. The effect of calcium on ASR was most probably due to the additional calcium facilitated the gelation of expansive ASR products. The results provided an indication that the deficiency of calcium in geopolymer concrete pore solution could account for the ASR resistance of the geopolymer concrete.
- The influence of the aluminum on the ASR mitigation in OPC concrete was reported to be due to the incorporation of aluminum into the silica structure on the aggregate surfaces, resulting a reduction of the silica dissolution rate. While the incorporation of the aluminum into the aggregate was not detected after the reaction of the geopolymer pore solution with the reactive aggregate, it suggested that the ASR resistance of the geopolymer concrete was probably not attributed to the aluminum presented in the pore solution.
- The geopolymer precursor could be produced from the ASR-suspicious rocks by the thermal treatment on a mix of rocks, alumina and sodium hydroxide in the powder form. The crystalline phases within the rocks were converted into an amorphous precursor. The structure of the precursor was less polymerized with the increase of the amount of the alumina and sodium hydroxide.

7.2 Future work

Due to the low efficiency of pore solution extraction on geopolymer mortars, the pore solution of the geopolymer pastes was extracted and analyzed without considering the influences of the aggregates on the pore solution. It is suggested to conduct a comparable study on the pore solution of the corresponding geopolymer mortars, which are more representative to the geopolymer concrete in practical situations.

In Chapter 4, the effect of the pore solution alkalinity on the ASR expansion of the geopolymer concrete was studied. The pore solution of the geopolymer MK_1.5 was increased by adjusting the activating solution while alkalinity was still slightly lower

compared to that of the OPC pore solution. It is suggested to extend the experiments to a geopolymer with higher alkalinity in the activating solution to further confirm conclusion in Chapter 4. The sodium silicate solution that was used for the activation of MK_1.5 geopolymer is almost saturated with the sodium ions. Other types of activating solution with higher alkalinity, such as NaOH solution should be used instead of the sodium silicate solution.

In Chapter 4, the expansion of the MK_1.5 concrete prisms in CPT was explained to be attributed to the further condensation of aluminosilicate species in the pore solution after the age of 28 d. Despite some indirect evidences provided, the explanation lacks of direct evidence to support. It is suggested to systematically investigate the content, the structure and the volume change of the geopolymer binders at the age from 7 to 56 d to understand the potential source of expansion.

In Chapter 5 and 6, the accelerated mortar bar test according to ASTM 1260 was applied to evaluate the ASR expansion of the AAS and the geopolymer mortars for a rapid test. The method was proposed based on the conventional cementitious material. It would raise following issues when it was applied to alkali-activated concrete. The aggressive condition in AMBT was reported to influence the chemical stability of the geopolymer matrix, and it may lead to the transition of amorphous geopolymers to crystalline zeolitic phases (Fernandez-Jimenez et al., 2007; García-Lodeiro et al., 2007; Nguyen and Škvára, 2016). In addition, the 1-M NaOH storage solution will leach alkali and hydroxide from the mortar bars with higher concentration in their pore solution. Both issues makes the applicability of this method to alkali-activated concrete questionable. Despite that, it is still the most commonly used test applied in evaluating ASR in alkali-activated concrete (Provis and van Deventer, 2014), due to the lack of other accelerated test. The other standard accelerated ASR tests that applied to alkali-activated concrete should be developed.

In the thesis, the ASR resistance of the geopolymer concrete was studied by using two types reactive aggregates, *i.e.*, novaculite (Table 4.1) and local JRC rocks (Table 6.1), which are both siliceous aggregates with minor content of alkalis and calcium. The conclusion drawn in the study may not apply to certain reactive aggregate types such as soda-lime glass, volcanic glass and some alkali-containing aggregates, as the

reactive aggregates may act as a source of alkali and calcium ions during the dissolution of the aggregates, which could influence the pore solution alkalinity and the gelation process of the silicate species. Thus, the research is suggested to be extended to cover more types of reactive aggregates.

In the thesis, the ASR resistance of the geopolymer concrete was only studied through laboratory investigations according to ASTM C 1293 and ASTM C 1260. It is suggested to study the ASR in geopolymer concrete in a larger sample size and exposed to natural environment, which is more close to the condition of practical applications, to increase the reliability of the test results.

In Chapter 6, the geopolymer binder was produced employing thermal treatment on the JRC rocks mixed with alumina and sodium hydroxide. The reactivity of the precursor was compromised due to the formation of crystal during the cooling process. It is suggested to further increase the precursor reactivity by quenching the molten glass after thermal treatment. In addition, life cycle assessment is suggested to be conducted on the produced geopolymer binder from the locally available rocks to analyze the cost benefits and environmental impacts of the proposed method.

Appendix

The deconvolution results of the ^{29}Si MAS NMR spectra of the geopolymer precursors are presented below.

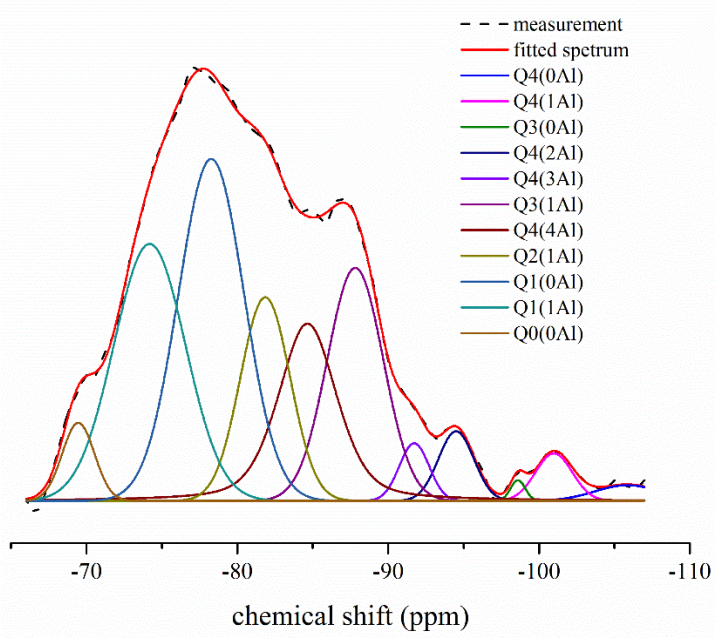

Fig. A1 Deconvolution of the ^{29}Si MAS NMR spectra of the precursor Al1.5-Na2.5.

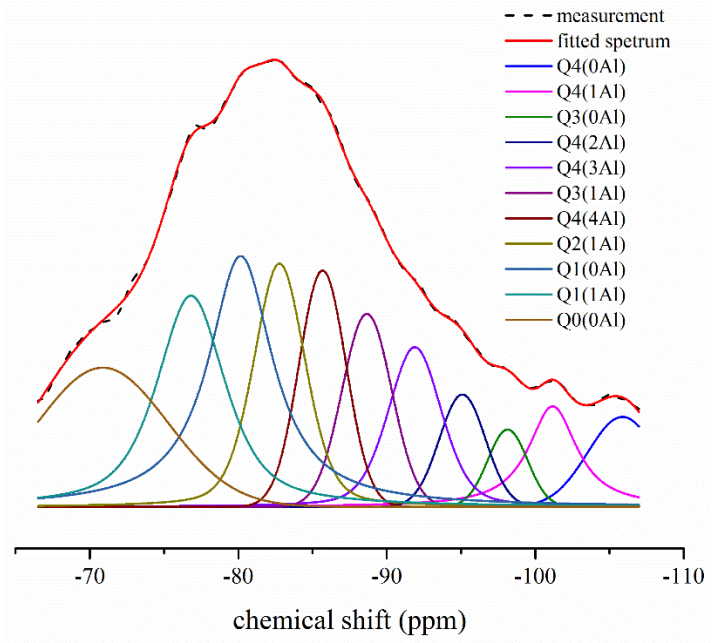

Fig. A2 Deconvolution of the ^{29}Si MAS NMR spectra of the precursor Al2.0-Na2.5.

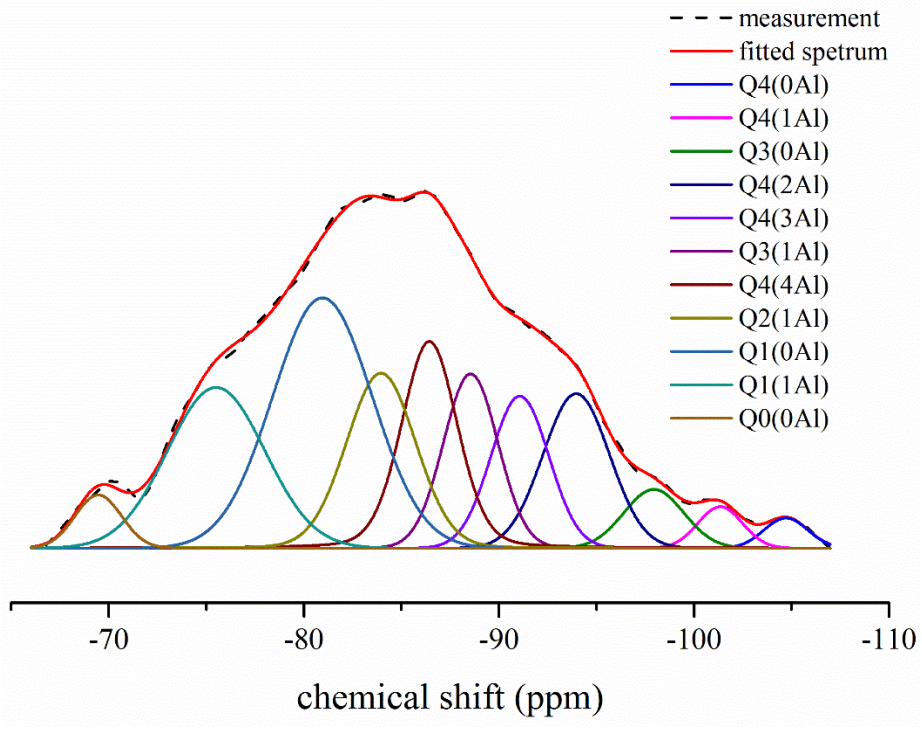

Fig. A3 Deconvolution of the ^{29}Si MAS NMR spectra of the precursor Al2.5-Na2.5.

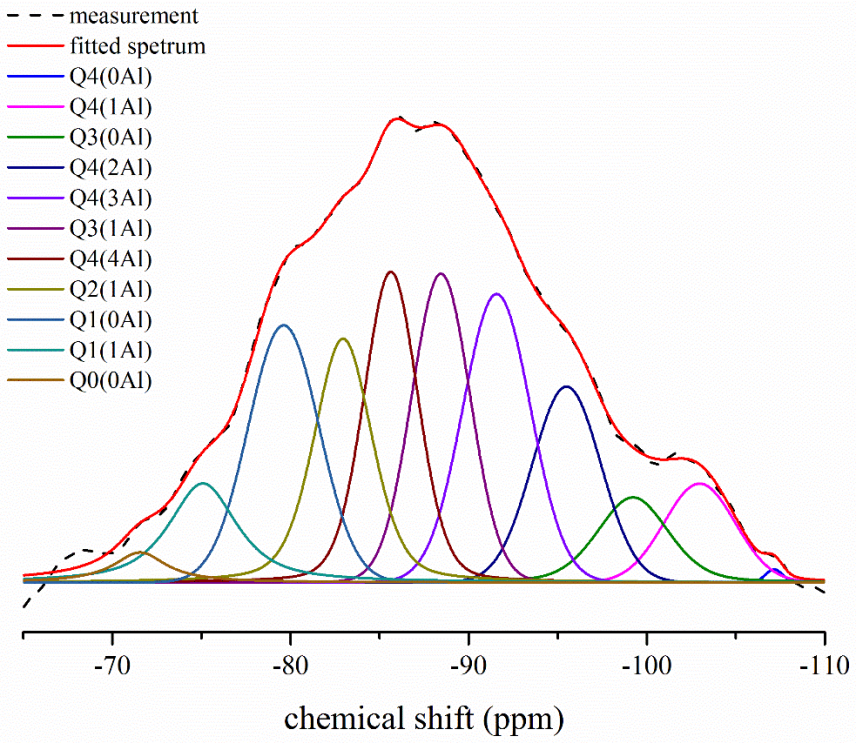

Fig. A4 Deconvolution of the ^{29}Si MAS NMR spectra of the precursor Al3.0-Na2.5.

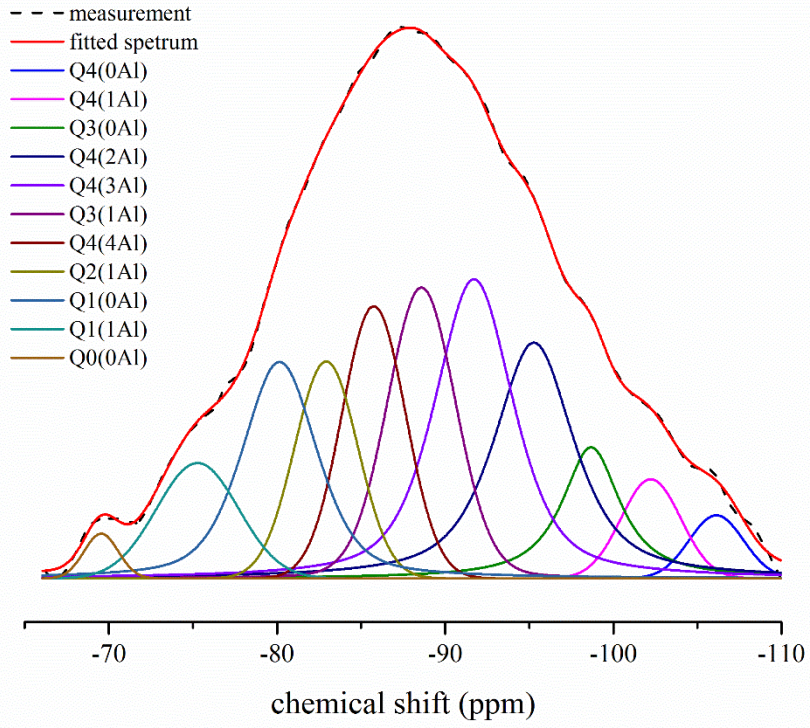

Fig. A5 Deconvolution of the ^{29}Si MAS NMR spectra of the precursor Al3.5-Na2.5.

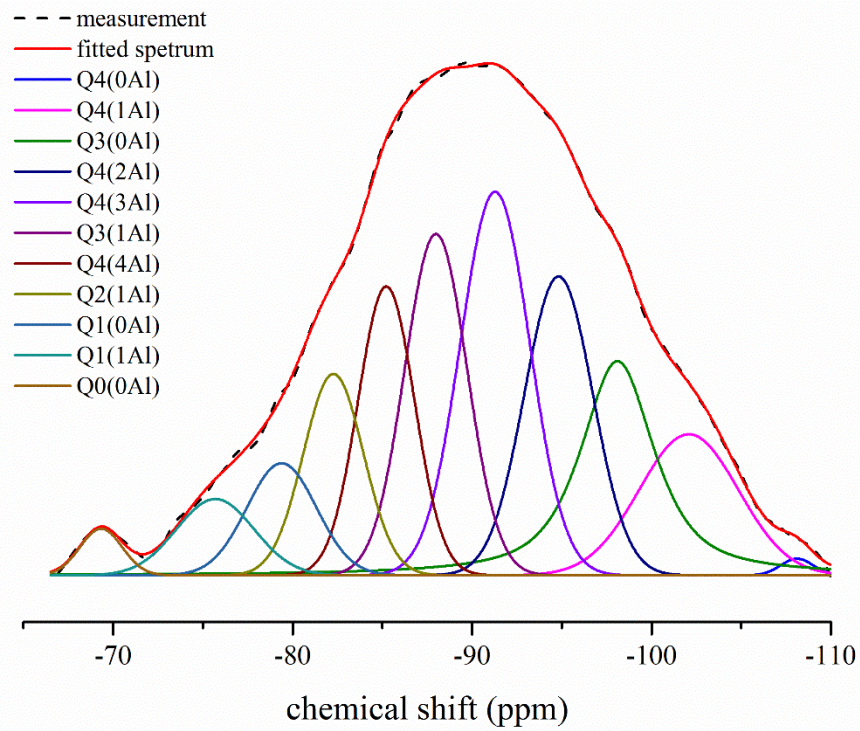

Fig. A6 Deconvolution of the ^{29}Si MAS NMR spectra of the precursor Al3.0-Na2.0.

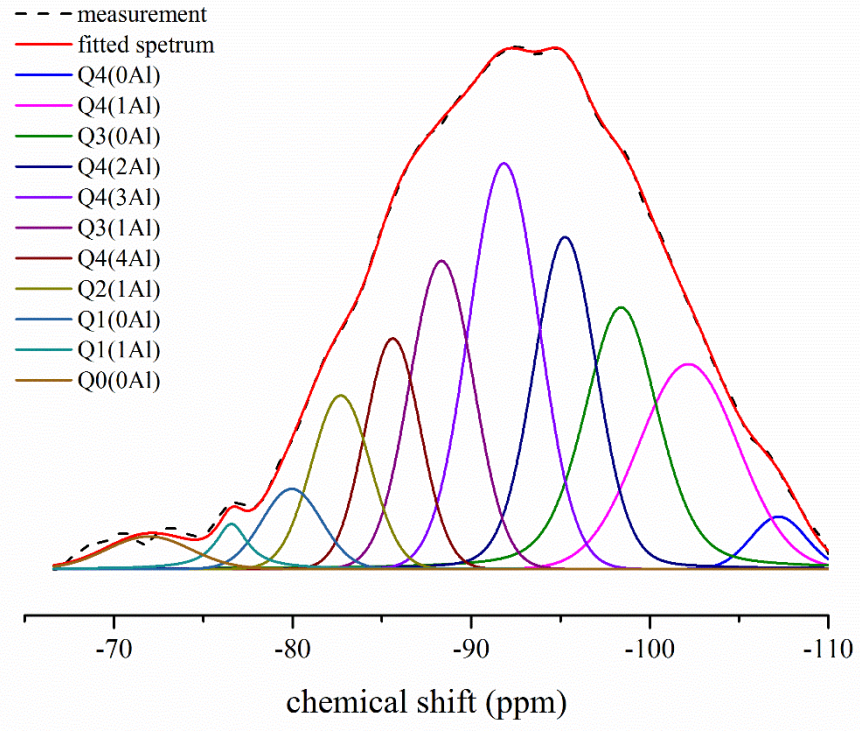

Fig. A7 Deconvolution of the ^{29}Si MAS NMR spectra of the precursor Al3.0-Na1.5.

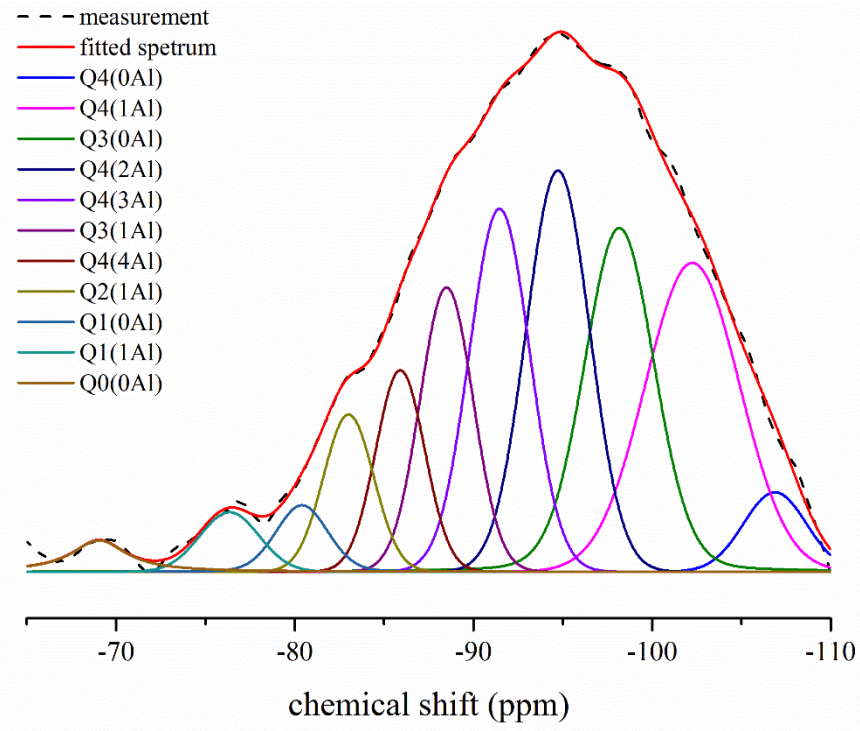

Fig. A8 Deconvolution of the ^{29}Si MAS NMR spectra of the precursor Al3.0-Na1.0.

References

Abdullah, M. M. A., Kamarudin, H., Bnhussain, M., Khairul, N. I., Rafiza, A. R. and Zarina, Y. (2011). The Relationship of NaOH Molarity, Na_2SiO_3/NaOH Ratio, Fly Ash/Alkaline Activator Ratio, and Curing Temperature to the Strength of Fly Ash-Based Geopolymer. Advanced Materials Research, 328–330, 1475–1482.

Alasali, M. M. and Malhotra, V. M. (1991). Role of Concrete Incorporating High Volumes of Fly Ash in Controlling Expansion due to Alkali-Aggregate Reaction. ACI Materials Journal, 88(2), 159–163.

Andersen, M. D., Jakobsen, H. J. and Skibsted, J. (2003). Incorporation of Aluminum in the Calcium Silicate Hydrate (C-S-H) of Hydrated Portland Cements: A High-Field ^{27}Al and ^{29}Si MAS NMR Investigation. Inorganic Chemistry, 42(7), 2280–2287.

Aquino, W., Lange, D. A. and Olek, J. (2001). The Influence of Metakaolin and Silica Fume on the Chemistry of Alkali - Silica Reaction Products. Cement and Concrete Composites, 23(8), 485–493.

ASTM C1293-08b (2015), Standard Test Method for Determination of Length Change of Concrete Due to Alkali-Silica Reaction, Annual Book of ASTM Standards.

ASTM C1260-14 (2014), Standard Test Method for Potential Alkali Reactivity of Aggregates (Mortar-Bar Method), Annual Book of ASTM Standards.

Azizi, S. N. and Ehsani-Tilami, S. (2009). Theoretical and Experimental ^{27}Al NMR Chemical Shift Studies on End-Group Aluminates Linked to Different Silicate Species. Journal of the Chinese Chemical Society, 2009, 56, 898-907.

Bakharev, T. (2005). Durability of Geopolymer Materials in Sodium and Magnesium Sulfate Solutions. Cement and Concrete Research. 35(6), 1233-1246

Barbosa, V. F., MacKenzie, K. J., and Thaumaturgo, C. (2000). Synthesis and Characterisation of Materials Based on Inorganic Polymers of Alumina and Silica: Sodium Polysialate Polymers. International Journal of Inorganic Materials, 2(4), 309-317.

Barneyback, R. S. and Diamond, S. (1981). Expression and Analysis of Pore Fluids from Hardened Cement Pastes and Mortars. Cement and Concrete Research, 11(2), 279–285.

Bass, J. L. and Turner, G. L. (2002). Anion Distributions in Sodium Silicate Solutions. Characterization by ^{29}Si NMR and Infrared Spectroscopies and Vapor Phase Osmometry. The Journal of Physical Chemistry B, 101(50), 10638-10644.

Bell, A. T. (1999). NMR Applied to Zeolite Synthesis. Colloids and Surfaces A: Physicochemical and Engineering Aspects. 158(1-2), 221-234.

Bernal, S. A., de Gutierrez, R. M., Provis, J. L. and Rose, V. (2010). Effect of Silicate Modulus and Metakaolin Incorporation on the Carbonation of Alkali Silicate-Activated Slags. Cement and Concrete Research, 40(6), 898-907.

Bernal, S. A. and Provis, J. L. (2014). Durability of Alkali-Activated Materials: Progress and Perspectives. Journal of the American Ceramic Society, *97*(4), 997–1008.

Bernal, S. A., Provis, J. L., Fernández-Jiménez, A., Krivenko, P. V., Kavalerova, E., Palacios, M., and Shi, C. (2014). Binder chemistry - High-calcium alkali-activated materials. Alkali Activated Materials, 59-91.

Bleszynski, R. F. and Thomas, M. D. A. (1998). Microstructural Studies of Alkali-Silica Reaction in Fly Ash Concrete Immersed in Alkaline Solutions. Advanced Cement Based Materials, *7*(2), 66–78.

Brough, A. R. and Atkinson, A. (2002). Sodium Silicate-Based, Alkali-Activated Slag Mortars - Part I. Strength, Hydration and Microstructure. Cement and Concrete Research, 32(6), 865-879.

Brus, J., Abbrent, S., Kobera, L., Urbanova, M. and Cuba, P. (2016). Advances in ^{27}Al MAS NMR Studies of Geopolymers. Annual Reports on NMR Spectroscopy, (Vol. 88, pp. 79-147), Academic Press.

Buchwald, A., Hohmann, M., Posern, K. and Brendler, E. (2009). The Suitability of Thermally Activated Illite/Smectite Clay as Raw Material for Geopolymer Binders. Applied Clay Science, 46(3), 300-304.

Buchwald, A., Zellmann, H. D. and Kaps, C. (2011). Condensation of Aluminosilicate Gels-Model System for Geopolymer Binders. Journal of Non-Crystalline Solids, 357(5), 1376-1382.

Burciaga-Díaz, O. and Escalante-García, J. I. (2013). Structure, Mechanisms of Reaction, and Strength of an Alkali-Activated Blast-Furnace Slag. Journal of the American Ceramic Society, 96(12), 3939-3948.

Chappex, T. and Scrivener, K. (2012a). Alkali Fixation of C-S-H in Blended Cement Pastes and Its Relation to Alkali Silica Reaction. Cement and Concrete Research, 42(8), 1049–1054.

Chappex, T. and Scrivener, K. (2012b). The Influence of Aluminium on the Dissolution of Amorphous Silica and Its relation to Alkali Silica Reaction. Cement and Concrete Research, 42(12), 1645–1649.

Chappex, T. and Scrivener, K. (2013). The Effect of Aluminum in Solution on the Dissolution of Amorphous Silica and Its Relation to Cementitious Systems. Journal of the American Ceramic Society, 96(2), 592–597.

Chatterji, S. (1979). The Role of $Ca(OH)_2$ in the Breakdown of Portland Cement Concrete due to Alkali-Silica Reaction. Cement and Concrete Research, 9(2), 185–188.

Chatterji, S., Jensen, A. D., Thaulow, N. and Christensen, P. (1986). Studies of Alkali-Silica Reaction. Part 3. Mechanisms by Which NaCl and $Ca(OH)_2$ Affect the Reaction. Cement and Concrete Research, 16(2), 246–254.

Chatterji, S., Thaulow, N. and Jensen, A. D. (1987). Studies of Alkali-Silica Reaction. Part 4. Effect of Different Alkali Salt Solutions on Expansion. Cement and Concrete Research, 17(5), 777–783.

Chen, W. and Brouwers, H. J. H. (2007). The Hydration of Slag, part 1: Reaction Models for Alkali-Activated Slag. Journal of Materials Science, 42(2), 428-443.

Choi, M., Matsunaga, K., Oba, F., and Tanaka, I. (2009). Al NMR chemical shifts in oxide crystals: a first-principles study. Journal of Physical Chemistry C, 113(9), 3869-3873.

Cyr, M. and Pouhet, R. (2016). Carbonation in the Pore Solution of Metakaolin-Based Geopolymer. Cement and Concrete Research, 88, 227–235.

Cyr, M., Rivard, P., Labrecque, F. and Daidié, A. (2008). High-Pressure Device for Fluid Extraction from Porous Materials: Application to Cement-Based Materials. Journal of the American Ceramic Society, 91(8), 2653–2658.

Dang, F., Mikuni, A., Hirano, Y., Komatsu, R. and Ikeda, K. (2005). Preparation of Geopolymeric Materials from Fly Ash Filler by Steam Curing with Special Reference to Binder Products. Journal of the Ceramic Society of Japan,

Davidovits, J. (1991). Geopolymers - Inorganic Polymeric New Materials. Journal of Thermal Analysis, 37(8), 1633–1656.

Davidovits, J. (1994). High-Alkali Cements for 21st Century Concretes. Special Publication, 144, 383–398.

Davidovits, J. (1999). Chemistry of Geopolymeric Systems, Terminology. In Second International Conference on Geopolymer.

Davies, G. and Oberholster, R. E. (1988). Alkali-Silica Reaction Products and Their Development. Cement and Concrete Research, 18(4), 621–635.

Diamond, S. (1975). A Review of Alkali-Silica Reaction and Expansion Mechanisms 1. Alkalies in Cements and in Concrete Pore Solutions. Cement and Concrete Research, 5(4), 329–345.

Diamond, S. (1983a). Alkali Reactions in Concrete-Pore Solution Effects. Proceedings of the 6th International Conference on Alkalis in Concrete, Danish Concrete Association, Copenhagen, 1983, pp. 155-166.

Diamond, S. (1983b). Effects of Microsilica (Silica Fume) on Pore-Solution Chemistry of Cement Pastes. Journal of the American Ceramic Society, 66(5), C-82.

Diamond, S. (1989). ASR-Another Look at Mechanisms. Proceedings of the 8th International Conference on Alkali-Aggregate Reaction, Kyoto, Japan (pp. 83–94).

Dietel, J., Warr, L. N., Bertmer, M., Steudel, A., Grathoff, G. H. and Emmerich, K. (2017). The Importance of Specific Surface Area in the Geopolymerization of Heated Illitic Clay. Applied Clay Science. 139, 99-107.

Duchesne, J. and Bérubé, M. A. (1994). The Effectiveness of Supplementary Cementing Materials in Suppressing Expansion due to ASR: Another Look at the Reaction Mechanisms Part 2: Pore Solution Chemistry. Cement and Concrete Research, 24(2), 221–230.

Duxson, P., Fernández-Jiménez, A., Provis, J. L., Lukey, G. C., Palomo, A. and van Deventer, J. S. (2007). Geopolymer Technology: The Current State of the Art. Journal of Materials Science, 42(9), 2917-2933.

Duxson, P., Lukey, G. C., Separovic, F. and van Deventer, J. S. (2005). Effect of Alkali Cations on Aluminum Incorporation in Geopolymeric Gels. Industrial and Engineering Chemistry Research, 44(4), 832–839.

Duxson, P. and Provis, J. L. (2008). Designing Precursors for Geopolymer Cements. Journal of the American Ceramic Society, 91(12), 3864-3869.

Duxson, P., Provis, J. L., Lukey, G. C., Mallicoat, S. W., Kriven, W. M. and van Deventer, J. S. (2005). Understanding the Relationship between Geopolymer Composition, Microstructure and Mechanical Properties. Colloids and Surfaces A: Physicochemical and Engineering Aspects, 269(1–3), 47–58.

Duxson, P., Provis, J. L., Lukey, G. C., Separovic, F. and van Deventer, J. S (2005). ^{29}Si NMR Study of Structural Ordering in Aluminosilicate Geopolymer Gels. Langmuir, 21(7), 3028-3036.

Engelhardt, G., Fahlke, B., Mägi, M. and Lippmaa, E. (1983). High-Resolution Solid-State ^{29}Si and ^{27}Al NMR of Aluminosilicate Intermediates in Zeolite A Synthesis. Zeolites, 3(4), 292-294.

Engelhardt, G. (1989). Multinuclear Solid-State NMR in Silicate and Zeolite Chemistry. Trends in Analytical Chemistry, 8(9), 343-347.

Feng, D., Provis, J. L. and van Deventer, J. S. (2012). Thermal Activation of Albite for the Synthesis of One-Part Mix Geopolymers. Journal of the American Ceramic Society, 95(2), 565-572.

Fernández-Jiménez, A., García-Lodeiro, I. and Palomo, A. (2007). Durability of alkali-activated fly ash cementitious materials. Journal of Materials Science, *42*(9), 3055–3065.

Fernández-Jiménez, A. and Puertas, F. (2002). The Alkali-Silica Reaction in Alkali-Activated Granulated Slag Mortars with Reactive Aggregate. Cement and Concrete Research, 32(7), 1019–1024.

Fernández-Jiménez, A., Puertas, F., Sobrados, I. and Sanz, J. (2003). Structure of Calcium Silicate Hydrates Formed in Alkaline-Activated Slag: Influence of the Type of Alkaline Activator. Journal of the American Ceramic Society, 86(8), 1389-1394.

Fletcher, R. A., MacKenzie, K. J. D., Nicholson, C. L. and Shimada, S. (2005). The Composition Range of Aluminosilicate Geopolymers. Journal of the European Ceramic Society, 25(9), 1471-1477.

Fournier, B. and Bérubé, M. A. (2000). Alkali-Aggregate Reaction in Concrete: A Review of Basic Concepts and Engineering Implications. Canadian Journal of Civil Engineering, 27(2), 167–191.

Gaboriaud, F., Nonat, A., Chaumont, D. and Craievich, A. (1999). Aggregation and Gel Formation in Basic Silico−Calco−Alkaline Solutions Studied: A SAXS, SANS, and ELS Study. The Journal of Physical Chemistry B, 103(28), 5775–5781.

Garcia-Lodeiro, I., Palomo, A. and Fernández-Jiménez, A. (2015). An Overview of the Chemistry of Alkali-Activated Cement-Based Binders. In Handbook of Alkali-Activated Cements, Mortars and Concretes, pp. 19-47, Woodhead Publishing.

García-Lodeiro, I., Palomo, A. and Fernández-Jiménez, A. (2007). Alkali-Aggregate Reaction in Activated Fly Ash Systems. Cement and Concrete Research, 37(2), 175–183.

Geng, G., Myers, R. J., Li, J., Maboudian, R., Carraro, C., Shapiro, D. A. and Monteiro, P. J. M. (2017). Aluminum-Induced Dreierketten Chain Cross-Links Increase the Mechanical Properties of Nanocrystalline Calcium Aluminosilicate Hydrate. Scientific Reports, 7, 44032.

Glasser, L. D., and Harvey, G. (1984). The Unexpected Behaviour of Potassium Aluminosilicate Solutions. Journal of the Chemical Society, Chemical Communications, (10), 664-665.

Glasser, L. D. and Kataoka, N. (1981). The Chemistry of "Alkali-Aggregate" Reaction. Cement and Concrete Research, 11(1), 1–9.

Glasser, L. D. and Kataoka, N. (1982). On the Role of Calcium in the Alkali-Aggregate Reaction. Cement and Concrete Research, 12(3), 321–331.

Glukhovsky, V. D., Rostovskaja, G. and Rumyna, G. V. (1980). High Strength Slag-Alkaline Cements. In 7th International Congress on the Chemistry of Cement, Paris, pp. 164–168.

Glukhowsky, V. D. (1967). Soil Silicate Articles and Structures. Russian, Budivel'nyk Publish., Kiev.

Gunasekara, C., Law, D. W. and Setunge, S. (2016). Long Term Permeation Properties of Different Fly Ash Geopolymer Concretes. Construction and Building Materials, 124, 352-362.

Haha, M. B., Le Saout, G., Winnefeld, F. and Lothenbach, B. (2011). Influence of Activator Type on Hydration Kinetics, Hydrate Assemblage and Microstructural

Development of Alkali Activated Blast-Furnace Slags. Cement and Concrete Research, 41(3), 301-310.

Hamilton, J. P., Brantley, S. L., Pantano, C. G., Criscenti, L. J. and Kubicki, J. D. (2001). Dissolution of Nepheline, Jadeite and Albite Glasses: Toward Better Models for Aluminosilicate Dissolution. Geochimica et Cosmochimica Acta, 65(21), 3683-3702.

Hansen, W. C. (1944). Studies Relating to the Mechanism by Which the Alkali–Silica Reaction Proceeds in Concrete. Journal of the American Concrete Institute, 15, 213–227.

Helmuth, R., Stark, D., Diamond, S. and Moranville-regourd, M. (1993). Alkali-Silica Reactivity : An Overview of Research. Concrete. Contract, 100, 202.

Hench, L. L. Clark, D. E. (1978). Physical Chemistry of Glass Surfaces. Journal of Non-Crystalline Solids, 28(1), 83–105.

Hong, S. Y. and Glasser, F. P. (2002). Alkali Sorption by C-S-H and C-A-S-H Gels: Part II. Role of Alumina. Cement and Concrete Research, 32(7), 1101–1111.

Hou, X., Kirkpatrick, R. J., Struble, L. J. and Monteiro, P. J. (2005). Structural Investigations of Alkali Silicate Gels. Journal of the American Ceramic Society, 88(4), 943–949.

Iler, K. R. (1979). The Chemistry of Silica: Solubility, Polymerization, Colloid and Surface Properties and Biochemistry of Silica.

Kawamura, M., Kayyali, O. A. and Haque, M. N. (1988). Effects of a Fly Ash on Pore Solution Composition in Calcium and Sodium Chloride-Bearing Mortars. Cement and Concrete Research, 18(5), 763–773.

Kim, M. S., Jun, Y., Lee, C. and Oh, J. E. (2013). Use of CaO as an Activator for Producing a Price-Competitive Non-Cement Structural Binder Using Ground Granulated Blast Furnace Slag. Cement and Concrete Research, 54, 208-214.

Kinrade, S. D. and Swaddle, T. W. (1989). Direct Detection of Aluminosilicate Species in Aqueous Solution by Silicon-29 and Aluminum-27 NMR Spectroscopy. Inorganic Chemistry, 28(10), 1952-1954.

Knudsen, T. and Thaulow, N. (1975). Quantitative Microanalyses of Alkali-Silica Gel in Concrete. Cement and Concrete Research, 5(5), 443–454.

Kollek, J. J., Varma, S. P. P. and Zaris, C. (1986). Measurement of OH^- Ion Concentrations of Pore Fluids and Expansion due to Alkali-Silica Reaction in Composite Cement Mortars. In 8th International Congress on the Chemistry of Cement. Rio de Janeiro, Vol 4, pp. 183-189.

Krivenko, P. (1997). Alkaline Cements: Terminology, Classification, Apspects of Durability. In 10th International Congress on the Chemistry of Cement, Vol. 4.

Krivenko, P., Drochytka, R., Gelevera, A. and Kavalerova, E. (2014). Mechanism of Preventing the Alkali-Aggregate Reaction in Alkali Activated Cement Concretes. Cement and Concrete Composites, 45, 157–165.

Krivenko, P. (1994). Alkaline Cements. Proceedings of the 1st International Conference on Alkaline Cements and Concretes, Kiev, Ukraine, 1994.

Krizan, D. and Zivanovic, B. (2002). Effects of Dosage and Modulus of Water Glass on Early Hydration of Alkali-Slag Cements. Cement and Concrete Research, 32(8), 1181-1188.

Kuehl, H. (1908). Slag Cement and Process of Making the Same. U.S. Patent No. 900,939. Washington, DC: U.S. Patent and Trademark Office.

Kupwade-Patil, K. and Allouche, E. N. (2012). Impact of Alkali Silica Reaction on Fly Ash Based Geopolymer Concrete. Journal of Materials in Civil Engineering, 25(1), 131-139.

Lahoti, M., Wong, K. K., Tan, K. H. and Yang, E. H. (2017). Use of Alkali-Silica Reactive Sedimentary Rock Powder as a Resource to Produce High Strength Geopolymer Binder. Construction and Building Materials, 155, 381-388.

Lahoti, M., Wong, K. K., Tan, K. H. and Yang, E. H. (2018). Effect of Alkali Cation Type on Strength Endurance of Fly Ash Geopolymers Subject to High Temperature Exposure. Materials and Design, 154, 8-19.

Leemann, A., Bernard, L., Alahrache, S. and Winnefeld, F. (2015). ASR Prevention - Effect of Aluminum and Lithium Ions on the Reaction Products. Cement and Concrete Research, 76, 192–201.

Leemann, A., Le Saout, G., Winnefeld, F., Rentsch, D. and Lothenbach, B. (2011). Alkali-Silica Reaction: The Influence of Calcium on Silica Dissolution and the Formation of Reaction Products. Journal of the American Ceramic Society, 94(4), 1243–1249.

Li, C., Sun, H. and Li, L. (2010). A Review: The Comparison between Alkali-Activated Slag (Si + Ca) and Metakaolin (Si + Al) Cements. Cement and Concrete Research, 40(9), 1341-1349.

Lippmaa, E., Mági, M., Samoson, A., Tarmak, M. and Engelhardt, G. (1981). Investigation of the Structure of Zeolites by Solid-State High-Resolution ^{29}Si NMR Spectroscopy. Journal of the American Chemical Society, 103(17), 4992-4996.

Lippmaa, E., Samoson, A. and Magi, M. (2005). High-Resolution Aluminum-27 NMR of Aluminosilicates. Journal of the American Chemical Society, 108(8), 1730-1735.

Lloyd, R. R., Provis, J. L. and van Deventer, J. S. (2010). Pore Solution Composition and Alkali Diffusion in Inorganic Polymer Cement. Cement and Concrete Research, 40(9), 1386–1392.

Markovic, S., Dondur, V. and Dimitrijevic, R. (2003). FTIR Spectroscopy of Framework Aluminosilicate Structures: Carnegieite and Pure Sodium Nepheline. Journal of Molecular Structure, 654(1-3), 223-234.

Martineau, C., Taulelle, F. and Haouas, M. (2016). The Use of ^{27}Al NMR to Study Aluminum Compounds: A Survey of the Last 25 Years. PATAI'S Chemistry of Functional Groups, 1-51.

McLellan, B. C., Williams, R. P., Lay, J., Van Riessen, A. and Corder, G. D. (2011). Costs and Carbon Emissions for Geopolymer Pastes in Comparison to Ordinary Portland Cement. Journal of Cleaner Production, 19(9-10), 1080-1090.

Mobili, A., Belli, A., Giosuè, C., Bellezze, T. and Tittarelli, F. (2016). Metakaolin and Fly Ash Alkali-Activated Mortars Compared with Cementitious Mortars at the Same Strength Class. Cement and Concrete Research, 88, 198-210.

Nguyen, A. D., and Škvára, F. (2016). The influence of ambient pH on fly ash-based geopolymer. Cement and Concrete Composites, *72*, 275–283.

Pacheco-Torgal, F., Abdollahnejad, Z., Camões, A. F., Jamshidi, M. and Ding, Y. (2012). Durability of Alkali-Activated Binders: A Clear Advantage over Portland Cement or an Unproven Issue? Construction and Building Materials, 30, 400-405.

Pallagi, A., Tasi, A., Gácsi, A., Csáti, M., Pálinkó, I., Peintler, G. and Sipos, P. (2012). The Solubility of $Ca(OH)_2$ in Extremely Concentrated NaOH Solutions at 25°C. Central European Journal of Chemistry, 10(2), 332-337.

Payá, J., Agrela, F., Rosales, J., Morales, M. M. and Borrachero, M. V. (2019). Application of Alkali-Activated Industrial Waste. In New Trends in Eco-efficient and Recycled Concrete, pp. 357-424, Woodhead Publishing.

Phair, J. W. and van Deventer, J. S. (2002). Effect of the Silicate Activator pH on the Microstructural Characteristics of Waste-Based Geopolymers. International Journal of Mineral Processing, 66(1-4), 121-143.

Pimraksa, K., Chindaprasirt, P., Rungchet, A., Sagoe-Crentsil, K. and Sato, T. (2011). Lightweight Geopolymer Made of Highly Porous Siliceous Materials with Various Na_2O/Al_2O_3 and SiO_2/Al_2O_3 ratios. Materials Science and Engineering A, 528(21), 6616-6623.

Pouhet, R., and Cyr, M. (2015). Alkali–Silica Reaction in Metakaolin-Based Geopolymer Mortar. Materials and Structures, 48(3), 571–583.

Powers, T. C. and Steinour, H. H. (1955). An Interpertation of Some Published Researches on the Alkali-Aggregate Reaction Part I- the Chemical Reactions and

Mechanism of Expansion. Journal of the American Concrete Institute, 51(2), 497–516.

Provis, J. L. (2018). Alkali-activated materials. Cement and Concrete Research, 114, 40-48.

Provis, J. L., Duxson, P., Lukey, G. C., and Van Deventer, J. S. J. (2005). Statistical thermodynamic model for Si/Al ordering in amorphous aluminosilicates. Chemistry of Materials, *17*(11), 2976–2986.

Provis, J. L. and van Deventer, J. S. (2014). Alkali Activated Materials: State-of-the-Art Report, RILEM TC 224-AAM. Springer.

Puertas, F., Fernández-Jiménez, A. and Blanco-Varela, M. T. (2004). Pore Solution in Alkali-Activated Slag Cement Pastes. Relation to the Composition and Structure of Calcium Silicate Hydrate. Cement and Concrete Research, 34(1), 139-148.

Puertas, F., Palacios, M., Gil-Maroto, A. and Vázquez, T. (2009). Alkali-Aggregate Behaviour of Alkali-Activated Slag Mortars: Effect of Aggregate Type. Cement and Concrete Composites, 31(5), 277–284.

Puertas, F., Palacios, M., Manzano, H., Dolado, J. S., Rico, A. and Rodríguez, J. (2011). A Model for the C-A-S-H Gel Formed in Alkali-Activated Slag Cements. Journal of the European Ceramic Society, 31(12), 2043-2056.

Purdon, A. O. (1940). The Action of Alkalis on Blast Furnace Slag. Journal of the Society of Chemical Industry, 59, 191–202.

Rajabipour, F., Giannini, E., Dunant, C., Ideker, J. H. and Thomas, M. D. (2015). Alkali-Silica Reaction: Current Understanding of the Reaction Mechanisms and the Knowledge Gaps. Cement and Concrete Research, 76, 130–146.

Ramlochan, T., Thomas, M. D. A. and Hooton, R. D. (2004). The Effect of Pozzolans and Slag on the Expansion of Mortars Cured at Elevated Temperature: Part II: Microstructural and Microchemical Investigations. Cement and Concrete Research, 34(8), 1341–1356.

Ravikumar, D. and Neithalath, N. (2012). Effects of Activator Characteristics on the Reaction Product Formation in Slag Binders Activated Using Alkali Silicate Powder and NaOH. Cement and Concrete Composites, 34(7), 809-818.

Ruiz-Santaquiteria, C., Fernández-Jiménez, A., Skibsted, J. and Palomo, A. (2013). Clay Reactivity: Production of Alkali Activated Cements. Applied Clay Science, 73, 11-16.

Saetta, A. V., Schrefler, B. A. and Vitaliani, R. V. (1993). The Carbonation of Concrete and the Mechanism of Moisture, Heat and Carbon Dioxide Flow through Porous Materials. Cement and Concrete Research, 23(4), 761–772.

Sagoe-Crentsil, K. and Weng, L. (2007). Dissolution Processes, Hydrolysis and Condensation Reactions during Geopolymer Synthesis: Part II. High Si/Al Ratio Systems. Journal of Materials Science, 42(9), 3007-3014.

Samadi-Maybodi, A., Azizi, S. N., Naderi-Manesh, H., Bijanzadeh, H., McKeag, I. H. and Harris, R. K. (2001). Highly Resolved ^{27}Al NMR Spectra of Aluminosilicate Solutions. Journal of the Chemical Society, Dalton Transactions, (5), 633-638.

Scrivener, K., Snellings, R. and Barbara, L. (2018). A Practical Guide to Microstructural Analysis of Cementitious Materials. Crc Press.

Shehata, M. H. and Thomas, M. D. (2006). Alkali Release Characteristics of Blended Cements. Cement and Concrete Research, 36(6), 1166–1175.

Shi, C., Jiménez, A. F. and Palomo, A. (2011). New Cements for the 21st Century: The Pursuit of an Alternative to Portland Cement. Cement and Concrete Research, 41(7), 750-763.

Shi, C., Krivenko, P. V and Roy, D. (2006). Alkali-Activated Cements and Concretes. Alkali-Activated Cements and Concretes. CRC Press.

Shi, C., Qu, B. and Provis, J. L. (2019). Recent Progress in Low-Carbon Binders. Cement and Concrete Research, 122, 227-250.

Shi, Z., Shi, C., Zhao, R. and Wan, S. (2015). Comparison of Alkali–Silica Reactions in Alkali-Activated Slag and Portland Cement Mortars. Materials and Structures, 48(3), 743-751.

Stade, H. and Müller, D. (1987). On the Coordination of Al in Ill-crystallized C-S-H Phases Formed by Hydration of Tricalcium Silicate and by Precipitation Reactions at Ambient Temperature. Cement and Concrete Research, 17(4), 553–561.

Stanton, T. (1940). Expansion of Concrete through Reaction between Cement and Aggregate. In Proceedings of American Society of Civil Engineers, 66, pp. 1781–1811.

Struble, L. J. (1988). The Influence of Cement Pore Solution on Alkali-Silica Reaction. Ph.D. Thesis, Purdue University.

Struble, L. J. and Diamond, S. (1981). Swelling Properties of Synthetic Alkali Silica Gels. Journal of the American Ceramic Society, 64(11), 652–655.

Sun, G. K., Young, J. F. and Kirkpatrick, R. J. (2006). The Role of Al in C-S-H: NMR, XRD, and Compositional Results for Precipitated Samples. Cement and Concrete Research, 36(1), 18–29.

Swamy, R. (1992). The Alkali-Silica Reaction in Concrete. CRC Press.

Taylor, H. F. (1997). Cement Chemistry. 2nd Edition. Academic Press.

Thomas, M. D. (1998). The Role of Calcium in Alkali–Silica Reaction. In Proceedings of the Sidney Diamond Symposium on Materials Science and Engineering of Concrete and Cementitious Based Composites, American Ceramic Society, pp. 325–335.

Thomas, M. D. (2001). The Role of Calcium Hydroxide in Alkali Recycling in Concrete. Materials Science of Concrete Special, 225–236.

Thomas, M. D., Fournier, B. and Folliard, K. J. (2013). Alkali-Aggregate Reactivity (AAR) Facts Book. (No. FHWA-HIF-13-019). United States. Federal Highway Administration. Office of Pavement Technology.

Thomas, M. D., Fournier, B., Folliard, K., Ideker, J. and Shehata, M. (2006). Test Methods for Evaluating Preventive Measures for Controlling Expansion due to Alkali-Silica Reaction in Concrete. Cement and Concrete Research, 36(10), 1842–1856.

Thomas, M. D., Hooton, R. D. and Rogers, C. A. (1997). Prevention of Damage Due to Alkali-Aggregate Reaction (AAR) in Concrete Construction-Canadian Approach. Cement, Concrete and Aggregates, 19(1), 26-30.

Urhan, S. (1987). Alkali Silica and Pozzolanic Reactions in Concrete. Part 1: Interpretation of Published Results and an Hypothesis Concerning the Mechanism. Cement and Concrete Research, 17(1), 141–152.

Valentini, L., Contessi, S., Dalconi, M. C., Zorzi, F. and Garbin, E. (2018). Alkali-Activated Calcined Smectite Clay Blended with Waste Calcium Carbonate as a Low-Carbon Binder. Journal of Cleaner Production, 184, 41-49.

van Deventer, J. S. J., Provis, J. L., Duxson, P., and Lukey, G. C. (2007). Reaction mechanisms in the geopolymeric conversion of inorganic waste to useful products. Journal of Hazardous Materials, 139(3), 506–513.

Vayghan, A. G., Rajabipour, F. and Rosenberger, J. L. (2016). Composition-Rheology Relationships in Alkali-Silica Reaction Gels and the Impact on the Gel's Deleterious Behavior. Cement and Concrete Research, 83, 45–56.

Wang-hong, A. Y. and Kirkpatrick, J. R. (1989). Hydrothermal Reaction of Albite and a Sodium Aluminosilicate Glass: A Solid-State NMR Study. Geochimica et Cosmochimica Acta, 53(4), 805-819.

Wang, H. and Gillott, J. E. (1991). Mechanism of Alkali-Silica Reaction and the Significance of Calcium Hydroxide. Cement and Concrete Research, 21(4), 647–654.

Wang, S. D. and Scrivener, K. L. (1995). Hydration Products of Alkali Activated Slag Cement. Cement and Concrete Research, 25(3), 561-571.

Wang, S. D. and Scrivener, K. L. (2003). ^{29}Si and ^{27}Al NMR Study of Alkali-Activated Slag. Cement and Concrete Research, 33(5), 769-774.

Wardhono, A. (2014). The Durability of Fly Ash Geopolymer and Alkali-Activated Slag Concretes. Ph.D. Thesis, RMIT University, Melbourne, Australia.

Warner, S., Ideker, J. H. and Schumacher, K. (2012). Alkali-Silica Reactivity and the Role of Alumina. In Proceedings of the 14th International Conference on Alkali-Aggregate Reactivity in Concrete (ICAAR), Austin, Texas.

Warner, S. J. (2012). The Role of Alumina in the Mitigation of Alkali-Silica Reaction. Master Thesis, Oregon State University.

Weng, L. and Sagoe-Crentsil, K. (2007). Dissolution Processes, Hydrolysis and Condensation Reactions during Geopolymer Synthesis: Part I-Low Si/Al Ratio Systems. Journal of Materials Science, 42(9), 2997-3006.

Williamson, T. and Juenger, M. C. G. (2016). The Role of Activating Solution Concentration on Alkali-Silica Reaction in Alkali-Activated Fly Ash Concrete. Cement and Concrete Research, 83, 124–130.

Winn, K., Ng, M. and Wong, L. N. Y. (2017). Stability Analysis of Underground Storage Cavern Excavation in Singapore. In Procedia Engineering, 191, 1040-1047.

Worrell, E., Price, L., Martin, N., Hendriks, C. and Meida, L. O. (2001). Carbon Dioxide Emissions from the Global Cement Industry. Annual review of energy and the environment, 26(1), 303-329.

Xu, H. and van Deventer, J. S. (2000). Geopolymerisation of Alumino-Silicate Minerals. International Journal of Mineral Processing, 59(3), 247–266.

Yuan, T., Wang, J. and Li, Z. (2010). Measurement and Modelling of Solubility for Calcium Sulfate Dihydrate and Calcium Hydroxide in NaOH/KOH Solutions. Fluid Phase Equilibria, 297(1), 129-137.

Zuhua, Z., Xiao, Y., Huajun, Z. and Yue, C. (2009). Role of Water in the Synthesis of Calcined Kaolin-Based Geopolymer. Applied Clay Science, 43(2), 218-223.